MAGNESIUM RICH PRIMER FOR THE CORROSION PROTECTION OF ALUMINUM

ALLOYS: INVESTIGATION, IMPROVEMENT AND APPLICATION

A Dissertation
Submitted to the Graduate Faculty
of the
North Dakota State University
of Agriculture and Applied Science

By

Junren Lin

In Partial Fulfillment of the Requirements
for the Degree of
DOCTOR OF PHILOSOPHY

Major Department:
Coatings and Polymeric Materials

April 2016

Fargo, North Dakota

North Dakota State University
Graduate School

Title

Magnesium Rich Primer for the Corrosion Protection of Aluminum Alloys:

Investigation, Improvement and Application

By

Junren Lin

The Supervisory Committee certifies that this *disquisition* complies with North Dakota State

University's regulations and meets the accepted standards for the degree of

DOCTOR OF PHILOSOPHY

SUPERVISORY COMMITTEE:

Dr. Dante Battocchi

Chair

Dr. Gordon P. Bierwagen

Dr. Andriy Voronov

Dr. Stuart Croll

Dr. Yechun Wang

Approved:

October, 18, 2016	Dr. Dean Webster
Date	Department Chair

ABSTRACT

The goals of this research are to develop deeper understanding of the corrosion protection mechanism of Mg-rich primer (MgRPs), improve corrosion protection performance of MgRPs, and extend the application of MgRPs. To address these research goals, the following studies were performed:

1. Early blistering problems encountered during constant immersion or ASTM B117 exposure of top-coated MgRPs over AA2024-T3 substrate were investigated. The results suggest that hydrogen entrapment by topcoat, instead of Al corrosion, contributes significantly to the formation of early blistering. Meanwhile, simultaneous real-time hydrogen collection and open circuit potential measurement was demonstrated as a new method for studying the corrosion protection mechanism of MgRPs. Moreover, the gas generated from MgRPs was unequivocally identified as hydrogen by cyclic voltammetry.

2. Degradation behaviors of MgRP in 1% NaCl solution and Dilute Harrison Solution (DHS) were compared through scanning electron microscopy, hydrogen volume collection and electrochemical tests. The effects of connection modes between Mg pigment and Al substrate, different ions on the formation and stability of Mg oxidation products, and cathodic reaction sites on the microstructure of MgRP were discussed. In addition, an in situ method for the estimation of remaining Mg pigment in MgRP was developed based on H_2 volume collection.

3. The effects of adding sodium benzoate (SB), sodium dodecylbenzenesulfonate (SDBS), and 8-hydroxyquinoline (HQ) to MgRP on its corrosion protection of AA 2024-T3 were investigated. The results show that addition of SB, SDBS and HQ into MgRP improved the corrosion protection performance of MgRP by decelerating the oxidation rate of Mg, improving coating barrier properties and inhibiting the corrosion of Al alloy substrate.

4. The (MgRP-powder topcoat) coating system was developed and characterized in this research for the corrosion protection of Al alloys. The results show that powder topcoat can be applied on top of MgRP through both fluidized bed and electrostatic spray methods. Moreover, this (MgRP-powder topcoat) coating system provided much longer corrosion protection time to Al substrate than the powder coat by itself, without degrading other coating properties.

ACKNOWLEDGMENTS

TABLE OF CONTENTS

LIST OF TABLES

LIST OF FIGURES

LIST OF ABBREVIATIONS

AA..Aluminum Alloy

AC..Alternating Current

Al...Aluminum

ASTM ....American Society for Testing and Materials

B117...Salt Spray Accelerated Weathering Testing Protocol, as per

ASTM B117

CPVC ....Critical Pigment Volume Concentration

CV ....Cyclic Voltammetry

DHS..Dilute Harrison Solution

DSC..Differential Scanning Calorimetry

ENM...Electrochemical Noise Methods

EDX ....Energy Dispersion X-Ray spectroscopy

EIS..Electrochemical Impedance Spectroscopy

FTIR...Fourier Transform Infrared Spectroscopy

HQ..8-hydroxyquinoline

LI..Localization Index

Mg..Magnesium

MgRP ....Magnesium Rich Primer

NDSU...North Dakota State University

OCP..Open Circuit Potential

PDS ....Potentiodynamic Scan

PVC..Pigment Volume Concentration

LIST OF SYMBOLS

A..Area

D..Density

e_a...Half-cell electrode potential of the oxidation reactions

e_c...Half-cell electrode potential of the reduction reactions

E_{Corr}..Corrosion Potential

$Ecorr\text{-}_{Al}$..Corrosion Potential of Al

$Ecorr\text{-}_{Mg}$...Corrosion Potential of Mg

E'corr ....Mixed Potential

$ia\text{-}_{Al}$..Anodic Current of Al

$ia\text{-}_{Mg}$...Anodic Current of Mg

$ic\text{-}_{Al}$..Cathodic Current of Al

$ic\text{-}_{Mg}$...Cathodic Current of Mg

$icorr\text{-}_{Al}$...Corrosion Current of Al

$icorr\text{-}_{Mg}$...Corrosion Current of Mg

$Mass_{Mg}$...Total mass of Mg Pigments

M_{Mg} ....Molar Mass of Mg

n_{H_2} ....Moles of Hydrogen

n_{Mg}..Moles of Mg

n_T ....Moles of Trapped Hydrogen

P_A..Adhesion Strength between Coatings and Substrate

P_T..Pressure Produced by Trapped Hydrogen

LIST OF APPENDIX FIGURES

CHAPTER 1. INTRODUCTION

Aluminum alloys, such as 2000 and 7000 series, have been the primary structure materials used in high-loaded aircraft structures for more than 80 years due to its high strength, superior toughness, great fatigue resistance, and high strength-to-weight ratio[1-3]. However, corrosion of aluminum alloys, especially the copper-rich 2000 series, is one of the major problems for the aerospace industry[4-6]. The structure failure of aircraft caused by corrosion could be disastrous: aside from putting humans and public safety at risk, these failures lead to severe inconvenience and numerous economic losses[7]. Therefore, protect aluminum alloys against corrosion becomes one of the major tasks for the aerospace industry.

Among all the corrosion prevention methods, protective coating is one of the most practical and effective methods. In the aerospace industry, the corrosion protection of Al alloys still relies significantly on chromate pretreatments and chromate primer systems[8]. However, hexavalent chromium (Cr^{6+}) is well known for its carcinogen nature[9-11]. Stringent regulations on the handling and use of Cr^{6+}-containing materials have been enacted by most governments[12, 13]. Therefore, there exists a severe need to develop an environmental-friendly coating system for replacing the chromate-based primer or pretreatment systems.

Mg-rich primers (MgRPs), in analogy to Zn-rich primers for steel, were first developed by Nanna, Battocchi and Bierwagen at North Dakota State University to provide cathodic protection for Al alloy substrate[14]. It is a very effective corrosion protective coating system to replace the chromate-based primer or pretreatment systems. The performance of MgRPs have been examined and studied using various techniques and shown equal or even better performance compared to the Cr-based coating systems[15-18]. The commercial product of MgRP (Aerodur®2100) was produced by Akzo Noble in 2007. Since then, investigation of corrosion

protection mechanism and further improvement of the performance of MgRP have been the topic of research by several researchers. Even though MgRP technology has advanced drastically since its conception, improvements are still occurring in MgRP technology, both in the academic and industrial laboratories and applications.

As the extension of Mg-rich primer technology, four parts of research were conducted in this Ph.D. project. The first part of research was to address the early blistering problem observed on topcoated MgRPs during lab exposure. Research in this work found that during lab tests, hydrogen generated rapidly from MgRP. Entrapment of hydrogen by the topcoat is the cause of early blistering. In the second part of research, corrosion protection mechanisms of MgRP in different solutions were compared. New insights of the corrosion protection mechanism were proposed. In addition, a new method was developed for the estimation of MgRP lifetime. Deeper understanding of corrosion protection mechanism of MgRPs over Al alloys was developed in the first two parts of research. In the third part of research, inhibitor-added MgRPs were formulated. These inhibitor-added MgRPs provide longer cathodic protection time and better coating barrier protection to Al substrate. Last, (Mg rich primer-powder topcoat) coating system was first developed in this research. The coating systems provided much longer corrosion protection time to Al substrate without degrading other coating properties. Successful development of this product extends the application of both MgRP and powder topcoat. In addition, it gives us guideline to develop other metal rich powder topcoat systems for the corrosion protection of various metal substrates.

Details of these studies will be demonstrated in this dissertation in chapter 3-6. In addition, a literature review on the history, development and future perspective of MgRPs will be given in chapter 2. The dissertation will be concluded with summary and future work.

1.1. References

1. J.C. Williams, and E. A. Starke, Acta Mater. 51 (2003): pp. 5775–5799.

2. A. Heinz, A Haszler, C. Keidel, S. Moldenhauer, R. Benedictus, and W. Miller, Mater. Sci. Eng. A 280 (2000): pp. 102–107.

3. T. Dursun, and C. Soutis, Mater. Des. 56 (2014): pp. 862–871.

4. R.T. Foley, Corrosion 42 (1986): pp. 277–288.

5. R. Akid, M. Gobara, and H. Wang, Electrochim. Acta 56 (2011): pp. 2483–2492.

6. D.W. Hoeppner, and C.A. Arriscorreta, Int. J. Aerosp. Eng. 2012 (2012).

7. D.A. Forman, R. Baty, E.F. Herzberg, A.R. Kelly, M. V. Kumaran, and N.T. O'Meara, "The Annual Cost of Corrosion for Air Force Aicraft and Missile Equipmwnt" (2009).

8. R.L. Twite, and G.P. Bierwagen, Prog. Org. Coatings 33 (1998): pp. 91–100.

9. K. Shekhawat, K., S. Chatterjee, and B. Joshi, Int. J. Adv. Res. 3 (2015): pp. 167–172.

10. A.A. Mamyrbaev, A., T.A. Dzharkenov, Z.A. Imangazina, and U.A. Satybaldieva, Environ. Health Prev. Med. 20 (2015): pp. 159–167.

11. P.L. Abreu, L.M.R. Ferreira, M.C. Alpoim, and a. M. Urbano, BioMetals 27 (2014): pp. 409–443.

12. "Chromium Compounds Hazard Summary," United State Environmental Protection Agency (2000), http://www3.epa.gov/airtoxics/hlthef/chromium.html (Jan. 1, 2015).

13. "RoHS Restricted Substance" (n.d.), http://www.rohsguide.com/rohs-substances.htm (Jan. 1, 2015).

14. M.E. Nanna, and G.P. Bierwagen, J. Coatings Technol. Res. 1 (2004): pp. 69–80.

15. G. Bierwagen, D. Battocchi, A. Simões, A. Stamness, and D. Tallman, Prog. Org. Coatings 59 (2007): pp. 172–178.

16. G.Bierwagen, R. Brown, D. Battocchi, and S. Hayes, Prog. Org. Coatings 67 (2010): pp. 48–61.

17. K. Pianoforte, "Aerospace Coatings Market," Coatings World (2015).

18. P. Visser, R. Waddell, and R. Walker, "Reflections," AkzoNobel Aerospace Coatings (2012).

CHAPTER 2. LITERATURE REVIEW

2.1. Introduction

In aerospace industry, the corrosion protection of structural Al alloys is a major challenge. Structural Al alloys such as AA 2024 T-3 and AA7075 T-6 are specially designed alloys that impart excellent mechanical properties to aircraft, but are prone to corrosion due to the addition of the alloying elements, especially copper[1-3]. Currently, the corrosion protection of aircraft Al alloys still relies significantly on chromate pretreatments and chromate primer systems[4, 5]. However, hexavalent chromium has been recognized as a toxic and carcinogenic material[6, 7]. Most governments have enforced strengthen regulations on the handling and use of Cr^{6+}-containing materials[8, 9]. The total replacement of chromates has been one of the major targets of US DOD environmental R&D programs for more than 20 years[10]. In the European Union, Cr^{6+} compounds will be completely forbidden by 2017[11]. Therefore, there exists a severe need to broaden the use of an environmental-friendly coating system to replace the chromate-coating systems.

Many alternative options for the protection of aircraft Al alloys have been considered and tested by researchers[5]. Among which, magnesium rich primer (MgRP) first developed at North Dakota State University by Nanna, Battocchi and Bierwagen is by far the most promising total Cr free alternative to provide corrosion protection for Al alloy[10]. The conception of MgRP was developed and tested in the early 2000s when it was realized that the particulate Mg pigments were available. The original work at NDSU generated a patent of "Magnesium rich coatings and coating systems" on 2004[12]. This technology was licensed to Akzo Nobel Aerospace Coatings and the first commercial product Aerodur® 2100 MgRP was launched in 2007. The performance of MgRP has been examined in the academic, industrial and military laboratories and

applications. This chrome free technology has repeatedly shown equal or superior corrosion protection performance compared to the Cr (VI) based primers[10, 13, 14]. In October 2014, the Aerodur® 2100 was approved to AMS 3095 and the newly released Mil-PRF-32239 specification[15]. This will apply to all DOD-AF aircraft. The usage of MgRP is on the upsurge.

This paper will review the research has been done on MgRPs and their qualifications for widespread use. Cathodic corrosion protection mechanism of MgRPs will be first presented for the better understanding of this primer technology. Focus will be given on important design issues of MgRPs, methods for the study/evaluation of MgRPs, and current development of high performance MgRPs. Finally, future perspective for MgRPs will be discussed.

2.2. Cathodic protection of Al/Al alloys by MgRP

The design hypothesis of MgRP was developed in analogy to the formulation of Zn-rich primer for the cathodic corrosion protection of steel. The corrosion of Al and the principle of cathodic protection can be explained by the Wagner-Traud mixed potential theory[16]. This theory consists of two hypotheses[17, 18]: (1) Any corrosion process can be divided into two or more partial oxidation and reduction reactions; (2) There is no net accumulation of electric charge during a corrosion process. That is, during corrosion of an electrically isolated metal sample, the total rate of oxidation must equal the total rate of reduction.

In the case of Al corrosion [19, 20] in aqueous medium, the oxidation of Al proceeds according to the Equation (2.1):

$$Al \rightarrow Al^{3+} + 3e \tag{2.1}$$

This reaction must be balanced by one or more simultaneous reduction reactions which capture the released electrons. In common aqueous medium, the following reduction reactions are thermodynamically possible:

(1) Reduction of H_2O:

$$2H_2O + 2e \rightarrow H_2 \uparrow +2OH^-$$ (2.2)

(2) Reduction of dissolved oxygen:

$$O_2 + 2H_2O + 4e \rightarrow 4OH^- \text{ (Neutral or alkaline media)}$$ (2.3)

$$O_2 + 4H^+ + 4e \rightarrow 2H_2O \text{ (Acidic media)}$$ (2.4)
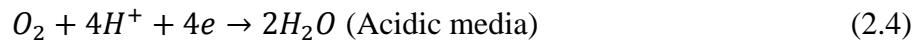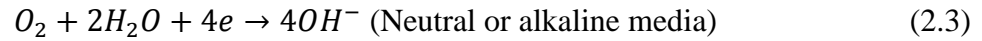
Each half-cell reaction has its own half-cell electrode potential and exchange current density. Corrosion occurs when at least one of the half-cell electrode potential of the reduction reactions (e_c) is higher than that of the oxidation reaction (e_a). The corrosion potential (E_{Corr}) lies between e_c and e_a by polarization, according to the mixed potential theory (Figure 2.1).
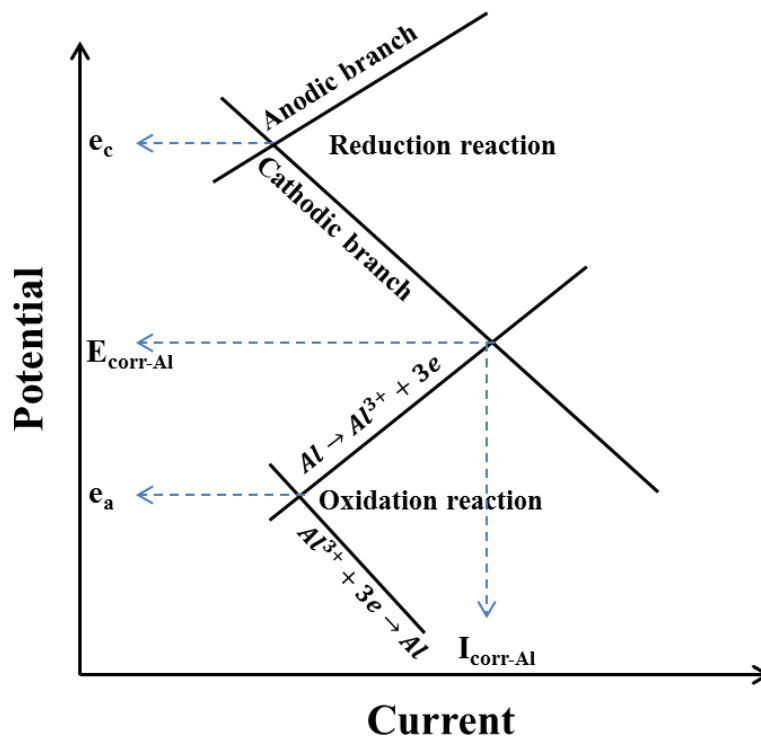
Figure 2.1. Diagram explaining corrosion of Al using mixed potential theory

When an excess of electron flow (through sacrificial anode or direct current source) is applied to the corroding Al electrode with $E_{corr\text{-}Al}$ and $i_{corr\text{-}Al}$ defined by mixed potential theory, the excess of electrons cause the electrode potential to shift negatively from $E_{corr\text{-}Al}$ to E'_{corr}. In the case of using MgRP for the corrosion protection of Al, MgRP acts as sacrificial anode since Mg is more electroactive than Al[21, 22]. According to the mixed potential theory, the E'_{corr} will be between $E_{corr\text{-}Al}$ and $E_{corr\text{-}Mg}$. And the excess of electrons suppresses the rate of the anodic reaction of Al from $i_{corr\text{-}Al}$ to $i_{a\text{-}Al}$, and increase the cathodic reduction reaction from $i_{corr\text{-}Al}$ to $i_{c\text{-}Al}$, as shown in Figure 2.2. Consequently, the corrosion of Al is suppressed. At the same time, the corrosion of Mg is accelerated, as the rate of the anodic reaction of Mg increases from $i_{corr\text{-}Mg}$ to $i_{a\text{-}Mg}$. The effect of cathodic protection is affected by the potential difference between Mg pigment and Al/Al alloys, resistance between Mg pigment and Al/Al alloys and relative exposed area of Mg pigment and Al/Al alloys[23, 24]. All these factors must be considered when formulating MgRPs.
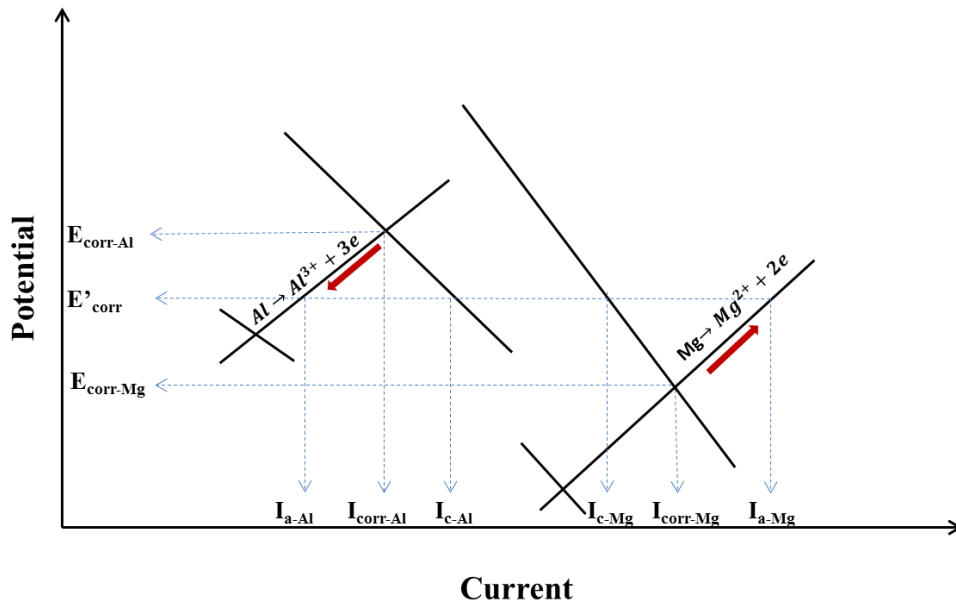
Figure 2.2. Diagram explaining cathodic protection of Al by Mg using mixed potential theory

2.3. Important design issues of MgRP

The development of a high-performance MgRP is very complex, since many factors would significantly influence the final properties of MgRP. This section will focus the discussions on some critical considerations for the design of MgRP, including the effect of pigment volume concentration, the choice of binder systems and the influence of surface pretreatment.

2.3.1. The effect of pigment volume concentration in MgRP

Volume effects are extremely important in the design of metal-rich coatings, since cathodic protection effect and many other performance behaviors of metal-rich coatings are influenced by the pigment volume concentration (PVC) of metal pigment in the primer[25, 26]. It was observed that for a pigmented coating, the breaks in many performance behaviors, such as the permeability, rusting, blistering, and gloss curves occur at a more or less definite point[27, 28]. This point was defined by Asbeck and Van loo as critical pigment volume concentration (CPVC), where "there are just sufficient binders to fill completely the voids left between the pigment particles incorporated in the film after volatilization of all thinner"[27]. Since CPVC is influenced by factors such as fundamental packing characteristics of the pigments, type of binder employed, types and amounts of special agents present, and fineness of grind of the system[29-31], the parameter Λ (= PVC/CPVC, reduced pigment volume concentration) was introduced by Bierwagen in 1975 to offer a guidelines for paint formulation based on pigment volume changes once a resin-pigmentation combination is chosen[32]. By using Λ in predicting and interpreting paint film behavior, one can isolate those properties dependent on Λ and those based on the chemical nature of the raw materials of the paint[32-34].

For effective sacrificial protection, the PVC of MgRP is usually formulated near or above the CPVC to ensure the total supply of Mg sacrificial anode material, and the electrical connectivity between Mg pigments as well as between Mg pigment and Al substrate. For example, Nanna and Bierwagen[22] studied MgRPs at 43, 46 and 50% PVC in 3% NaCl solution by open circuit potential and electrochemical impedance spectroscopy methods. The data indicated that MgRP at 46% PVC, which was the estimated CPVC for this system, provided the most effective protection. Li, et al.[35] determined the CPVC of MgRPs based on a two component epoxy resin through EIS measurement, and found that the CPVC was quite similar to the theoretical value 47.5%. They concluded that 50% PVC was the optimum in the formation of effective electrical contact. However, for coatings with Λ larger than 0.85, poor barrier protection was observed[25]. Thus, MgRPs formulated with Λ larger than 0.85 should be coated with a topcoat with low PVC to avoid a porous structure open to water/electrolyte intrusion.

Besides poor barrier properties, rapid consumption of Mg pigment might also be a problem for MgRPs formulated at high PVC. At high PVC, a large percent of Mg pigment is readily exposed to electrolyte, and thus might cause unnecessary oxidation of Mg pigment, giving no cathodic protection, before the substrate needs protection due to the high reactivity of Mg. King and Scully[36] investigated the effect of PVC in MgRPs through electrochemical methods, SEM and XRD analysis. They found that MgRPs with high PVC (65%) allowed a larger percent of the distributed Mg pigment to be utilized to protect remote defects. MgRPs with moderate PVC (45%) had a smaller amount of Mg available for remote protection. However, the remaining Mg pigment would be available to protect local defects as they occur throughout the coating's lifetime. In addition, there is some evidence that the electrical connectivity of the metal pigment carries over from the PVC = CPVC to PVC = volume percolation threshold (~30% by

9

volume for Zn spherical particles) [37-39]. Therefore, sacrificial protection might occur even MgRPs are formulated at lower PVC, which suggests that a balanced PVC where MgRPs can provide effective and longtime sacrificial protection, as well as acceptable barrier properties might be possible.

2.3.2. The effect of binders in MgRP

Coating matrix / binder provides both cohesion within a coating and adhesion between coatings and substrates. In addition, binder properties also affect corrosion protection, thermal and mechanical properties of coatings[40, 41]. Traditionally, the most commonly used binder system for metal-rich primers is a two component epoxy system, due to its good wetting of metal-metal oxide surface, excellent adhesion to most substrates, and stability at high pH environment caused by metal corrosion[31]. Li, et al.[35] investigated the effects of epoxy resin molecular mass, curing agent functionality, and epoxy/NH ratio on the performance of MgRPs. They found that among the binders tested, the optimized coating composition was based on the high MW epoxy resin, amide-functional curing agent, 1.0 epoxy/NH ratio and 50% PVC, which show very good corrosion protection for at least 3000 hrs of B117 salt spray exposure. Other binder systems have also been explored and tested for MgRPs. For example, Nanna and Bierwagen[22] compared dynamic and mechanical properties, flammability, and corrosion protection effect of conventional epoxy binders and a hybrid silane modified epoxy-urea IPNs. They found MgRPs performed better with the hybrid silane modified epoxy-urea IPNs. Ravindran et al.[42] found silane-modified glycidyl carbamate resins to be a promising binder system especially in the aspect of high temperature stability. All the above mentioned binder systems are solvent based. Considering the environmental effect and the progress in the coating industry, it would be desirable if MgRP could be formulated as powder primer.

10

2.3.3. The effect of surface pretreatment

Surface pretreatments are usually applied to metal prior to the actual coating process to improve the adhesion between the substrate and coating and also to impart corrosion protection[43]. Most commonly used pretreatment techniques for aerospace Al alloys is chromate conversion coatings, which offer strong corrosion resistance properties[44]. However, hexavalent chromium poses environmental hazards and thus chromate conversion coatings are excluded from MgRP coating systems, which were developed to replace all chromates in coating systems and have been proved performing effectively over sandblasting/Prekote® (nonfilm-forming, non-chrome surface pretreatment) pretreated Al / Al alloy substrates[10].

For MgRP, the electrical resistance imparted by the pretreatment should also be considered, since it might limit or delay sacrificial anode-based cathodic protection. Kannan, King, and Scully[45] compared the role of conversion coatings, anodized coatings on the performance of MgRP on AA2024-T3 to clean and desmutted surfaces and those with a Prekote pretreatment. They found that conversion coatings and anodized coatings caused delayed galvanic coupling between MgRP and AA 2024-T3 substrate. The delayed time is influenced by the thickness and chemistry of pretreatments.

More surface pretreatment methods were applied to metal surface to improve the performance of MgRP. For example, Schulz et al.[46] used a plasma polymerization method to grow thin SiC-based films on Al-2024. They found the trimethylsilane derived films showed good barrier properties and did not negate the galvanic activity of the Mg-based primer anode. Lu et al. evaluated a micro-arc oxidation treatment on the performance of MgRP on AZ91D magnesium alloy[47] and they also pretreated AZ91D magnesium alloy surface with silane pretreatment[48]. For both methods, they found the adhesive strength of the Mg-rich primer to

AZ91D alloy substrate is remarkably increased, and the failure time for the coating system is obviously prolonged after pretreatment. However, the electrical resistance imparted by the pretreatment was not investigated. They attribute the prolonged corrosion protection time to the improved barrier effect of the coating system, which impeded both the permeation of the electrolytes to the substrate and the diffusion of the corrosion products outward.

2.4. Characterization and performance of MgRP

Electrochemical techniques as well as chemical and surface analysis have been used to evaluate and study the performance of MgRPs in different environments as complements to the visual inspection and traditional coating characterization methods.

2.4.1. Weathering tests

Coating performance is significantly influenced by its service environment. That is to say, the same coating might show entirely different performance characteristics when exposed to different environments. The most reliable and easy-performed way to evaluate coating performance is to perform actual live weathering in the given climate[49, 50]. For example, AkzoNobel Aerospace Coatings and the Norwegian Air Force have been evaluating Aerodur 2100 MgRP since 2010 by painting half an F16 with Aerodur 2100 based coating system (the Aerodur 2100MgRP primer was applied over Prekote pretreatment, and was topcoated with AkzoNobel's advanced Military topcoat, Aerodur 5000). In 2012, after thorough evaluation on this flying platform as well as independent lab tests, the Royal Norwegian Air Force has decided to approve Aerodur 2100[51]. Also, US Department of Defense are testing up to 100 doors, port-hole covers, and other small parts on the exterior of aircraft coated with MgRP systems that are performing in a more than satisfactory manner in use[52,53].

While the actual live weathering test is the most accurate method, it is also the most time consuming. It may take several years or more to see the results. Many manufactures do not have several years to wait and see if a new and improved product is truly an improvement. In order to save time, accelerated weathering tests are often used for R & D, quality control and materials certification. Commonly, accelerated weathering tests are divided into two categories: outdoor / natural accelerated weathering tests and laboratory accelerated weathering tests[54, 55].

Outdoor accelerated weathering tests of MgRPs are usually conducted on sites of high known corrosion rates, such as Daytona Beach, FL[52], rain forest and marine sites in Hawaii[56], Kennedy Space Center, FL, and Charlottesville, Virginia[57,58]. At all test sites, MgRPs provided very effective and longtime protection to Al alloys. Even though outdoor accelerated weathering tests are generally agreed to be the most reliable tests in terms of correlation to the end-use service life, some variables exist that do not guarantee repeatable results, including variability due to climate, time of year, and test design[54]. Test standards such as ASTM D1014 and ASTM D 1654 could be used as guidelines for obtaining good outdoor exposure outcomes.

Because there is a need for more rapid evaluations of the resistance of materials to weathering that can be obtained by outdoor exposure tests, devices that can simulate sun exposure, humidity, heat, corrosive conditions and etc. are generally used to accelerate the degradation. Historically, ASTM B117 continuous salt spray test is one of the most popular methods for the accelerated corrosion test. Also, it is the most widely used test to rank the corrosion protection effect of coatings on steel[59]. However, during more than 100 years of use, researchers have found out that the test results of B117 do not correlate well with the corrosion results seen in actual exposures. For example, the field exposure results show that topcoated MgRPs can provide very long time protection to Al alloys. But severe early blistering has been

13

observed during ASTM B117 test[53, 60]. This field vs. lab discrepancy suggests that more realistic accelerated weathering tests need to be developed for the qualification of the corrosion protection effect of metal-rich primers. Some improved laboratory accelerated corrosion tests such as ASTM G85 Prohesion test and customized tests[61-63] have been developed. These tests introduced cyclic weathering, humidity, radiation, and temperature control to better simulate the actual environment. However, the correlation of the laboratory accelerated corrosion test results to the real service performance remains a problem[64, 65].

2.4.2. Electrochemical techniques

Open circuit potential (OCP) measurement, galvanic current measurement, and potentiodynamic scan (PDS) are intuitional and simple ways to verify the cathodic protection provided by MgRP to Al/Al alloys. These methods are usually conducted on MgRP coated samples without a topcoat, because the high resistance of topcoat might modify the measured potential and current by introducing an ohmic potential drop. It is generally agreed that the OCP of a coated Al/Al alloy system should be at least 100 mV below the OCP of the substrate to realize effective cathodic protection[66]. Measurements of the OCP of MgRP coated Al alloys have proved that MgRP can polarized Al alloys to low enough potential and thus provide effective cathodic protection[21, 22, 67]. The cathodic protection ability of MgRP has also been proved through galvanic current measurement and PDS: cathodic current flows from MgRP coated Al alloy to an identical Al alloy without primer were detected by galvanic current measurement[36, 68, 69]; while lower corrosion potential, smaller corrosion current were observed on MgRP coated Al alloys when compared to bared Al alloys in PDS[36, 70, 71]. In addition, the OCP changes of MgRP coated Al/Al alloy systems gave information of the status of the cathodic protection provided by the MgRP. For example, Nanna and Bierwagen proposed a three-period cathodic protection

mechanism provided by MgRPs through studying the OCP change of MgRP coated AA2024-T3 in 3% NaCl solution[22].

Like all the electrochemical techniques, OCP and galvanic current measurements only measure the electrochemically well connected Mg pigments. It has been noticed that Mg pigments insulated by polymer matrix still preserved in MgRP after the OCP of MgRP coated AA 2024-T3 rose above the OCP of AA2024-T3 or after the current flow from MgRP coated Al alloy to an identical Al alloy without primer became anodic[36]. That is to say, the OCP, galvanic current measurements, or probably all electrochemical tests should be used cautiously as an indication of the depletion of Mg pigment, especially for short time exposure of MgRPs. EIS has been widely used for the study and evaluation of degradation behavior of MgRPs. Useful information, such as coating barrier properties, water uptake information, and coating degradation process could be obtained from EIS results[72, 73]. The barrier properties of MgRP based coating systems have been investigated through measuring the impedance at low frequency (lower than 1Hz)[67, 74]. Generally, if the impedance is above 10^9 ohm, it means the coating can provide effective barrier protection. If the impedance is below 10^6 ohm, the barrier protection is poor. The humidity changes between topcoat and MgRP have been studied by tracking the high frequency impedance (higher than 10 kHz) change through embedded sensors[75]. Besides the barrier properties and water uptake phenomena, more information, such as double layer capacitance, electrolyte diffusion process, and charge transfer resistance was obtained from EIS measurement by fitting the data to an equivalent electrical circuit model or transmission line model[69, 76-78].

ENM is another electrochemical method that has been applied to studying the performance of MgRPs[79, 80]. Studies by Allahar et al.[79] showed that the change in the value of

noise resistance (R_n) was consistent with the changes in low frequency impedance, and the changes in the localization index (LI) supported that cathodic protection was due to a more uniform corrosion of the Mg particles, and the loss of cathodic protection resulted in a change toward a more localized corrosion. However, the trends for LI and shot noise parameter (q) were not monotonic and do not provide a simple relationship for tracking the real time loss of cathodic protection. Future work is necessary to understand and interpret the relationship between the parameters obtained from ENM and the features related to corrosion[81-83].

Traditional electrochemical techniques only give surface-averaged information on the system. The defect in a coating or the development of corrosion on a metal substrate usually occurs in a very small area. Therefore, localized techniques, such as scanning vibrating electrode technique (SVET) [67, 74, 84], scanning electrochemical microscopy (SECM) [67, 74, 84] and scanning Kelvin probe (SKP) [85] have been used to investigate the corrosion protection mechanism of MgRPs at smaller scale. It has been found that MgRPs provided cathodic protection to AA2024-T3 substrate by both preventing pit nucleation and inhibiting the growth of the pre-existing pits[84].

2.4.3. Chemical and morphology analysis

The performance of MgRPs depends critically on the severity of the environment of exposure, which affects the evolving voids in the primer, the Mg oxidation products, the migration of ions in primer film and etc. In order to better understanding the protection mechanism of MgRP, chemical and morphology analyses such as microscopy, SEM/EDX, FTIR, XRD, XPS, and Raman spectroscopy have been conducted to analyze Mg oxidation products and their distribution in MgRP. It was found that when the CO_2 concentration was low, i.e., in the salt spray chamber, Mg hydroxide was formed. When the CO_2 concentration was high, Mg carbonate was formed. Pathak et al. have suggested that the magnesium carbonate layer is thicker

and more compact than the magnesium hydroxide layer. The carbonate film inhibits both the anodic and the cathodic corrosion processes[86]. Field studies show that even though Mg is converted from the metallic state to a non-metallic compound, a system based on MgRPs still retains a high degree of corrosion resistance in long term exposure[14]. It is suggested by some researchers that besides cathodic protection, certain barrier protection developed through the precipitation of Mg oxidation products is possible[87]. Other protection mechanism such as dissolved Mg ions could also provide protection has also been proposed.

Since Al is susceptible to basic corrosion, the pH changes on Al substrate under MgRPs were investigated. Maier et al.[85] believed that cathodic corrosion of AA2024-T3 will occurs if the amount of CO_2 is not enough to buffer OH^- from magnesium corrosion products and oxygen reduction. However, Bierwagen et al.[10] have noted that the natural Mg oxidation products precipitate at pH around 10.5 and do not yield a pH high enough to corrode and dissolve Al (pH > 11).

As mentioned before, electrochemical techniques only sense the electrochemically well-connected Mg pigments. King and Scully[36] proposed two possible modes of galvanic protection: long-range protection of remote defects by well-connected Mg pigment and local or short-range protection by buried pigment particle. They developed a method based on XRD measurement for estimating the remaining capacity of MgRPs for each mode of protection.

2.5. Current development of high-performance MgRPs

The highly reactive nature of Mg and the intense galvanic action between Mg pigment and Al substrate cause rapid dissolution of Mg pigment, which reduces the time of cathodic protection. Thus, most improvements on MgRP have been focus on controlling the activity of Mg pigment, including using Mg alloys instead of pure Mg as pigment[88-90], surface pretreatment

of Mg pigment[91-93], and addition of corrosion inhibitive components into MgRP[68,94-98]. Out of the scope of controlling the activity of Mg pigment, only one research on nanostructured Mg composite coatings has been conducted[99].

2.5.1. Mg alloys as pigment in MgRP

Xu et al.[89] investigated three different Mg alloys (AM60, AZ91B, and LNR91) in pigmentary form in an epoxy-polyamide polymer system at various PVC values. Testing results showed that the primers with Mg alloys as pigments could provide cathodic protection to AA2024-T3 substrate, and pigments with smaller particle sizes and better controlled shapes would result in a better primer performance. Plagemann et al. produced zinc-magnesium pigments in different compositions and formulated them in zinc-magnesium rich coatings. A durability of more than 10,000 h in salt spray test was observed on AA 2024 unclad substrate[90]. Wang et al. found that a Mg-Al rich primer with 20% Mg and 30% Al show better protection and prolonged lifetime than a Mg-rich primer with 50% Mg. They believed the improved performance is because the addition of Al particles increased barrier property and inhibited intense galvanic coupling[88].

2.5.2. Surface pretreatment of Mg pigment

Pathak et al.[91, 93] treated magnesium powder with aqueous carbonic acid and formulated the treated magnesium powder into a Mg-rich primer. They found that the Mg-rich primer formulated with the treated Mg powder performed better in the salt-fog test than the primer based on untreated Mg powder. Wang et al.[92] formulated Mg-rich primer with magnesium powder treated with phosphoric acid. They found the phosphate layer had no negative influence on the cathodic protection of the Mg-rich primer for Al alloy but can reduce the consumption rate of Mg particles. In addition, a phosphate compound layer was formed on the surface of

substrate alloy, which decreased the corrosion rate of Al alloy. The barrier effect of the primer is improved and the lifetime is extended.

2.5.3. Addition of corrosion inhibitive components into MgRP

Zuo et al.[64, 94-96] examined the effect of 8-hydroxyquinoline (8-HQ), aluminum tri-polyphosohate (SAP), ZnO and ceria on the corrosion performance of MgRP on AZ91D magnesium alloy. Their findings suggest that by adding corrosion inhibitive components into MgRP, the cathodic protection time of an MgRP could be prolonged through one of the following effects, such as formation of an insoluble complex on Mg particles, pH buffering effect, or increasing electrical conductivity between Mg particles. The barrier property of MgRP can be improved through increase physical crosslink density of the coating matrix or formation of insoluble Mg oxidation products that can fill the voids in primer. Merten et al.[97] observed anti-corrosion and anti-blistering effects on formulations containing Li_2CO_3, $Mg(NO_3)_2$, and a low percentage of Mg metal particulates. They found that $Mg(NO_3)_2$ can reduce blistering and Li_2CO_3 can enhance defect protection through facilitating the production of $Mg(OH)_2$ and $MgCO_3$ precipitates. Visser and Hayes[99] formulated lithium salts into MgRP for anti-corrosion performance and reduced blistering. Optimal results were achieved with the use of 3-9 vol. % Li_2CO_3.

2.5.4. Nanostructured Mg composite coatings

Dennis et al.[100] found a way to synthesized Mg nanoplatelets by the solution-phase reduction of MeMgCl using lithium naphthalide in anhydrous THF. A coating consists of dispersed Mg nanoplatelets in poly(ether imide) matrix was developed for the corrosion protection of steel[99]. The use of nanostructured Mg allows for reduced coating thicknesses and a smoother surface finish. Results showed that this nanostructured Mg composite coating

19

significantly outperform galvanized Zn and Zn-rich primer coatings of comparable thickness.

2.6. Summary and future work

MgRP has been proved to be a very promising environmental friendly alternative to the hexavalent chromate based coating systems. The technology has progressed drastically since its conception. However, deeper understanding of the corrosion protection mechanism and further improvement of MgRP for better performance and wider applications are still necessary. Most of the research on understanding the corrosion protection mechanism provided by MgRP focused on the effect of Cl^- and CO_2, effects of other corrosive specials, such as NH_4^+ and SO_4^{2-} on the corrosion behavior of MgRP haven't been well discussed. Also, correlating lab and field performance of MgRP is currently difficult and the test standards used (often mis-used) for the qualification of MgRP, such as ASTM B117 have been challenged. More realistic accelerated weathering tests and qualification standards need to be developed. In addition, developing MgRP powder coat may be highly beneficial from environmental perspective. Continued progress in the field will yield MgRPs that possess better performance and wider applications.

2.7. References

1.   J.C. Williams, and E.A. Starke, Acta Mater. 51 (2003): pp. 5775–5799.

2.   A. Heinz, A Haszler, C. Keidel, S. Moldenhauer, R. Benedictus, and W.Miller, Mater. Sci. Eng. A 280 (2000): pp. 102–107.

3.   R.T. Foley, Corrosion 42 (1986): pp. 277–288.

4.   E. Musingo, Alum. Int. Today 27 (2015): p. 46.

5.   R.L. Twite, and G.P. Bierwagen, Prog. Org. Coatings 33 (1998): pp. 91–100.

6.   A.A. Mamyrbaev, T.A. Dzharkenov, Z.A. Imangazina, and U.A. Satybaldieva, Environ. Health Prev. Med. 20 (2015): pp. 159–167.

7.   K. Shekhawat, S. Chatterjee, and B. Joshi, Int. J. Adv. Res. 3 (2015): pp. 167–172.

8. "RoHS Restricted Substance" (n.d.), http://www.rohsguide.com/rohs-substances.htm (Jan. 1, 2015).

9. "Chromium Compounds Hazard Summary," United State Environmental Protection Agency (2000), http://www3.epa.gov/airtoxics/hlthef/chromium.html (Jan. 1, 2015).

10. G. Bierwagen, R. Brown, D. Battocchi, and S. Hayes, Prog. Org. Coatings 67 (2010): pp. 48–61.

11. S. Pommiers, J. Frayret, A. Castetbon, and M. Potin-Gautier, Corros. Sci. 84 (2014): pp. 135–146.

12. M.E. Nanna, and D. Bierwagen, Gordon P. Battocchi, Method of Applying a Magnesium-Containing Powder to the Surface of an Aluminum or Aluminum Alloy Substrate, No. 8,568,832. 29, 2013.

13. P. Visser, R. Waddell, and R. Walker, "Reflections," AkzoNobel Aerospace Coatings (2012).

14. W.H. Abbott, The Long Term Degradation of Paint Systems: Effects of Environmental Severity and Acceleration Factors. A Summary of 7 Year Results (Columbus, OH: In Press, n.d.).

15. K. Pianoforte, "Aerospace Coatings Market," Coatings World (2015).

16. C. Wagner, and W. Traud, Corrosion 62 (2006): pp. 844–855.

17. G.S. Frankel, "Wagner-Traud to Stern-Geart; Development of Corrosion Kinetics," in Corros. Sci. A Retrosp. Curr. Status Honor Robert P Frankenthal (Pennington, NJ.: The Electrochemical Society Inc., 2002), pp. 33–41.

18. E. McCafferty, "Kinetics of Corrosion," in Introd. to Corros. Sci. (New York, NY.: Springer, 2010), pp. 119–176.

19. C. Vargel, Corrosion of Aluminum (Elsevier, 2004).

20. J.R. Davis, Corrosion of Aluminum and Aluminum Alloys (OH: ASM International, 1999).

21. S.S. Pathak, S.K. Mendon, M.D. Blanton, and J.W. Rawlins, Metals (Basel). 2 (2012): pp. 353–376.

22. M.E. Nanna, and G.P. Bierwagen, J. Coatings Technol. Res. 1 (2004): pp. 69–80.

23. D.A. Jones, "Cathodic Protection," in Princ. Prev. Corros., 2nd ed. (NJ: Prentice-Hall Inc., 1996), pp. 439–476.

24. Z. Ahmad, "Cathodic Protection," in Princ. Corros. Eng. Corros. Control (Oxford, UK.: Butterworth-Heinemann, 2006), pp. 271–351.

25. G.P. Bierwagen, and A.M. Houvinen, "Paint Formulation," in Shrier's Corros. (Elsevier, 2010), pp. 2643–2665.

26. G.P. Bierwagen, Prog. Org. Coatings 28 (1996): pp. 43–48.

27. W.K. Asbeck, and M. Van Loo, Ind. Eng. Chem. 41 (1949): pp. 1470–1475.

28. W.K. Asbeck, J. Coatings Technol. 64 (1992): pp. 47–58.

29. G.P. Bierwagen, J. Paint Tech. 44 (1972): p. 46.

30. G.P. Bierwagen, and R.G. Mallinger, J. Coatings Technol. 54 (1982): p. 73.

31. G.P. Bierwagen, J. Coatings Technol. 64 (1992): pp. 71–75.

32. G.P. Bierwagen, and T.K. Hay, Prog. Org. Coatings 3 (1975): pp. 281–303.

33. G. Bierwagen, J. Coatings Technol. Res. 5 (2008): pp. 133–155.

34. R.S. Fishman, D. a. Kurtze, and G.P. Bierwagen, Prog. Org. Coatings 21 (1993): pp. 387–403.

35. J. Li, J. He, B.J. Chisholm, M. Stafslien, D. Battocchi, and G.P. Bierwagen, J. Coatings Technol. Res. 7 (2010): pp. 757–764.

36. A.D. King, and J.R. Scully, Corrosion 67 (2011): pp. 1–22.

37. S.R. Böhm, J. Holness, H.N. McMurray, and D.A. Worsley, "Charge Percolation and Sacrificial Protection in Zinc-Rich Organic Coatings" (London, 2000).

38. G. Bierwagen, K. Allahar, B. Hinderliter, and H. Jung, "Zn-Rich Coatings Revisited," in Tri-Service Corros. Conf. (Denver, Co., 2007).

39. V.I. Roldughin, and V. V. Vysotskii, Prog. Org. Coatings 39 (2000): pp. 81–100.

40. A.R. Marrion, "Binders for Conventional Coatings," in Chem. Phys. Coatings, 2nd ed. (Cambridge, UK.: The Royal Society of Chemistry, 2004), pp. 96–150.

41. Z.W. Wicks, F.N. Jones, S.P. Pappas, and D.A. Wicks, "What Are Coatings?," in Org. Coatings Sci. Technol., 3rd ed. (Hoboken, NJ.: John Wiley & Sons, Inc., 2007), pp. 1–6.

42. N. Ravindran, A.Z. Dipak K. Chattopadhyay, D. Battocchi, D.C. Webster, and G.P. Bierwagen, Polym. Degrad. Stab. 95 (2010): pp. 1160–1166.

43. L. Fedrizzi, H. Terryn, and A. Simoes, Innovative Pre-Treatment Techniques to Prevent Corrosion of Metallic Surface (Cambridge, UK.: Woodhead Publishing, 2007).

44. F.W. Eppensteiner, and M.R. Jenkins, Met. Finish. 100 (2002): pp. 479–491.

45. B. Kannan, A.D. King, and J.R. Scully, 71 (2015): pp. 1093–1109.

46. D.L. Schulz, R. A. Sailer, C. Braun, A. Wagner, N. Klaverkamp, K. Mattson, J. Sandstrom, D. Bunzow, S. Payne, J. He, J. Li, and B. Chisholm, Prog. Org. Coatings 63 (2008): pp. 149–154.

47. X. Lu, X. Feng, Y. Zuo, C. Zheng, S. Lu, and L. Xu, Surf. Coatings Technol. 270 (2015): pp. 227–235.

48. X. Lu, Y. Zuo, X. Zhao, and Y. Tang, Corros. Sci. 60 (2012): pp. 165–172.

49. F. Deflorian, S. Rossi, L. Fedrizzi, and C. Zanella, Prog. Org. Coatings 59 (2007): pp. 244–250.

50. F. Deflorian, S. Rossi, and M. Fedel, Corros. Sci. 50 (2008): pp. 2360–2366.

51. A. S. Richardson, "Reflections" (2010).

52. G. Bierwagen, R. Brown, D. Battocchi, and S. Hayes, "Observations on the Testing of Mg-Rich Primers for the Totally Chromate-Free Corrosion Protection of Aerospace Alloys," in Dep. Def. Corros. Conf. (Washington DC, 2009).

53. B. Abbott, CorrDefense 9 (2013): pp. 1–3.

54. L.F.E. Jacques, Prog. Polym. Sci. 25 (2000): pp. 1337–1362.

55. U. Schulz, Accelerated Testing: Nature and Artificial Weathering in the Coating Industry (Hannover, Germany: Vincentz Network, 2009).

56. S. Pathak, M. Blanton, S. Mendon, and J. Rawlins, Metals (Basel). 4 (2014): pp. 322–334.

57. A.D. King, B. Kannan, and J.R. Scully, c (2014): pp. 512–535.

58. A.D. King, B. Kannan, and J.R. Scully, 9312 (2014): pp. 536–557.

59. G.P. Bierwagen, and D.E. Tallman, Prog. Org. Coatings 41 (2001): pp. 201–216.

60. A.D. King, and J.R. Scully, "Blistering Phenomena in Early Generation Mg-Rich Primer Coatings on AA2024-T351 and the Effects of CO_2," in NACE DoD 2011 Conf. Proc. (Palm Springs, CA: DoD & NACE, 2011).

61. G.P. Bierwagen, L. He, J. Li, L. Ellingson, and D.E. Tallman, Prog. Org. Coatings 39 (2000): pp. 67–78.

62. B.S. Skerry, and C.H. Simpson, Corrosion 49 (1993): pp. 663–674.

63. E. Scrinzi, S. Rossi, and F. Deflorian, Corros. Rev. 29 (2011): pp. 275–285.

64. M.L. Tayle, M. Blanton, C. Konecki, J. Rawlins, and J.R. Scully, Corrosion 71 (2015): pp. 326–342.

65. K.R. Baldwin, and C.J.E. Smith, Aircr. Eng. Aerosp. Technol. 71 (1999): pp. 239–244.

66. G.K. Glass, Corros. Eng. (1999): pp. 286–290.

67. D. Battocchi, A.M. Simões, D.E. Tallman, and G.P. Bierwagen, Corros. Sci. 48 (2006): pp. 1292–1306.

68. X. Lu, Y. Zuo, X. Zhao, and Y. Tang, Electrochim. Acta 93 (2013): pp. 53–64.

69. X. Lu, Y. Zuo, X. Zhao, and S. Shen, 10 (2015): pp. 9586–9604.

70. D. Battocchi, A. M. Simões, D.E. Tallman, and G.P. Bierwagen, Corros. Sci. 48 (2006): pp. 2226–2240.

71. G. Bierwagen, D. Battocchi, A. Simões, A. Stamness, and D. Tallman, Prog. Org. Coatings 59 (2007): pp. 172–178.

72. G. Bierwagen, D. Tallman, J. Li, L. He, and C. Jeffcoate, Prog. Org. Coatings 46 (2003): pp. 148–157.

73. J. Li, C.S. Jeffcoate, G.P. Bierwagen, D.J. Mills, and D.E. Tallman, Corrosion 54 (1998): pp. 763–771.

74. A. Simões, D. Battocchi, D. Tallman, and G. Bierwagen, Prog. Org. Coatings 63 (2008): pp. 260–266.

75. V. Upadhyay, K.N. Allahar, and G.P. Bierwagen, Sensors Actuators B Chem. 193 (2014): pp. 522–529.

76. X. Lu, Y. Zuo, X. Zhao, Y. Tang, and X. Feng, Corros. Sci. 53 (2011): pp. 153–160.

77. K. N. Allahar, D. Battocchi, G.P. Bierwagen, and D.E. Tallman, J. Electrochem. Soc. 157 (2010): p. C95.

78. K. N. Allahar, D. Battocchi, M.E. Orazem, G.P. Bierwagen, and D.E. Tallman, J. Electrochem. Soc. 155 (2008): p. E143.

79. K. N. Allahar, D. Wang, D. Battocchi, G.P. Bierwagen, and S. Balbyshev, Corrosion 66 (2010): pp. 0750031–07500311.

80. D. Wang, D. Battocchi, K.N. Allahar, S. Balbyshev, and G.P. Bierwagen, Corros. Sci. 52 (2010): pp. 441–448.

81. G. Bierwagen, D. Tallman, and B. Skerry, "Electrochemical Noise Methods as a Possible In Situ Corrosion Sensing Technique," in Proc. 12th Int. Corros. Congr. (1993), pp. 4208–4218.

82. G.P. Bierwagen, J. Electrochem. Soc. 141 (1994): p. L155.

83. D.J. Mills, G.P. Bierwagen, D. Tallman, and B. Skerry, Mater. Perform. 34 (1995).

84. A.M. Simões, D. Battocchi, D.E. Tallman, and G.P. Bierwagen, Corros. Sci. 49 (2007): pp. 3838–3849.

85. B. Maier, and G.S. Frankel, Corrosion 67 (2011): pp. 055001–1–055001–15.

86. S.S. Pathak, M.D. Blanton, S.K. Mendon, and J.W. Rawlins, Corros. Sci. 52 (2010): pp. 1453–1463.

87. R.L. DeRosa, I. Szabo, G.P. Bierwagen, and D. Battocchi, Prog. Org. Coatings 78 (2015): pp. 455–461.

88. J. Wang, Y. Zuo, and Y. Tang, Int. J. Electrochem. Sci. 8 (2013): pp. 10190–10203.

89. H. Xu, D. Battocchi, D.E. Tallman, and G.P. Bierwagen, Corrosion 65 (2009): pp. 318–325.

90. P. Plagemann, J. Weise, and A. Zockoll, Prog. Org. Coatings 76 (2013): pp. 616–625.

91. T. Turel, S.S. Pathak, S.K. Mendon, M.D. Blanton, and J.W. Rawlins, J. Coatings Technol. Res. 10 (2012): pp. 475–483.

92. J. Wang, Y. Zuo, Y. Tang, and X. Lu, Appl. Surf. Sci. 292 (2014): pp. 93–99.

93. S. S. Pathak, M.D. Blanton, S.K. Mendon, and J.W. Rawlins, Corros. Sci. 52 (2010): pp. 3782–3792.

94. Y. Wang, X. Zhao, and X. Lu, 28 (2012): pp. 407–413.

95. S. Shen, and Y. Zuo, Corros. Sci. 87 (2014): pp. 167–178.

96. S. Shen, Y. Zuo, and X. Zhao, Corros. Sci. 76 (2013): pp. 275–283.

97. B. J. E. Merten, D. Battocchi, and G.P. Bierwagen, Prog. Org. Coatings 78 (2015): pp. 446–454.

98. P. Visser, and S.A. Hayes, Anti-Corrosive Coating Composition, US8628689 B2, 2014.

99. R.V. Dennis, L.T. Viyannalage, J.P. Aldinger, T.K. Rout, and S. Banerjee, Ind. Eng. Chem. Res. 53 (2014): pp. 18873–18883.

100. L. Viyannalage, V. Lee, R. V. Dennis, D. Kapoor, C.D. Haines, and S. Banerjee, Chem. Commun. 48 (2012): pp. 5169–5171.

CHAPTER 3. HYDROGEN EVOLUTION AND EARLY BLISTERING FROM MAGNESIUM RICH PRIMERS ON AA2024-T3[1]

3.1. Abstract

Early blistering was observed on topcoated magnesium-rich primers (MgRPs) over AA2024-T3 substrate under constant immersion or constant salt spray tests. Hydrogen evolution and the cause of early blistering were investigated in this research. Estimates are given for the first time for the amount of H_2 generated from MgRPs with and without topcoats. The measurement results along with blister formation on glass substrate, hydrogen pressure estimation, adhesion testing, and SEM images support the claim that hydrogen entrapment by topcoat, instead of Al corrosion, contributes significantly to the formation of early blistering on topcoated MgRPs. Meanwhile, simultaneous real-time hydrogen collection and open circuit potential measurement were demonstrated as a new method for studying the corrosion protection mechanism of MgRPs. Moreover, the gas generated from MgRPs was unequivocally identified as hydrogen by cyclic voltammetry scanning.

3.2. Introduction

The Mg-rich primer (MgRP) system, in analogy to Zn-rich primers for steel, was first developed by Nanna, Battocchi, and Bierwagen at North Dakota State University[1, 2]. The system is an alternative to the toxic hexavalent chromium (Cr^{6+})-based coating systems now used to provide protection for Al alloy substrates[3-6]. It is the only true Cr-free corrosion protective coating system to date that matches and/or exceeds the protection afforded by Cr^{6+} pigments[7].

Studies showed that MgRP provided more than 10,000 h of corrosion protection to Al substrate under cyclic prohesion exposure[8]. In addition, topcoated MgRPs have been found effective on field exposure at all sites where MgRPs have been studied[9, 10], and has been approved to AMS 3095 and the newly released Mil-PRF-32239 specification[11]. However, severe early blistering has been observed on topcoated MgRPs during constant immersion or ASTM B117 constant salt spray testing[8, 12-16]. This field versus lab discrepancy has hampered the acceptance of MgRPs, as blistering has consistently been interpreted as an under-film corrosion failure. For example, some researchers suggest that early blistering on topcoated MgRPs is caused by anodic undermining aided by H_2 production or cathodic corrosion of AA2024-T351 (UNS A92024).[(2),15] This interpretation may have some validity in a Cr^{6+} protection system, but not for MgRP systems, because much of the "blistering problems" have been solved by the use of inorganic and organic additives that decrease the rate of hydrogen evolution to the point that hydrogen can escape by diffusion instead of blister formation[17-18]. Some researchers have proposed that hydrogen entrapment by topcoat is the main cause for early blistering[8, 12] based on the fact that a large number of hydrogen bubbles are observed when MgRPs are exposed without topcoats under constant immersion or the ASTM B117 condition.

In this research, evidence is provided to support hydrogen entrapment as the major, if not the only, cause of early blistering on topcoated MgRPs. Also, blister formation is shown on a topcoated MgRP on glass substrate that cannot corrode. In addition, simultaneous real-time hydrogen collection and open circuit potential (OCP) measurement was used to study the corrosion protection mechanism of MgRPs. While there have been studies on the use of the H_2 measurement test on sheets of Mg, other metals, or metal alloys[19-23], this research is the first to

---

[(2)] UNS numbers are listed in *Metals and Alloys in the Unified Numbering System*, published by the Society of Automotive Engineers (SAE International) and cosponsored by ASTM International.

apply the test to MgRPs. Because the mols of Mg pigment oxidized are equal to the mols of hydrogen generated, studying H_2 evolution would be a new approach of studying the protection mechanism of MgRPs. Moreover, even though the gas generated from MgRPs is assumed to be hydrogen, no experiment has proven this assumption. In this paper, the gas was clearly identified by cyclic voltammetry scanning.

3.3. Experimental procedures

3.3.1. Materials and sample preparation

The AA2024-T3 panels used in this study were purchased from Q-Lab[†]. The chemical composition of AA2024-T3 is shown in Table 3.1 as provided by the manufacturer. The glass panels were purchased from VWR International[†]. The epoxy resin system used was a two component system (Epon 828[†] and Epikure 3164[†]) purchased from Hexion Inc. BYK 346[†], from BYK-Chemi, was used as dispersant, tert-butyl acetate (from TCI American[†]) and P-xylene (from Sunnyside Corporation[†]) were the solvents used. The Mg pigments were supplied by READE Advanced Materials[†]. The topcoat was Aerodur 5000[†] military aircraft topcoat supplied by Akzo Nobel. The concentration of all of the solutions used in this research is expressed as wt%.

The AA2024-T3 panels were blasted with Al_2O_3 grit to remove the oxide layer, grease, and oils. The panels were then rinsed with hexane until no residue was observed. The glass panels were cleaned with hexane. MgRPs were prepared by dispersing Mg pigments into the epoxy phase. The pigment volume concentration (PVC) was 40%. MgRPs were applied to AA2024-T3 panels and glass panels by air spray. MgRP coated panels were cured at room temperature for 7 d before being tested or topcoated. The thickness of the dry primer was

---

[†] Trade name.

approximately 55 µm (±10 µm) and the thickness of the topcoat was about 50 µm (±10 µm), as measured with a digital thickness gauge (Elcometer 345[†]) for AA2024-T3 panels and with a caliper for glass panels. The topcoated panels (on both AA2024-T3 and glass substrate) were scribed so electrolyte could easily penetrate MgRPs. Subsequent references to these two topcoated systems will be denoted as MgRP-Al-T and MgRP-G-T, respectively.

Table 3.1. Percent chemical composition of AA2024-T3 used as a substrate in this research

Al	Cr	Cu	Fe	Mg	Mn	Si	Ti	Zn	Others (total)
Bal.	0.1	3.8-4.9	0.5	1.2-1.8	0.3-0.9	0.5	0.15	0.25	0.15

3.3.2. H_2 identification by cyclic voltammetry measurement

The cyclic voltammetry (CV) experiments were performed in 1 wt% NaCl solution. The setup, as shown in Figure 3.1(a), was used to detect gas generated from MgRPs. A MgRP-coated AA2024-T3 panel (MgRP-Al) was clamped to a glass cell with a 12 cm^2 exposure area to generate gas. A saturated calomel electrode (SCE) was used as the reference electrode and two Pt electrodes were used as the working and counter electrode, respectively. The Pt electrodes were polished on a microcloth pad using a series of water-based alumina slurries (1 µm, 0.3 µm, and 0.05 µm). Electrochemical cleaning was performed in H_2SO_4 (0.1 M) cycling between –0.5 V_{SCE} and –1 V_{SCE}. The CV scan started after exposing MgRPs for 30 min to the 1% NaCl solution to make sure that there was enough gas to react on the Pt surface. The CV scan was performed between –0.8 V_{SCE} and 0.1 V_{SCE} at a scan rate of 100 mV/s. The oxidation/reduction peaks of pure hydrogen gas were measured in a beaker with 1% NaCl solution purged with high purity hydrogen gas (Figure 3.1b). The same experiment was conducted in a beaker with 1% NaCl solution as control.

3.3.3. Formation of blisters on glass substrate

The blister formation test was conducted by immersing MgRP-G-T in 3.5 wt% NaCl solution in a beaker. An X shaped scribe was made along the coating until the glass substrate was reached. The edges and back of the sample were sealed with tape to prevent leakage penetration of the electrolyte.
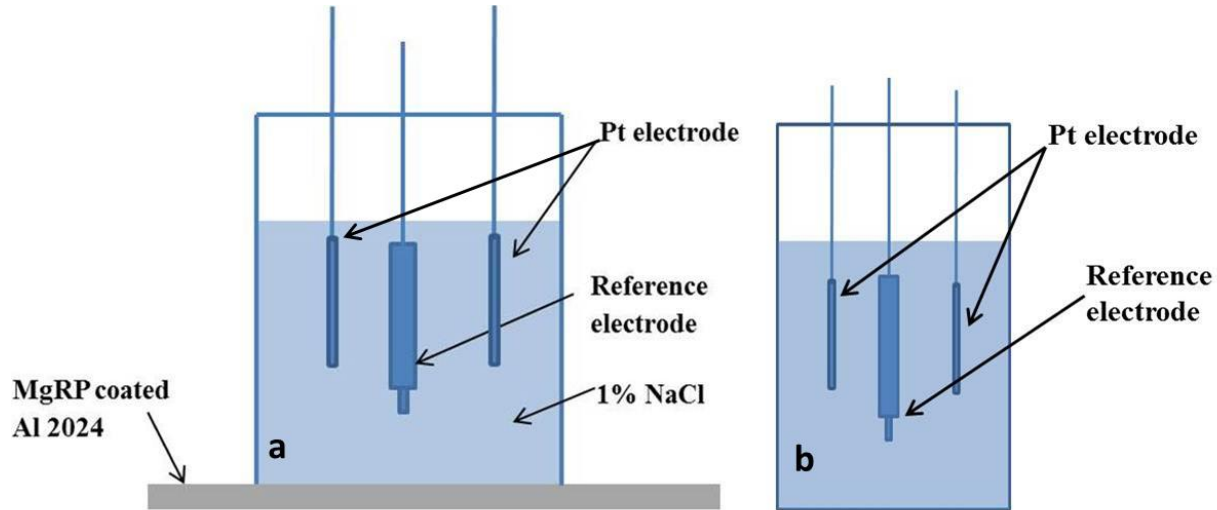
Figure 3.1. Setups of cyclic voltammetry measure, (a) over MgRP, (b) without MgRP

3.3.4. Hydrogen collection and open circuit potential measurement

A full immersion hydrogen testing assembly was modified to simultaneously measure the OCP and the volume of H_2 gas evolved on a MgRP-Al panel[22-23]. The experimental setup consisted of a glass funnel placed inside of a beaker. An inverted volumetric burette was attached to the end of a glass funnel to collect H_2 bubbles. A MgRP-Al panel was placed at the bottom of the beaker, inside the glass funnel. The exposed area of the coating was 9 cm^2. A wire was connected to the reverse side of the Al panel using conductive epoxy for OCP measurement. The edges and the back of the sample were sealed with epoxy and taped to prevent the penetration of electrolyte. SCE was used as the reference electrode. The same setup was used for the

measurement of scribed MgRP-Al-T panels. A schematic of the setup is shown in Figure 3.2. The electrolyte was saturated with H_2 gas prior to exposing the MgRP sample by cathodically polarizing the electrolyte using two Pt electrodes. The potential was set at -1.5 V_{SCE} for 6,000 s prior to any sample exposure. OCP was measured using a Gamry[†] potentiostat. The test electrolyte was 3.5 wt% NaCl. The pH of the solution was 8.5.
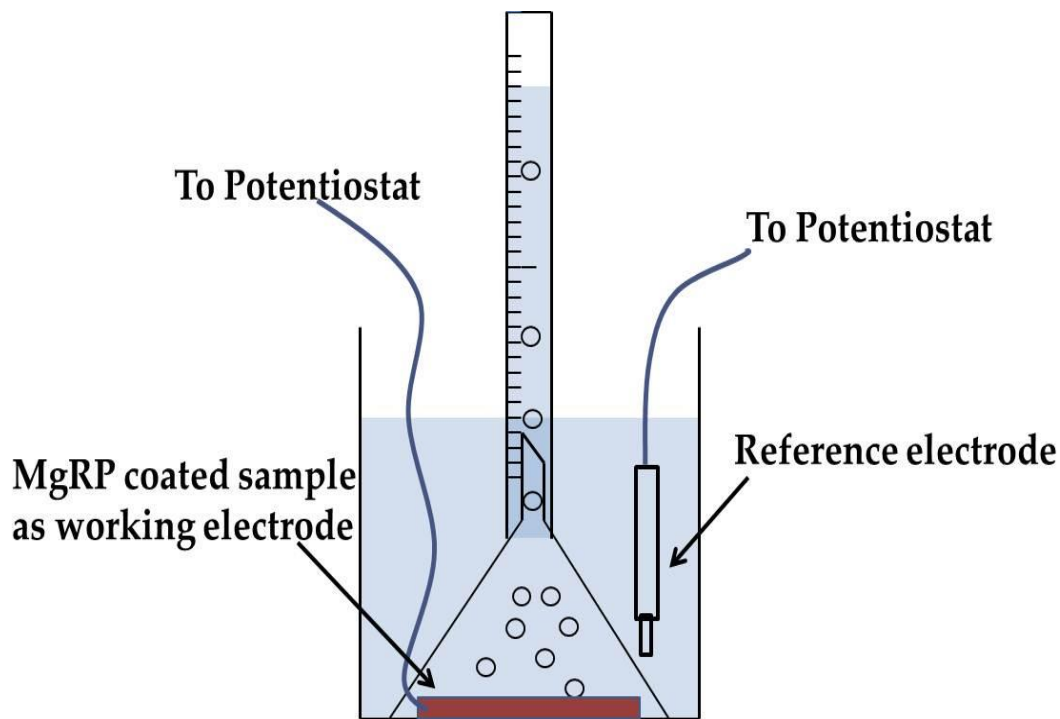
Figure 3.2. Experimental set-up to simultaneously collect evolved H2 gas and measure OCP

3.3.5. Scanning electron microscope

For scanning electron microscope (SEM) investigations, coating cross sections were prepared by ion mill using a JEOL IB09010CP[†] cross-section polisher. Then samples were mounted on aluminum mounts and coated with gold using a Hummer II[†] sputter coater. Images of the cross section of blisters were taken using a JEOL JSM-6490LV[†] SEM in back scatter mode with 15 keV acceleration voltage.

32

3.3.6. Adhesion test

Pull-off adhesion testing was conducted on MgRP-Al according to the ASTM D4541-09. Three sets of measurements were conducted. The dolly used for the test had a diameter of 14 mm and the pull off rate was 0.7 MPa/s.

3.4. Results and discussion

3.4.1. H_2 identification

Figure 3.3 shows the CV results recorded over MgRP-Al (dash line) in 1% NaCl solution, in 1% NaCl solution without MgRP (dot line), and in 1% NaCl solution without MgRP but purged with high purity hydrogen gas (solid line). When recorded in 1% NaCl solution without MgRP, the CV response shows no signal as a result of H_2. When recorded in 1% NaCl solution above MgRP-Al, a large number of bubbles were observed, indicating the evolution of gas from MgRP. The oxidation/reduction peaks of the gas generated from MgRP were at the same position as the peaks obtained from high purity hydrogen, which confirms that the gas generated from MgRP was H_2.
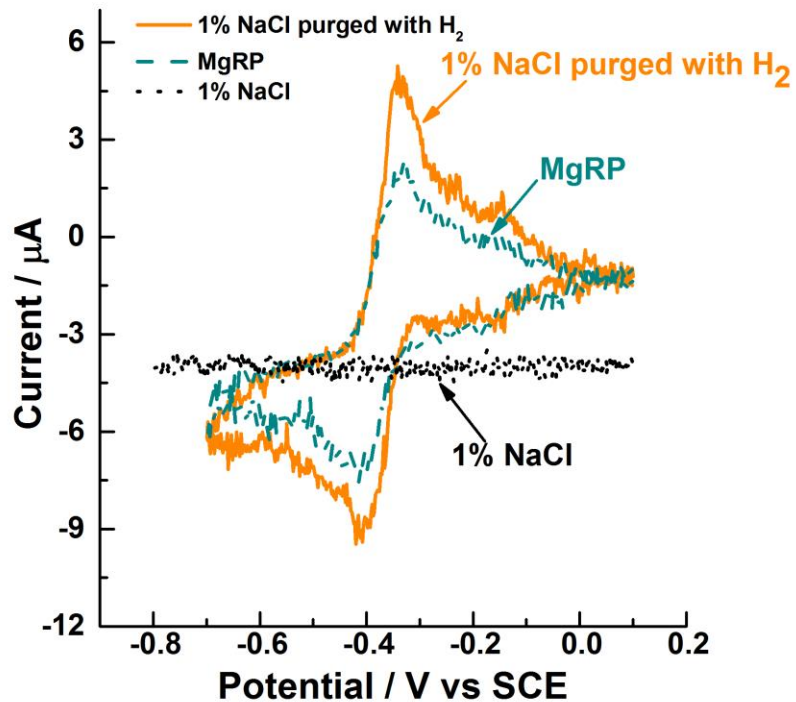
Figure 3.3. CV recorded in NaCl solution over MgRP, without MgRP, and purged with hydrogen

3.4.2. Blister formation on glass substrate

In order to totally exclude AA2024-T3 corrosion as a main cause of early blistering, immersion tests with glass substrates were conducted. The replacement of AA2024-T3 substrate does not stop the generation of H_2, but eliminates the generation of AA2024-T3 corrosion product. If entrapment of H_2, instead of corrosion of AA2024-T3, is the main cause of early blistering, then blisters should also be observed on glass substrates. As can be seen in Figure 3.4, blisters are observed on the MgRP-G-T after 3 d of constant immersion in 3.5% NaCl solution. The formation of blisters on glass substrate indicates that corrosion products of AA2024-T3 are not necessarily the cause of blistering.
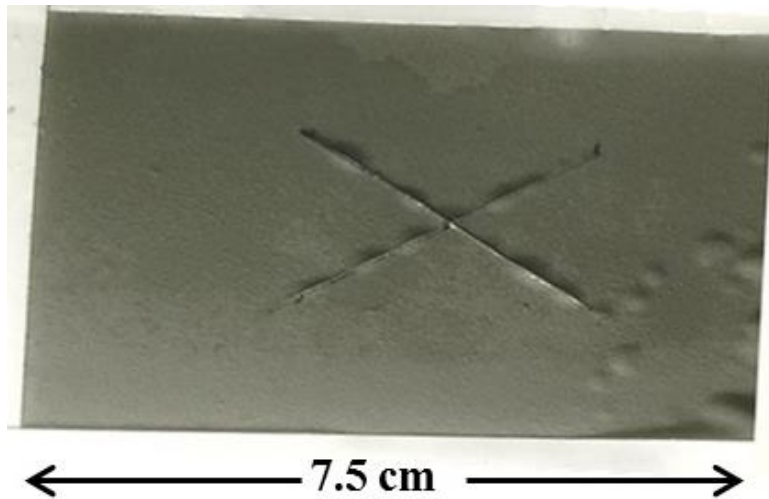
Figure 3.4. Image of topcoated MgRP on glass substrate after constant immersion

3.4.3. Hydrogen volume measurement and early blistering

Figure 3.5 shows the volume of H_2 collected as a function of time from MgRP-Al and

MgRP-Al-T in 3.5% NaCl solution. For MgRP-Al, the volume of H_2 increased rapidly in the first

24 h. Then, the rate slowed until finally reaching an asymptotic plateau after 168 h of immersion.

The amount of H_2 collected from MgRP-Al after 200 h of immersion is 10.6 mL. For MgRP-Al-

T, the volume of H_2 slowly increased and the amount of H_2 collected from MgRP-Al-T after 200

h of immersion is less than 2 mL. The volume of H_2 collected from MgRP-Al-T is much less

than those from MgRP-Al. This difference is a result of the barrier properties of topcoat, which

hinder the penetration of electrolyte, as well as the escape of hydrogen gas from coating,

permitting only slow diffusion loss of H_2 from the surface.

During the H_2 measurement test, blisters were observed near the scribe on the topcoated

MgRPs. Figure 3.6(a) shows the image of MgRP-Al-T after the H_2 measurement test. The total

area and volume of the blisters are estimated to be 0.07 cm^2 and 0.014 cm^3, respectively, by

assuming the blisters are hemispherical (detailed estimation process is provided in Appendix).

The SEM image in Figure 3.6(b) clearly illustrates the cross section of a blister. The image shows no accumulation of corrosion product inside the blister that would attribute to the formation of a blister, which again indicates that corrosion of Al is not the cause of blistering.

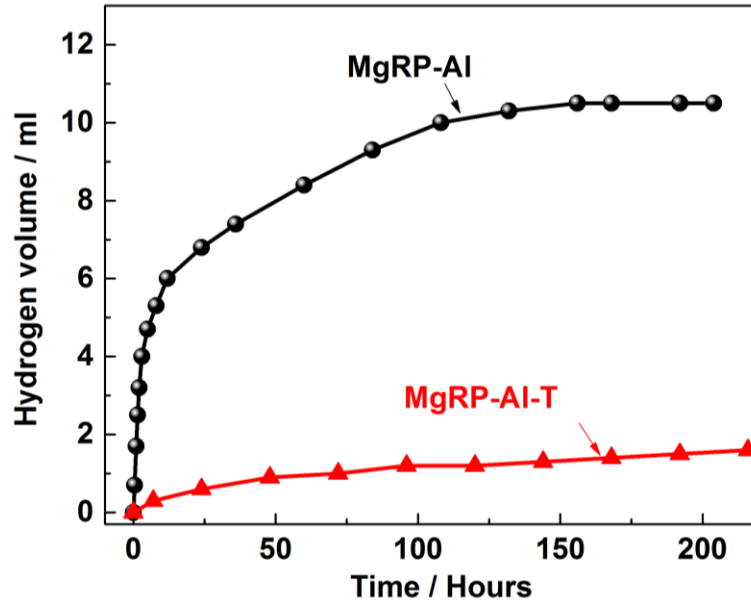Figure 3.5. Volume of hydrogen collected as a function of time in 3.5% NaCl solution: (a) MgRP-Al, (b) MgRP-Al-T
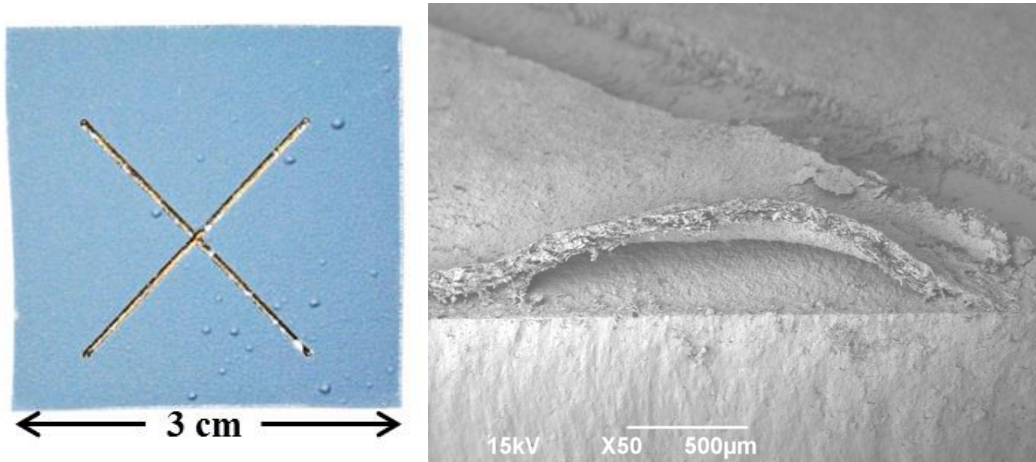
Figure 3.6. (a) Image of MgRP-Al-T after the H_2 measurement test, (b) SEM image of cross-section of blister

3.4.4. Determining the cause of early blistering

Though some researchers suggest that corrosion of Al alloy is the main cause of early blistering[15], results from this research exclude this cause. In addition, hydrogen entrapment by the topcoat (when presented) was observed during immersion test. Therefore, early blistering is believed to form when the pressure generated by trapped hydrogen exceeds the adhesion strength between coatings and substrate. The adhesion strength between MgRP and AA2024-T3 substrate was measured using the pull-off adhesion test, and the value was 8.03±0.68 MPa. Next, the amount of trapped H_2 that can cause greater pressure than the adhesion strength is estimated.

According to ideal gas law, the pressure generated by trapped H_2 can be calculated using Equation (3.1):

$$P_T = \frac{n_T RT}{V_T} \tag{3.1}$$

where P_T is the pressure produced by trapped H_2, n_T is the mols of trapped H_2, V_T is the volume that trapped H_2 occupied, R is the ideal gas constant (0.0826 L·atm/mol·K), and T is the temperature.

Before blisters formed, H_2 was trapped in voids between coatings and AA2024-T3 substrate, so V_T is a very small value. Consequently, very small amount of H_2 trapped by topcoat will result in $P_T > P_A$, and causes early blistering.

After blister formation, the volume of blisters ($V_b \approx 0.014$ cm^3) is approximately the volume of trapped H_2. Assuming the pressure generated by trapped H_2 remained the same after blisters formed and equal to the adhesion strength between MgRP and AA2024-T3 substrate, then from Equation (3.1), if the mols of trapped H_2 exceed 5.7×10^{-5} mol, then $P_T > P_A$.

From the independent hydrogen volume measurement discussed earlier and described in Figure 3.5, it was obtained that 10.6 mL of H_2 were generated from MgRP without a topcoat,

37

which equals 4.3×10^{-4} mol of H_2. Therefore, compared to non-topcoated MgRP, even if only 15% of H_2 was generated and trapped by topcoat, the pressure generated by trapped H_2 exceeds the adhesion strength between MgRP and AA2024-T3 substrate. This result was obtained by assuming $V_b \approx V_T$. In fact, before blister formation, V_T was much smaller than the volume of blisters, which means that much less H_2 trapped by topcoat will cause early blistering. In addition, the discussion earlier was based on the average value of the adhesion strength. In fact, neither the adhesion strength nor the pressure generated by trapped H_2 is homogeneous throughout the surface. In some spots, the pressure required to create a blister may be lower. Once the pressure generated by trapped H_2 was greater than the adhesion strength locally, blisters formed.

From the above estimation, it was successfully proven that the entrapment of H_2 by the topcoat is the main cause of early blistering on topcoated MgRPs on AA2024-T3 substrate. The total area and volume of the blisters were estimated, and the interior of the blisters was observed by SEM. Compared to ASTM D714-02, which only evaluates the size, frequency, shape, and pattern of distribution of blistering by visual observation, this approach of evaluating blisters is more accurate and informative. Also, these findings of the cause of early blistering suggest that more realistic accelerated weathering tests need to be developed for the qualification of the corrosion protection effect of metal-rich primers. Tests developed for steel, which assume that corrosion products are the only source of blistering, have no validity when there is another source of blistering present.

3.4.5. Hydrogen evolution rate and open circuit potential measurement

Figure 3.7(a) shows the hydrogen evolution rate derived from Figure 3.5(a) as a function of time. Four distinct stages (S_i, i = 1 to 4) are apparent in the data. The first stage (S_{1a}) is

approximately the first hour of exposure where the hydrogen evolution begins and the rate of evolution is increasing. In the second stage (S_{2a}), after initial exposure, the hydrogen evolution rate drops dramatically. The third stage (S_{3a}) is the steady decrease of the hydrogen evolution rate between 24 h and 168 h, after which the hydrogen evolution rate decreases to an asymptotic plateau.

The OCP data measured simultaneously are shown in Figure 3.7(b), which correspond very well to the earlier interpretation. In the first stage (S_{1b}), the E_{ocp} dropped from −1.0 V to −1.3 V. Then the E_{ocp} increase dramatically to −1.1 V by the end of the second stage (S_{2b}). After a steady increase of E_{ocp} in the third stage (S_{3b}), the E_{ocp} increased dramatically toward the potential of the bare AA2024-T3. As explained by Bierwagen and Battocchi[6, 24], the first stage is the "activation" period. As the electrolyte diffuses through the coating, Mg pigments start to react. Thus, the hydrogen evolution rate increased and the E_{ocp} dropped. The cathodic protection reached its peak at the end of this stage, reaching a maximum Mg-Al area ratio. Then the hydrogen evolution rate decreased and the E_{ocp} increased as a result of the consumption of Mg pigment and the build-up of Mg corrosion products. As suggested[25], there are two possible modes of protection by Mg pigments: long-range protection by well-connected Mg and local protection by isolated Mg pigments. It is quite possible that after the second stage, most of the well-connected Mg pigments have been consumed or covered with corrosion products. The gradual decrease in the hydrogen evolution rate and a steady increase of E_{ocp} observed in the third stage could be a result of continued reaction of isolated Mg pigments. Finally, after 168 h of constant immersion, the hydrogen evolution rate decreased to an asymptotic plateau, and the E_{ocp} increased dramatically toward the E_{ocp} of bare AA2024-T3, which indicated a mass loss of detectable Mg pigments and a direct path to the underlying AA2024-T3.
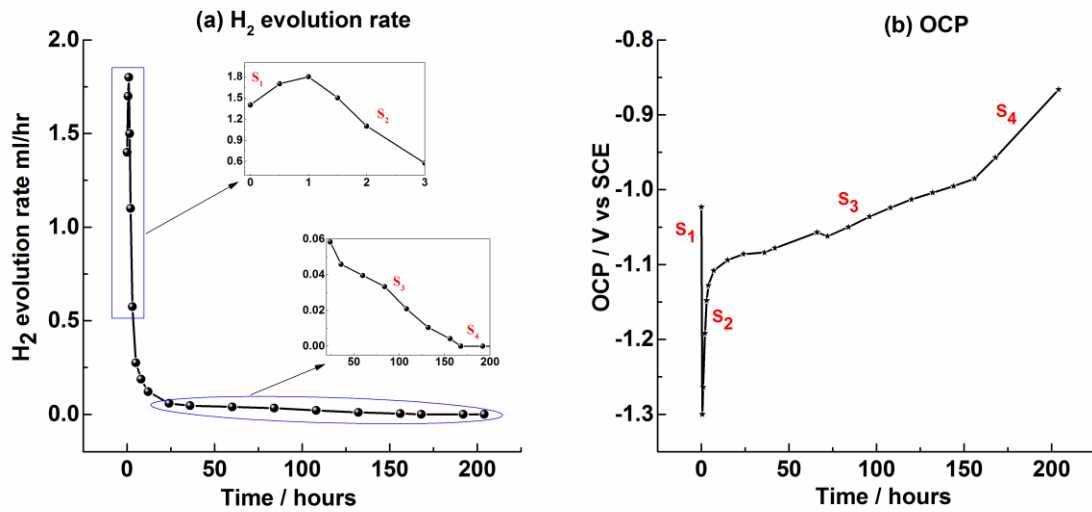
Figure 3.7. (a) Hydrogen evolution rate of MgRP-Al as a function of time in 3.5% NaCl, (b) OCP of MgRP-Al as a function of time in 3.5% NaCl solution

3.5. Conclusions

1. The gas generated from MgRPs was unequivocally identified as hydrogen by cyclic voltammetry scan.

2. Corrosion of AA2024-T3 is very unlikely to be the cause of early blistering, because (a) blisters were observed on topcoated MgRP on glass substrate (no Al present), and (b) on AA2024-T3 substrate, no Al corrosion product was observed inside the blisters. The pressure produced by trapped hydrogen was estimated and compared to adhesion strength between MgRP and AA2024-T3 substrate. The results suggest that trapped hydrogen is very likely to produce enough pressure to cause early blistering.

3. Compared to ASTM D714-02, this approach of evaluating blisters seems to be more accurate and informative. Also, the findings of the cause of early blistering suggest that a more

realistic accelerated weathering test needs to be developed for the qualification of the corrosion protection effect of metal-rich coating systems.

4. Simultaneous real-time hydrogen collection and open circuit potential measurement was demonstrated as a new approach for studying the protection mechanism of MgRPs. Hydrogen evolution rate and OCP results correspond to each other very well, which captured a four-period process: activation, long range and local protection by MgRPs, local protection by MgRPs, and mass loss of Mg pigments.

3.6. Acknowledgments

3.7. References

1.   P. Plagemann, J. Weise, A. Zockoll, Prog. Org. Coatings 76 (2013): pp. 616-625.

2.   M.E. Nanna, G.P. Bierwagen, J. Coatings Technol. Res. 1 (2004): pp. 69-80.

3.   E. Gaggelli, F. Berti, N. D'Amelio, N. Gaggelli, G. Valensin, L. Bovalini, A. Paffetti, L. Trabalzini, Environ. Health Perspect. 110 (2002): pp. 733-738.

4.   J. Sinko, Prog. Org. Coatings 42 (2001): pp. 267-282.

5.   D. Battocchi, A. M. Simões, D.E. Tallman, G.P. Bierwagen, Corros. Sci. 48 (2006): pp. 1292-1306.

6.   R.L. Twite, G.P. Bierwagen, Prog. Org. Coatings 33 (1998): pp. 91-100.

7.   P. Visser, R. Waddell, R. Walker, AkzoNobel Aerospace Coatings Reflections 13 (2012): pp.9.

8.   G. Bierwagen, R. Brown, D. Battocchi, S. Hayes, Prog. Org. Coatings 67 (2010): pp. 48-61.

9.   A.D. King, B. Kannan, J.R. Scully, Corrosion 70, 5 (2014): pp. 536-557.

10.   W.H. Abbott, The Long Term Degradation of Paint Systems: Effects of Environmental Severity and Acceleration Factors. A Summary of 7 Year Results Greyden Press (Columbus, OH: In Press).

11.   K. Pianoforte, Coatings World May (2015).

12.   S.S. Pathak, M.D. Blanton, S.K. Mendon, J.W. Rawlins, Corros. Sci. 52 (2010): pp. 1453-1463.

13.   H. Xu, D. Battocchi, D.E. Tallman, G.P. Bierwagen, Corrosion 65 (2009): pp. 318-325.

14.   G. Bierwagen, D. Battocchi, A. Simões, A. Stamness, D. Tallman, Prog. Org. Coatings 59 (2007): pp. 172-178.

15.   A.D. King, J.R. Scully, "Blistering Phenomena in Early Generation Mg-Rich Primer Coatings on AA2024-T351 and the Effects of CO_2," DoD Corrosion Conference 2011 (Houston, TX: NACE International/DoD, 2011).

16.   B. Abbott, CorrDefense 9 (2013): pp. 1-3.

17.   B.J.E. Merten, D. Battocchi, G.P. Bierwagen, Prog. Org. Coatings 78 (2015): pp. 446-454.

18.   P. Visser, S.A. Hayes, "Anti-Corrosive Coating Composition," U.S. Patent 8628689 B2, 2014.

19.   N.T. Kirkland, N. Birbilis, M.P. Staiger, Acta Biomater. 8 (2012): pp. 925-936.

20.   G. Song, A. Atrens, Adv. Eng. Mater. 5 (2003): pp. 837-858.

21.   M. Reboul, Rev. l'Aluminium (1973): pp. 399-412.

22.   G.S. Frankel, A. Samaniego, N. Birbilis, Corros. Sci. 70 (2013): pp. 104-111.

23.   A.D. King, N. Birbilis, J.R. Scully, Electrochim. Acta 121 (2014): pp. 394-406.

24.   R.L. DeRosa, I. Szabo, G.P. Bierwagen, D. Battocchi, Prog. Org. Coatings 78 (2015): pp. 455-461.

25.   A.D. King, J.R. Scully, Corrosion 67 (2011): pp. 1-22.

CHAPTER 4. DEGRADATION OF MAGNESIUM RICH PRIMERS OVER AA2024-T3 DURING CONSTANT IMMERSION IN DIFFERENT SOLUTIONS [(1)]

4.1. Abstract

Degradation of Mg-rich primer (MgRP) during constant immersion in 1 wt. % NaCl solution and in Dilute Harrison Solution was compared. The effects of different ions, Mg pigment connection modes, and cathodic reaction sites on the degradation of MgRP were discussed. In addition, an in situ method for the estimation of remaining Mg pigment content in MgRP was developed based on H_2 volume collection. The estimation confirmed that there was still Mg pigment preserved in MgRP for continued protection of Al even though the open circuit potential (OCP) of MgRP had risen above the OCP of bare AA2024-T3 substrate.

4.2. Introduction

The Mg-rich primer (MgRP) system first developed by Nanna, Battocchi and Bierwagen at North Dakota State University is an effecive Cr-free corrosion protective coating system that duplicates / exceeds the protection afforded by Cr^{6+} pigments[1-5]. The primary protection mechanism of MgRP is cathodic protection of Al substrate through sacrificial anodic reaction of Mg pigment[6-9]. Therefore, the protection efficiency of MgRP depends critically upon several factors, including the connection between Mg pigment, Al substrate and electrolyte, the corrosion behavior of Mg pigment under exposure condition, and the Mg pigment content in MgRP, etc.

[(1)] The material in this chapter was co-authored by Junren Lin, Dante Battocchi, and Gordon P. Bierwagen. Junren Lin had primary responsibility for conducting experiment, collecting and interpreting data. Junren Lin was the primary developer of the conclusions that are advanced here. Junren Lin also drafted and revised all versions of this chapter. Dante Battocchi, and Gordon P. Bierwagen served as proofreaders and checked the data obtained by Junren Lin.

Previous research on metal-rich primers[10-11] has noticed that connection between metal pigment, substrate and exposure electrolyte play an important role on the corrosion protection by metal-rich primers. For example, Morcillo, et al.[11] discussed different electronic and ionic conductive paths in zinc rich primers (ZRP). They found that the attack mechanisms for zinc particles in ZRP are different, depending on the connections between zinc paricles and steel substrate. King et al.[10] suggested two possible modes of protection in MgRP: well-connected Mg pigment provides long range protection to remote defects while Mg pigment buried in the polymer matrix might provide local or short range protection. Built on previous research, a more general and comprehensive description of the connection modes between Mg pigment, Al substrate and electrolyte is proposed in this paper. The effects of the connection modes on the corrosion protection by MgRPs are discussed. The proposed connection modes also work for other metal-rich primer systems.

The role of exposure condition in the degradation behavior of MgRP has been studied in previous research. Majority of the research has focused on the effect of Cl^- or CO_2 on the corrosion protection by MgRP[12–15]. Dilute Harrison Solution (DHS), which consists of 0.35 wt% $(NH_4)_2SO_4$ and 0.05 wt% NaCl in distilled water, has been used extensively in MgRP studies[15–17]. The incorporation of $(NH_4)_2SO_4$ is considered to better emulate atmospheric conditions often encountered by airplanes (acid rain) than NaCl along. Research on the corrosion of Mg / Mg alloys in the presence of NH_4^+ and SO_4^{2-} has found different behavious from those in NaCl solution. Battochi, et al. [16]have found for a Mg electrode smaller corrosion rates in NaCl than in DHS. Buggio et al. [18] have observed uniform corrosion and remarkable reactivity on AZ31 Mg alloy in the presence of NH_4^+. However, the effect of NH_4^+ and SO_4^{2-} on the corrosion behavior

44

of MgRP hasn't been well discussed. In this paper, degradation behaviors of MgRP during constant immersion in 1 wt. % NaCl solution and in DHS were compared.

Lifetime of an MgRP relies significantly on Mg pigment content in the primer as the metal content defines the cathodic protection. Therefore, the information of the remaining Mg pigment content in an MgRP should aid in predicting the lifetime of an MgRP in various environments. XRD has been used to quantitativly assess the amount of elemental Mg remainging in MgRPs after full immersion[10]. The result revealed that Mg pigment that was buried in polymeric matrix was preserved in MgRPs after immersion, but electrochemical methods can not sense the buried Mg pigment. Therefore, methods that are capable to predict the lifetime of MgRPs more accurately should be developed, especially methods that would allow easy, non-destructive and *in-situ* measurement.

This research compares the corrosion mechanism of Mg pigment and the degradation behaviors of MgRP in 1% NaCl solution and in DHS during constant immersion. Eventhough some evidence indicates that constant immersion produce results in disagreement with field experience, constant immersion remains a common test for the qualification of paint systems. The MgRP formula originally developed by NDSU was used in this reseach instead of a commercial product of MgRP, in order to eliminate the influence of unknown additives in commercial products. Dissolution of Mg pigment and immersion of Mg pellet electrodes were performed to assess the corrosion rate and corrosion forms of Mg pigment in DHS and 1% NaCl solution. Electrochemical measurements, scanning electron microscope analysis and hydrogen volume collection were conducted on MgRP with no topcoat in order to better observe the processes that occur in the primer when the topcoat is scratched or chinked.

45

4.3. Experimental procedures

4.3.1. Materials and sample preparation

The AA2024-T3 panels were purchased from Q-Lab[†]. The epoxy resin used in this study was a two component system (Epon 828 and Epikure 3164) purchased from Hexion Inc[†]. BYK 346 (from BYK-Chemie[†]) was used as dispersant, tert-butyl acetate (from TCI American[†]) and p-xylene (from Sunnyside Corporation[†]) were the solvents used. The Mg pigment was supplied by READE Advanced Materials[†].

The AA2024-T3 panels were blasted with Al_2O_3 grit to remove the oxide layer, grease, and oils. The panels were then rinsed with hexane until no residues were observed. Mg-rich primer (MgRP) was prepared by dispersing Mg pigment into the epoxy phase. The pigment volume concentration was 40%. MgRP was applied to Al panels by air spray. MgRP coated panels were cured at room temperature for 7 days before being tested. The thickness of the dry primer was about 70 µm (±10 µm), which was measured with a digital thickness gauge (Elcometer 345[†]).

Mg pellets were made by compressing Mg powder using an International Crystal Laboratories press[†] at 4000 psi. The pellet was then mounted inside a Tefzel flat specimen holder purchased from Princeton Applied Research[†]. The exposed area was $1cm^2$.

Two electrolytes: 1% NaCl solution and DHS were used in this research. The pH of 1% NaCl solution was 6.06±0.18 and the pH of DHS was 5.81±0.14.

[†] Trade name

4.3.2. Reaction of Mg pigment

Same amount (0.015g) of Mg pigment was added into 15 ml DHS and into 15 ml 1% NaCl solution to compare the dissolution rate of Mg pigment in these two electrolytes. The dissolution process of Mg pigment was recorded. Solution pH was measured after 15 mins of adding Mg pigment. The same experiement was repeated three times.

Immersion of Mg pellet electrode was performed to determine corrosion forms of Mg in 1% NaCl solution and in DHS. A Mg pellet electrode was immersed vertically in 50ml electrolyte and removed from the electrolyte periodically in order to collect the image of Mg pellet surface. Mg pellet surface was rinsed with deionized water and dried with air before taking an image. Solution pH was measured during the immersion test. Three replicates were performed in each electrolyte.

4.3.3. Constant immersion and electrochemical measurement

The setup of the constant immersion test was consisted of a PVC tube adhered to an MgRP coated AA2024-T3 panel. The tube was filled with electrolyte for the duration of the experiment. The exposed area of the MgRP was 12 cm^2. The electrolyte was replaced once per week. Open circuit potential (OCP) and electrochemical impedance spectroscopy (EIS) were conducted periodically during the constant immersion using a Gamry potentiostat[†]. The electrochemical measurements were performed using a three-electrode setup. The MgRP coated sample was the working electrode. A saturated calomel electrode (SCE) was used as reference electrode and a Pt mesh was used as counter electrode. A 10 mV amplitude perturbation potential with respect to the open circuit potential was used for the EIS measurement. Frequency range of 10^5 to 10^{-2} Hz was applied during measurement with an acquisition rate of 10 points per decade. Three replicates were performed in 1% NaCl solution and in DHS.

4.3.4. H_2 Volume collection

A full immersion hydrogen testing assembly[19-21] was used to measure the volume of H_2 gas generated from a MgRP coated AA2024-T3 panel. The experimental setup consisted of a glass funnel placed inside a beaker. An inverted volumetric burette was attached to the end of the glass funnel to collect H_2 bubbles. A MgRP coated Al panel was placed at the bottom of the beaker, inside the glass funnel. The exposed area of the MgRP was 9cm^2. The edges and the back of the sample were sealed with epoxy and taped to prevent the penetration of electrolyte. A schematic of the setup is shown in Figure 4.1. The electrolyte was saturated with H_2 gas prior to exposing the sample by purging with high purity H_2. Three replicates were performed in 1% NaCl solution and in DHS.
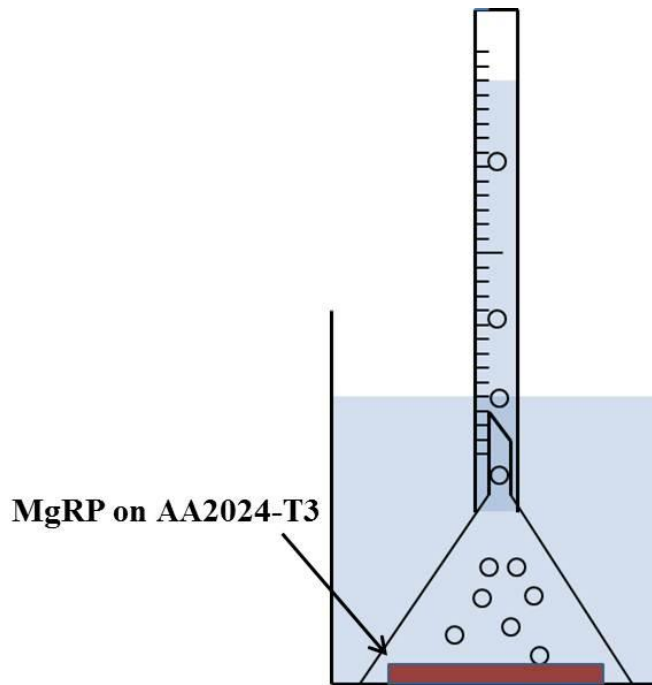

Figure 4.1. Experimental setup for H_2 volume collection

4.3.5. Scanning electron microscope

For scanning electron microscope (SEM) investigations, coating cross-sections were prepared by ion mill using a JEOL IB09010CP cross section polisher (from JEOL Ltd[†]). Then samples were mounted on aluminum mounts and coated with gold using a Hummer II sputter coater[†]. Images of the cross-section were taken using a JEOL JSM-6490LV scanning electron microscope (from JEOL Ltd) in back scattering mode with 15KeV acceleration voltage. Energy-dispersive X-ray spectroscopy (EDX) information was obtained via a Thermo NORAN EDS detector[†].

4.4. Results and discussion

4.4.1. Effect of Cl^-, NH_4^+, SO_4^{2-} on the formation of Mg corrosion products

0.015g Mg pigment was added into 15 ml DHS and into 15 ml 1% NaCl solution. The dissolution process of Mg pigment was recorded for 5 mins as a supplemental material (with 4 times the speed). Figure 4.2 shows that after 5 mins, more Mg piment remains in 1% NaCl solution than in DHS, indicating that Mg pigment dissolved slower in 1% NaCl solution than in DHS. The pH of 1% NaCl solution increased to 10.93±0.15 and the pH of DHS increased to 9.73±0.06 after 15 mins of adding Mg pigment.
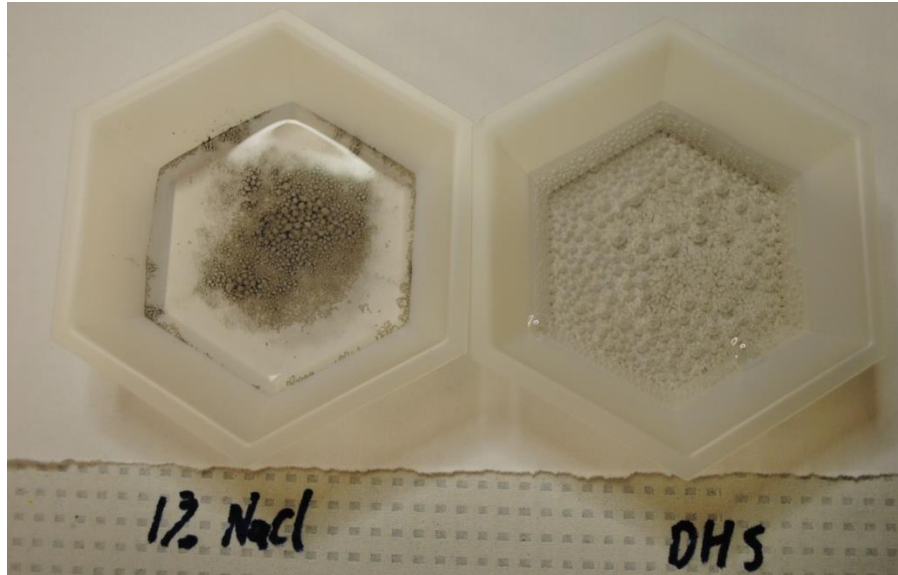
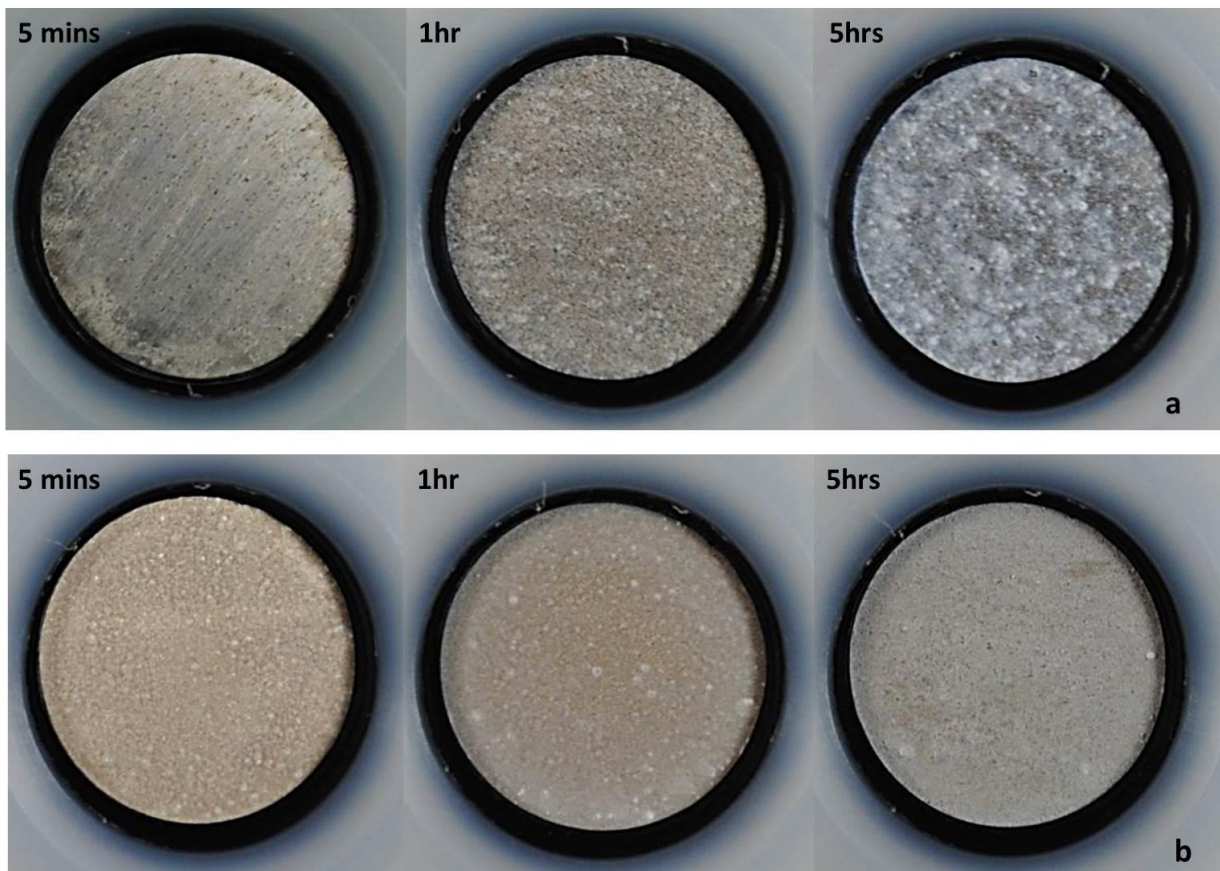Figure 4.2. Remaining Mg pigment after 5 mins adding into 1% NaCl solution and DHS

Figure 4.3. Images of the corroded Mg pellet surfaces during immersion in (a) 1% NaCl solution (b) DHS

To determine corrosion forms of Mg in 1% NaCl solution and in DHS, immersion of Mg pellet electrode was performed. Representative images of the corroded surfaces during the immersion test are showed in Figure 4.3. In 1% NaCl soultion, pits were observed on Mg pellet surface after 5 mins of immersion. With increased immersion time, oxide layer was developed on Mg pellet surface. In DHS, uniform corrosion with formation of a thin surface layer was observed. Changes of electrolyte pH during the immersion test are shown in Figure 4.4.
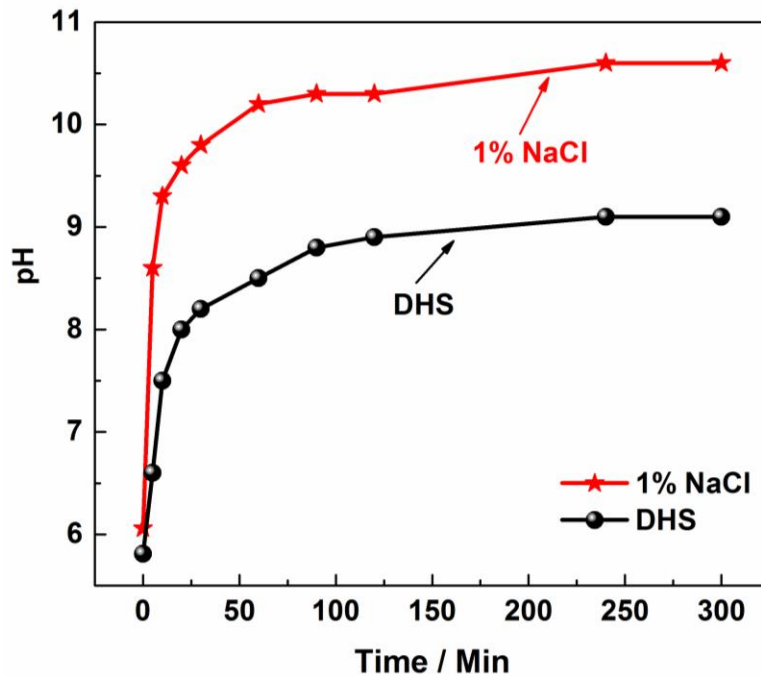
Figure 4.4. Changes of electrolyte pH during Mg pellet electrode immersion test

To interpret the different behaviors between Mg pigment in 1% NaCl solution and in DHS, the effects of different ions on the formation and dissolution of Mg corrosion products should be considered. Initially, the pH value of DHS (5.81±0.14) is slightly lower than that of 1% NaCl solution (6.06±0.18). It is known that Mg is more reactive in lower pH electrolyte. With corrosion reactions going on, the cathodic reduction of H_2O produces OH^-. It is known that

$Mg(OH)_2$ tends to precipitate and form a protective layer at high pH (~10.5)[17]. In 1% NaCl solution, accumulation of OH⁻ leaded to the increase of pH (Figure 4.4) and thus the precipitation of Mg corrosion products. Even though Cl⁻ can penetrate through the protective layer and cause pitting corrosion[22,23], the corrosion rate of Mg decreased to some extent due to the formation of the partial protective layer.

Figure 4.5. Distribution of Mg^{2+} species in (a) 1% NaCl solution and (b) DHS
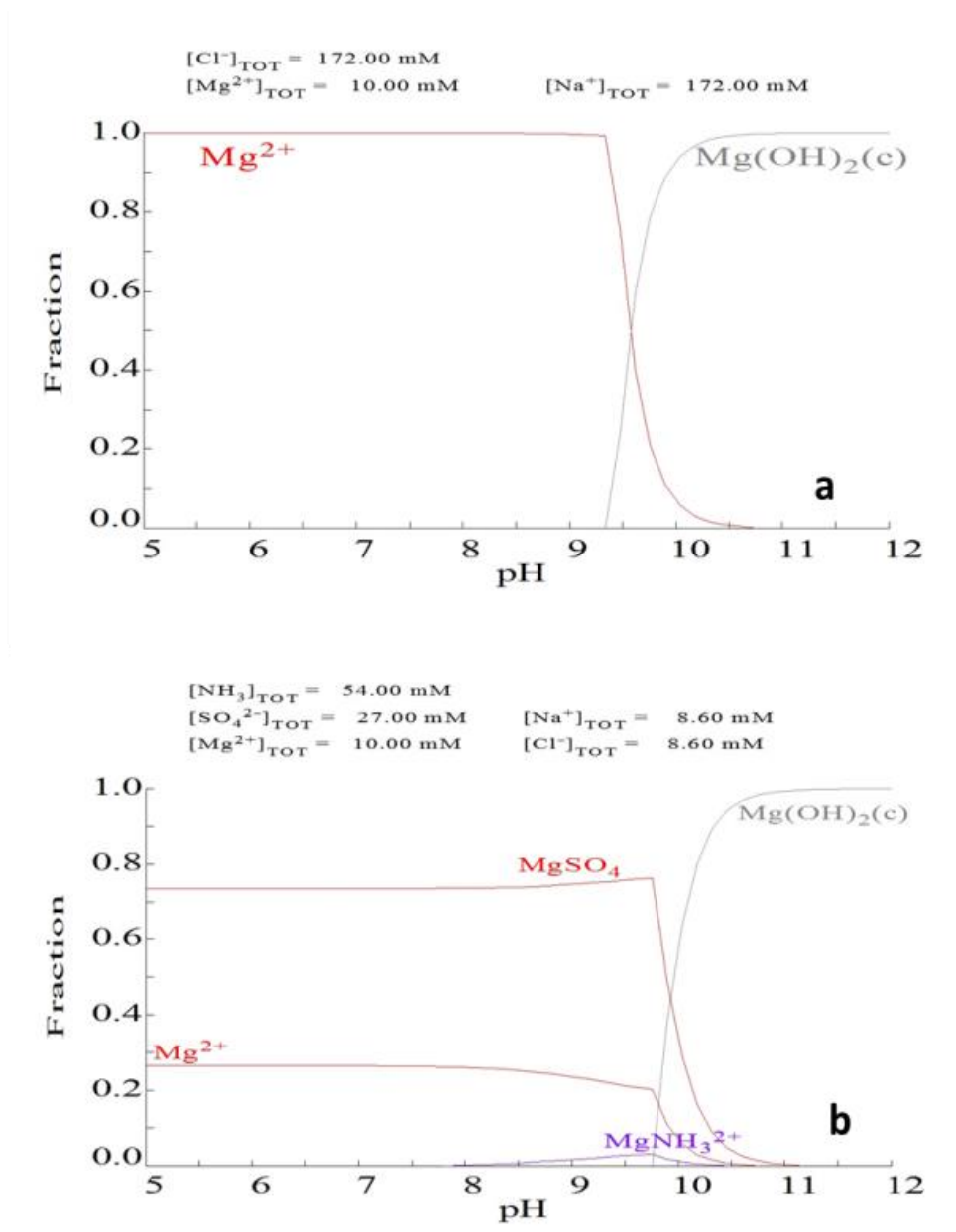
While in DHS, due to the buffering effect of NH_4^+ (Equation 4.1)[24,25], OH⁻ was consumed. Consequently, the increase of pH and the precipitation of insoluble Mg corrosion product were delayed in DHS (Figure 4.3 &4.4).

$$NH_4^+ + OH^- \rightarrow NH_3 + H_2O \tag{4.1}$$

In addition, the approximate equilibrium calculation using Hydra Medusa© software[1] shows that the onset pH for the precipitation of $Mg(OH)_2$ increases from around 9.3 in 1% NaCl solution (Figure 4.5a) to around 9.75 in DHS (Figure 4.5b), due to the formation of $MgNH_3^{2+}$ and $MgSO_4$ soluble complexes. As a result of the slower precipitation of Mg corrosion product, the corrosion rate of Mg was higher in DHS than that in 1% NaCl solution.

4.4.2. Connection modes of Mg pigment

Built on previous work, it is proposed in this section that Mg pigment exists in MgRP with one or more of the three connection modes depending on the pigment volume concentration and the coarseness of the coating[26–28], as shown in Figure 4.6: (1) Insulated Mg pigment: Mg pigment is completely embedded in polymer matrix, not connected to voids or cracks that allow access to electrolyte; (2) Isolated Mg pigment: Mg pigment is connected to voids or cracks that allow access to electrolyte, but not connected to Al substrate; and (3) Well-connected Mg pigment: Mg pigment is connected to Al substrate as well as voids or cracks that allow access to electrolyte. The modes of connection are somewhat mutable. For example, new defects occur in the polymer matrix may transform the insulated Mg pigment into isolated or well-connected pigment; and well-connected Mg pigment may transform into isolated Mg pigment due to dissolution of Mg or formation of corrosion product.

When surface pretreatment is applied to Al substrate, connection between Mg pigment and Al substrate is affected by different surface pretreatments[29]. If the resistance of the pretreatment layer is high, the observation of well-connected Mg pigment will be delayed until conductive path developed through the pretreatment layer.
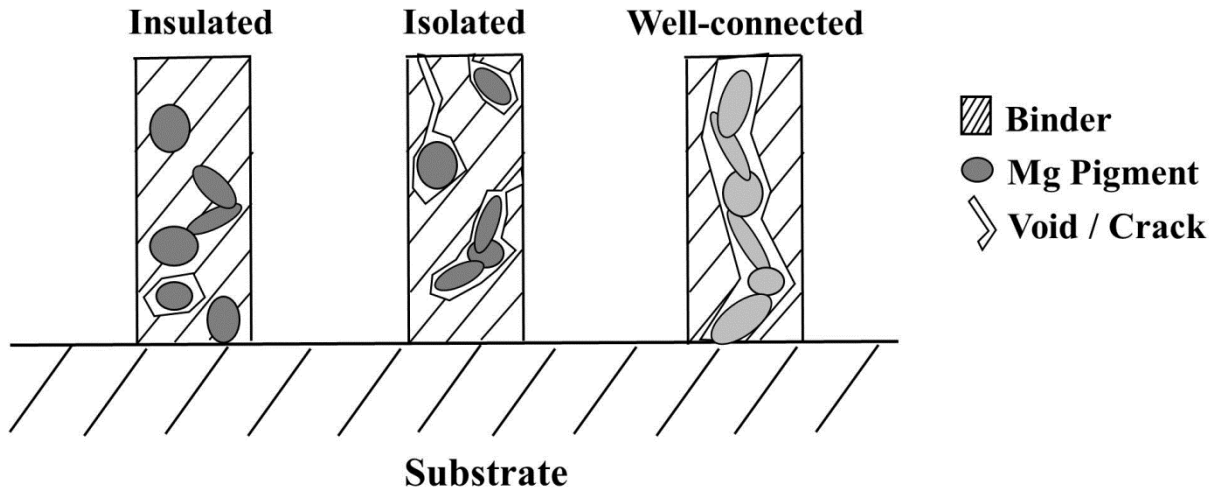
Figure 4.6. Schematic representation of connection modes of Mg pigment in MgRP

When MgRP is exposed to corrosive environment, reactions occur on both isolated and well-connected Mg pigments. No reaction occurs on insulated Mg pigment, unless it transform into isolated or well-connected pigment. While reactions happen, the well-connected Mg pigment can provide cathodic protection to Al substracte since the well-connected Mg pigment and Al substract form a galvanic couple. But isolated Mg pigment undertake self-corrosion without providing cathodic protection to Al substracte as no electronic connection between isolated Mg pigment and Al substrate. This suggests that eliminating the amount of isolated Mg pigment and balancing the ratio of insulated and well-connected Mg pigment are critial to theformulation of MgRPs with long term cathodic protection.

54

4.4.3. Cathodic reaction and microstructure of MgRP in DHS and 1% NaCl solution

4.4.3.1. SEM and EDX analysis

Scanning electron microscopy (SEM) image of Mg-rich primer prior to immersion was shown in Figure 4.7a. Energy-dispersive X-ray spectroscopy (EDX) analysis on Mg pigment (area 1) shows very low oxygen content (Table 4.1), suggesting that Mg pigment was largely unoxidized prior to immersion.

After constant immersion, MgRPs were cross-sectioned for SEM and EDX analysis. Two distinct areas (outer dark layer and inner bright area) were observed on most Mg pigment after immersion in 1% NaCl solution (Figure 4.7b). EDX results show that the outer dark area (area 2) has very high oxygen content, suggesting the formation of an oxide layer; and the inner bright area (area 3) shows similar elemental contents to the unexposed sample, suggesting unreacted Mg. These results indicate that after immersion in 1% NaCl solution, an oxide layer formed on the surface of most Mg pigment. In contrast, after immersion in DHS, MgRP shows a porous structure (Figure 4.7c). Few Mg particles are surrounded by a darker layer and EDX analysis show that remaining Mg pigment has similar elemental contents to the unexposed sample (area 4). This suggests that few Mg particles are covered by oxide layer after immersion in DHS.

(a)   (b)

(c)
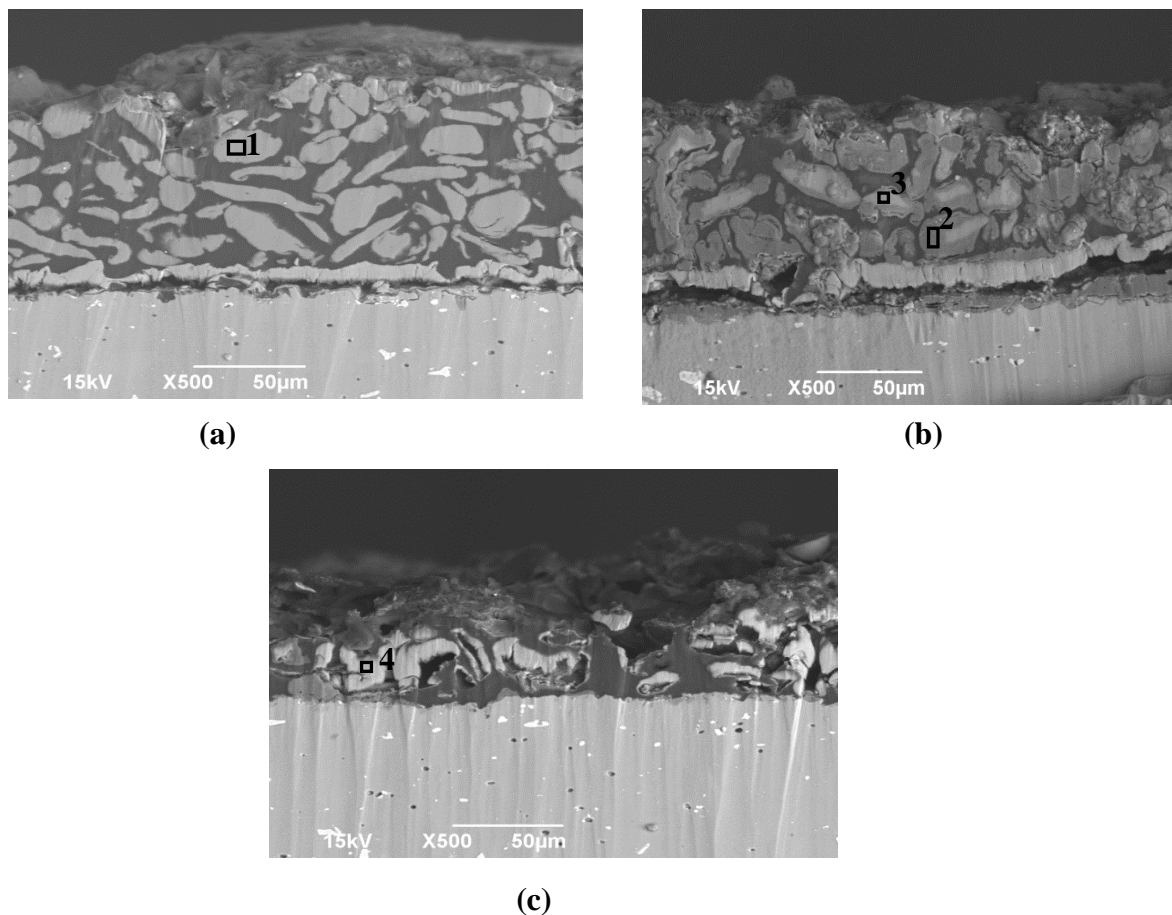
Figure 4.7. SEM images for MgRP (a) before immersion, (b) after immersion in 1% NaCl, (c) after immersion in DHS

Table 4.1. Elemental composition by EDX of Mg pigments before and after immersion

Area	Exposure condition	Elemental composition (Atom %)		
		C	O	Mg
1	Unexposed	32.25	0.21	67.54
2	After immersion in NaCl	7.94	68.72	22.48
3	After immersion in NaCl	26.11	2.15	71.74
4	After immersion in DHS	31.93	0.42	67.47

It has been discussed in previous section that the buffering effect of NH^{4+} and the formation of $MgNH_3^{2+}$ and $MgSO_4$ soluble complexes result in delayed precipitation of Mg corrosion product in DHS. In addition, the effect of cathodic reaction sites in MgRP might also

contribute to the different microstructures observed on MgRPs after immersion in DHS and 1% NaCl solution.

4.4.3.2. Effect of cathodic reaction sites on the microstructure of MgRP

Depending on whether Mg pigment is well-connected or isolated, cathodic reaction might occur in the MgRP system at different locations. When Mg pigment is isolated from AA2024-T3 substrate, both anodic and cathodic reactions occur on Mg pigment. Therefore, in both DHS and 1% NaCl solution, corrosion product (if present) will precipitate on the surface of isolated Mg pigment.

In the well-connected mode, Mg pigment and the bare zone of AA2024-T3 substrate form a galvanic couple. The cathodic reaction occurs mainly on the AA2024-T3 surface, with small portion taking place on Mg pigment. Therefore, the sites where corrosion products form depend on the relative mobility of Mg^{2+} and OH^- ions, as well as local pH value. In 1% NaCl solution, pitting corrosion occurred on Mg pigment in the primer. The pits provided sheltered areas that deterred easy mass transport between the pit interior and the exterior bulk solution. It was easier for OH^- to diffuse from AA2024-T3 surface to the pit mouth. Also, a high-pH microenvironment developed inside the pit due to the cathodic reaction that occurred on Mg pigment. Consequently, in 1% NaCl solution, corrosion products of Mg precipitated on Mg pigment, inside the pit or at the pit mouth when Mg^{2+} diffused to the exterior.

In DHS, uniform corrosion occurred on Mg pigment. There was no restriction for Mg^{2+} diffusing to the AA2024-T3 surface. In addition, higher pH value developed on AA2024-T3 surface than on Mg pigment surface due to extensive cathodic reaction on AA2024-T3 surface. Therefore, in DHS, corrosion products formed close AA2024-T3 surface

According to the discussion above, in 1% NaCl solution, most corrosion product precipitated on Mg surface no matter Mg pigment was isolated or well-connected. In DHS, few corrosion products precipitated on Mg pigment surface and lead to the porous structure of MgRP after immersion in DHS. In addition, the porous structure developed in DHS allowed more electrolyte penetrated into MgRP. Penetration of bulk electrolyte into MgRP lowers the pH value in the primer and increases ionic conductivity. As a result, Mg pigment dissolution was further accelerated in DHS.

4.4.4. H_2 volume measurement

4.4.4.1. H2 evolution from MgRPs

The volume of H_2 generated from MgRPs immersed in DHS and in 1% NaCl solution was collected for 240 hours (Figure 4.8). In DHS, the volume of H_2 increased rapidly during first 24 hours of immersion, and then increased in a very slow rate. In 1% NaCl solution, the volume of H_2 increased slower than in DHS during early stage of the test, but kept increasing steadily till the end of the test.
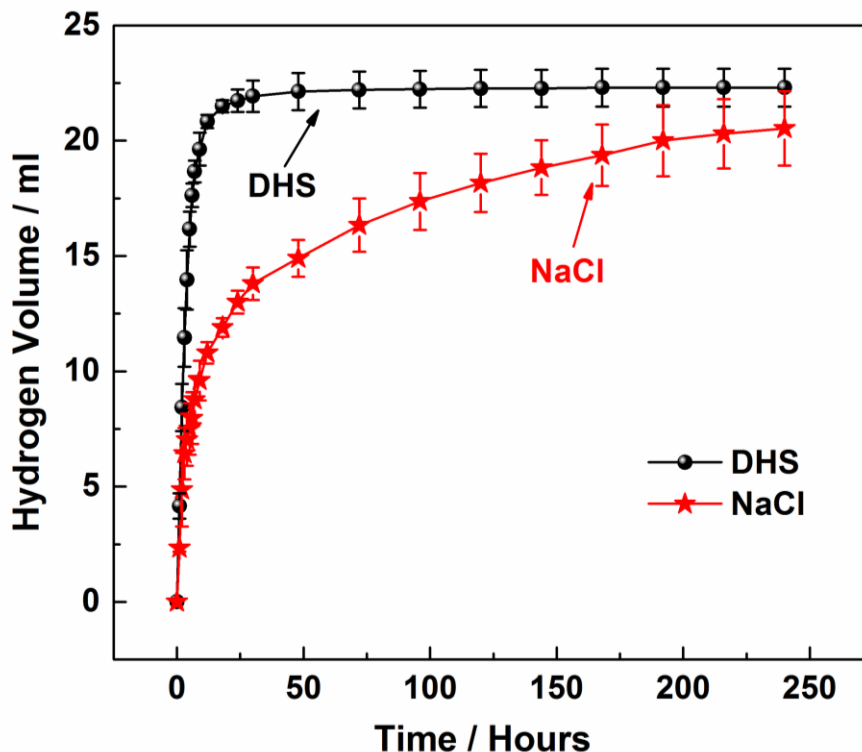
Figure 4.8. Volume of hydrogen collected as a function of time in DHS and in 1% NaCl solution

According to the corrosion reaction of Mg (Equation 4.2),

$$Mg + 2H_2O \rightarrow Mg(OH)_2 + H_2 \uparrow \tag{4.2}$$

during the degradation process of MgRP, the moles of hydrogen generated are equal to the moles of Mg pigment oxidized. Therefore, the amount and rate of H2 evolved from MgRP can be interpreted by the corrosion behavior of Mg pigment in MgRP.

H$_2$ evolution from MgRP shown in Figure 4.8 depends on both the H$_2$ generation rate and the diffusion rate of H$_2$ out of coatings. The corrosion rate of Mg in 1% NaCl solution was lower than that in DHS. That is to say, H$_2$ generation rate was lower in 1% NaCl solution than in DHS. In addition, the porous structure of MgRP after immersion in DHS allowed faster diffusion of H$_2$ out of MgRP. Consequently, higher hydrogen evolution rate was observed in DHS until the

readily exposed Mg was mostly consumed. Then due to the exhaustion of readily exposed Mg

pigment in DHS, the hydrogen evolution rate was lower in DHS than in 1% NaCl solution.

4.4.4.2. Estimation of the quantity of remaining Mg pigment in MgRP

The moles of hydrogen generated from MgRP (n_{H_2}) can be calculated using the ideal gas

law. Since the moles of hydrogen generated are equal to the moles of Mg pigment oxidized, the

moles of Mg consumed (n_{Mg}) can be obtained. By comparing the moles of Mg consumed and

the total mole of Mg in an MgRP, the remaining capacity of MgRP can be easily estimated at

any point of the H_2 volume collection as illustrated below.

The moles of Mg consumed (n_{Mg}) can be calculated using Equation 4.3:

$$n_{Mg} = n_{H_2} = \frac{pV_{H_2}}{RT}$$
(4.3)

where p is the atmosphere pressure , V_{H_2} is the volume of H_2 collected, R is the ideal gas

constant (0.0826 L·atm·mol^{-1}·K^{-1}), and T is the temperature.

Total moles of Mg in an MgRP (N_{Mg}) can be calculated using Equation 4.4:

$$N_{Mg} = \frac{Mass_{Mg}}{M_{Mg}} = \frac{PVC \times T \times A \times D_{Mg}}{M_{Mg}}$$
(4.4)

Where $Mass_{Mg}$ is the total mass of Mg pigments in a MgRP, M_{Mg} is the molar mass of Mg

(24g/mol), PVC is the pigment volume concentrate of the MgRP, T is the thickness of the MgRP

film, A is the exposed area of the MgRP, and D_{Mg} is the density of Mg pigments (1.738g/cm^3).

As an example, for the MgRPs used in this research (40% PVC, 9cm^2 exposed area and

70μm thickness), the total moles of Mg is 1.82×10^{-3} mole. After H_2 volume collection, in DHS,

where 22.5 ml of H_2 was collected, n_{Mg-DHS} =9.14×10^{-4} mole; and in 1%NaCl solution, where

21.2 ml of H_2 was collected, $n_{Mg-NaCl}$ =8.61×10^{-4} mole. So in both solutions, the amount of Mg

reacted is much less than the total amount of Mg in the MgRP, which suggests that there was Mg

pigment preserved in polymer matrix, as also observed by Scully, et al[10].

4.4.5. Electrochemical measurements on MgRPs

The open circuit potential (OCP) and electrochemical impedance spectroscopy (EIS)

measurements were taken periodically during the constant immersion. The OCP results were

shown in Figure 4.9. It is observed that the OCP of MgRP rose above the OCP of bare AA2024-

T3 after 72 hours of immersion in DHS and after 168 hours of immersion in 1% NaCl solution,

while both the SEM images and the estimation of remaining Mg pigment based on H_2 volume

collection show that there is Mg pigment remaining in MgRP even after 240 hours of constant

immersion. This confirms that OCP measurement only senses well-connected Mg pigment.

Therefore, the OCP of MgRP increases above the OCP of AA2024-T3 substrate when well-

connected Mg pigment is depleted, even though isolated and insulated Mg pigment remains in

MgRP. In DHS, as fast uniform corrosion occurred on Mg pigment and corrosion product did not

precipitate on the surface of well-connected Mg pigment, anodic reaction of Mg pigment lead to

rapid loss of electrical connection between Mg pigment and AA2024-T3 substrate. Consequently,

OCP of MgRP rose above the OCP of bare AA2024-T3 rapidly. In 1% NaCl solution, corrosion

product precipitated on the surface of well-connected Mg pigment, decreasing the electrical

connectivity between Mg pigment and AA2024-T3 substrate. However, the electrical

connectivity persisted until the oxide layer is too thick to be conductive or the depletion of well-

connected Mg pigment. Therefore, the OCP of MgRPs in 1% NaCl solution increased slower
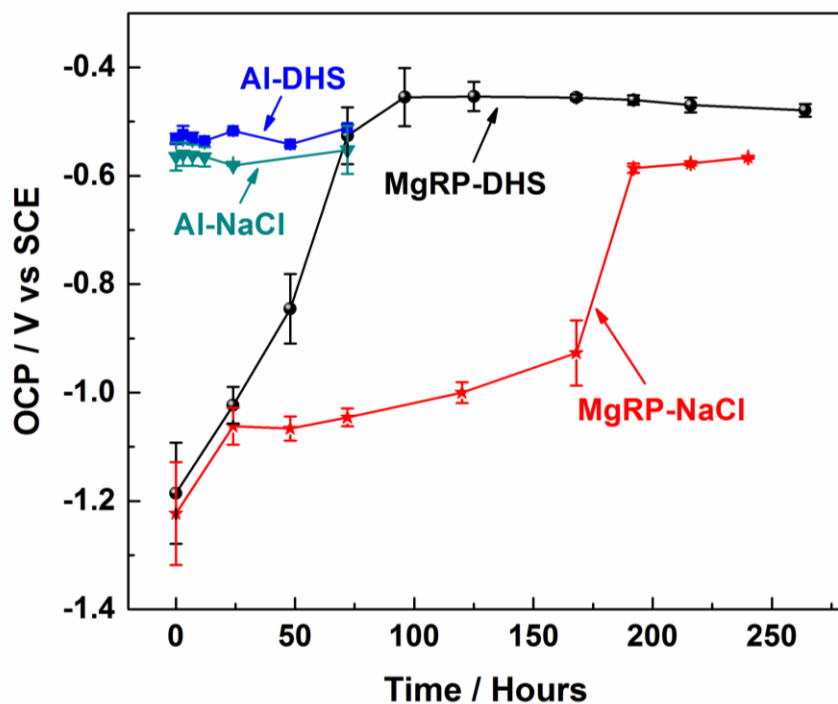
than that in DHS.

Figure 4.9. OCP of MgRP and bare Al in different solutions

The impedance measured at low frequency reflects the resistance information about the coating system, including the barrier properties of the coating film as well as the resistances occurring at the substrate/coating interface[30, 31]. Three replicates were performed in each electrolyte. The trends of the change of low frequency impedance were very similar in each electrolyte. Figure 4.10 shows the representative results of the change of the 0.01Hz impedance. The difference in the initial 0.01 Hz impedance could be attributed to the solution resistance: 1% NaCl solution has lower solution resistance resulting in lower 0.01Hz impedance. During first few hours of immersion, the 0.01Hz impedance decreased in both solutions. This stage can be described as the "activation" period, during which the electrolyte diffused through the primer and the electrochemical connection between Mg pigment and Al substrate was developed. After this period, the 0.01Hz impedance increased in both solutions, which may be due to the formation of

corrosion products/oxide layer on Mg or Al substrate surface, as well as the consumption of Mg

pigment, which increased the corrosion resistance of the primer. However, in DHS, the 0.01Hz

impedance decreased after 72 hours of immersion. While in 1% NaCl solution, the 0.01Hz

impedance kept increasing until 100 hours of immersion and then remained almost constant until

the end of the experiment. The decrease of 0.01Hz impedance in DHS after 72 hours of

immersion might be caused by the development of coating porosity due to the dissolution of

well-connected and isolated Mg pigment. The unchanged 0.01Hz impedance in 1% NaCl

solution suggests that the formation and dissolution of Mg corrosion product reached a balance
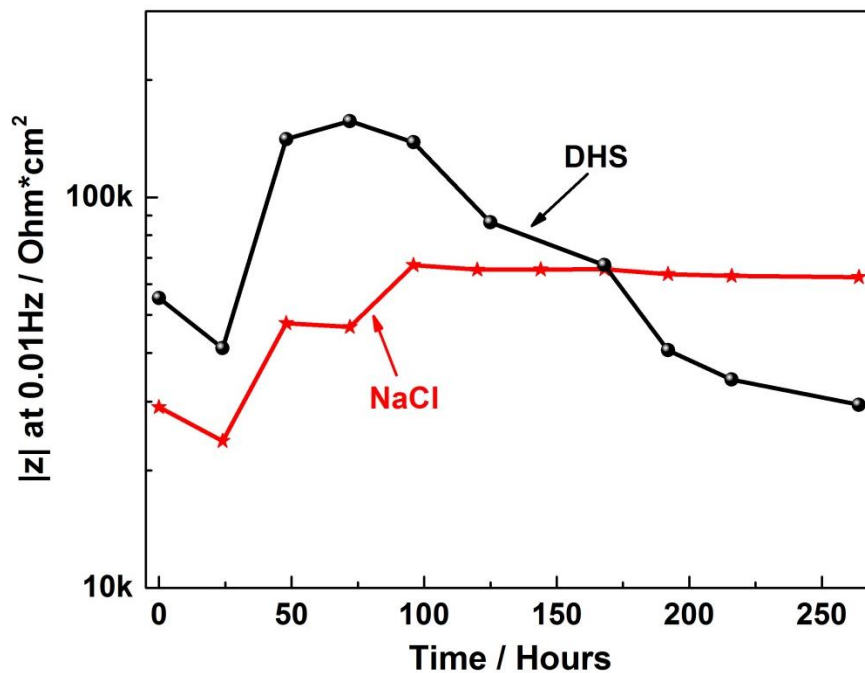
in 1% NaCl solution.

Figure 4.10. 0.01Hz impedance of MgRP during immersion in DHS and 1% NaCl solution

4.5. Conclusions

1. Corrosion of Mg in DHS and 1% NaCl solution was compared. The different corrosion

behavior in DHS when compared to 1% NaCl solution is attributed to the buffering effect of

NH_4^+ and the formation of soluble complexes, which retarded the precipitation of Mg corrosion products.

2. Readily exposed Mg pigment consumed faster in DHS than in 1% NaCl solution. MgRPs showed different microstructures after constant immersion in DHS and in 1% NaCl solution. Mg pigment connection modes and the effects of the connection modes on the corrosion protection by MgRPs were discussed. This effect along with the effect of different ions on the formation of Mg oxidation products and the effect of cathodic reaction sites in MgRP explained the different behaviors of MgRP in DHS and in 1% NaCl solution.

3. A method for the estimation of remaining Mg pigment content in MgRP was developed based on H_2 volume collection. The estimation data and the SEM analysis of MgRP confirmed that there was still Mg pigment preserved in MgRP for continued protection of Al even though the OCP of MgRP rose above the OCP of bare AA2024-T3 substrate.

4.6. Acknowledgements

4.7. References

1. G. Bierwagen, R. Brown, D. Battocchi, and S. Hayes, Prog. Org. Coatings 67 (2010): pp. 48–61.

2. M.E. Nanna, and G.P. Bierwagen, J. Coatings Technol. Res. 1 (2004): pp. 69–80.

3. K. Pianoforte, "Aerospace Coatings Market," Coatings World (2015).

4. P. Visser, R. Waddell, and R. Walker, "Reflections," AkzoNobel Aerospace Coatings (2012).

5.   W. H. Abbott, The Long Term Degradation of Paint Systems: Effects of Environmental Severity and Acceleration Factors. A Summary of 7 Year Results (Columbus, OH: In Press).

6.   D. Battocchi, A.M. Simões, D.E. Tallman, and G.P. Bierwagen, Corros. Sci. 48 (2006): pp. 1292–1306.

7.   A. M. Simões, D. Battocchi, D.E. Tallman, and G.P. Bierwagen, Corros. Sci. 49 (2007): pp. 3838–3849.

8.   G. Bierwagen, D. Battocchi, A. Simões, A. Stamness, and D. Tallman, Prog. Org. Coatings 59 (2007): pp. 172–178.

9.   S. S. Pathak, S.K. Mendon, M.D. Blanton, and J.W. Rawlins, Metals (Basel). 2 (2012): pp. 353–376.

10.   A. D. King, and J.R. Scully, Corrosion 67 (2011): pp. 1–22.

11.   M. Morcillo, R. Barajas, S. Feliu, and J.M. Bastidas, "A SEM Study on the Galvanic Protection of Zinc-Rich Paints," Journal of Materials Science (1990).

12.   A.D. King, and J.R. Scully, "Blistering Phenomena in Early Generation Mg-Rich Primer Coatings on AA2024-T351 and the Effects of CO_2," in NACE DoD 2011 Conf. Proc. (Palm Springs, CA: DoD & NACE, 2011).

13.   S.S. Pathak, M.D. Blanton, S.K. Mendon, and J.W. Rawlins, Corros. Sci. 52 (2010): pp. 1453–1463.

14.   A.D. King, B. Kannan, and J.R. Scully, Corrosion 70 (2014): pp. 512–535.

15.   B. Maier, and G.S. Frankel, Corrosion 67 (2011): pp. 055001–1–055001–15.

16.   D. Battocchi, a. M. Simões, D.E. Tallman, and G.P. Bierwagen, Corros. Sci. 48 (2006): pp. 2226–2240.

17.   R.L. DeRosa, I. Szabo, G.P. Bierwagen, and D. Battocchi, Prog. Org. Coatings 78 (2015): pp. 455–461.

18.   D. Buggio, M. Trueba, and S.P. Trasatti, Corros. Sci. (n.d.).

19.   G.S. Frankel, A. Samaniego, and N. Birbilis, Corros. Sci. 70 (2013): pp. 104–111.

20.   AD. King, N. Birbilis, and J.R. Scully, Electrochim. Acta 121 (2014): pp. 394–406.

21.   J. Lin, V. Upadhyay, X. Qi, D. Battocchi, and G.P. Bierwagen, Corrosion 72 (2016): pp. 377–383.

22.   Song, G., and A. Atrens, Adv. Eng. Mater. 5 (2003): pp. 837–858.

23.   Yang, L.J., Y.H. Wei, L.F. Hou, and D. Zhang, Corros. Sci. 52 (2010): pp. 345–351.

24.   Ogle, K., S. Morel, and D. Jacquet, J. Electrochem. Soc. 153 (2006): pp. B1–B5.

25.   Salgueiro Azevedo, M., C. Allély, K. Ogle, and P. Volovitch, Electrochim. Acta 153 (2015): pp. 159–169.

26.   Fishman, R.S., D. a. Kurtze, and G.P. Bierwagen, J. Appl. Phys. 72 (1992): pp. 3116–3124.

27.   Fishman, R.S., D. a. Kurtze, and G.P. Bierwagen, Prog. Org. Coatings 21 (1993): pp. 387–403.

28.   Fishman, R.S., E.F. Hill, T.K. Storsved, and G.P. Bierwagen, J. Appl. Phys. 79 (1996): p. 729.

29.   Kannan, B., A.D. King, and J.R. Scully, 71 (2015): pp. 1093–1109.

30.   Merten, B.J.E., D. Battocchi, and G.P. Bierwagen, Prog. Org. Coatings 78 (2015): pp. 446–454.

31.   Xu, H., D. Battocchi, D.E. Tallman, and G.P. Bierwagen, Corrosion 65 (2009): pp. 318–325.

CHAPTER 5. INHIBITORS FOR PROLONGING CORROSION PROTECTION OF MAGNESIUM RICH PRIMER ON AL ALLOY 2024-T3[1]

5.1. Abstract

This research investigated the possibility of adding inhibitors into magnesium rich primer (MgRP) to prolong the corrosion protection time of MgRP on Al alloy 2024-T3. Three inhibitors: sodium benzoate (SB), sodium dodecylbenzenesulfonate (SDBS), and 8-hydroxyquinoline (HQ), were tested and added into MgRPs separately. Potentiodynamic scans on pellet electrodes confirmed that the inhibitors reduced Mg corrosion rate. The coating systems with and without inhibitors were compared through electrochemical tests, hydrogen volume measurement, accelerated weathering tests and adhesion tests. It was observed that the addition of SB, SDBS and HQ into MgRPs could prolong cathodic protection time and improved barrier properties of MgRPs, without compromising adhesion strength.

5.2. Introduction

The Mg-rich primer (MgRP) system first developed by Nanna, Battocchi and Bierwagen at North Dakota State University is an effective Cr-free corrosion protective coating system that duplicates / exceeds the protection afforded by Cr^{6+} pigments[1-8]. The protection mechanism of MgRP is primarily cathodic protection of Al substrate through sacrificial anodic reaction of Mg pigment[9-12]. However, rapid consumption rate of Mg pigment in wet environment results in limited cathodic protection time of MgRPs, especially when a topcoat is not present[13]. One approach to prolong the cathodic protection time of MgRPs is adding corrosion inhibitive

components into MgRPs to moderate the consumption rate of Mg pigment[14–17]. For example, Yu Zuo, et al[15]. studied 8-hydroxyquinoline (HQ) added MgRP on AZ91D Mg alloy substrate and observed that HQ prolonged the cathodic protection time of the primer by forming an insoluble complex with Mg. However, these research focus on examining the inhibitor-added MgRPs on Mg alloy substrate. Research on the addition of organic inhibitors to prolong the corrosion protection of MgRPs on Al alloy substrate has not been reported.

Prior studies have shown that sodiumdodecylbenzenesulfonate (SDBS) and sodium benzoate (SB) are promising environmental friendly corrosion inhibitors for Mg, Al or their alloys by absorbing on metal surface and decelerating the metal dissolution rate [18–21]. Their effects as additives in MgRPs used on Al alloy have not been examined. In this research, SB, SDBS and HQ were added into MgRPs. The potential of these inhibitors to prolong the corrosion protection time of MgRPs on Al alloy was investigated. The inhibitor-added MgRPs were tested through hydrogen volume measurement, accelerated weathering tests, electrochemical tests and adhesion test.

5.3. Experimental procedures

5.3.1. Materials

The AA2024-T3 panels used in this study were purchased from Q-Lab†. The epoxy resin system used was a two component system (Epon 828 and Epikure 3164) purchased from Hexion Inc†. BYK 346, from BYK-Chemi†, was used as dispersant, tert-butyl acetate (from TCI American†) and p-xylene (from Sunnyside Corporation†) were the solvents used. The Mg pigments were supplied by READE Advanced Materials†. Particle size distribution of Mg pigment was measured using Accusizer 780 single particle optical particle sizing system (Figure

---

† Trade name

5.1). Sodium benzoate (SB) and 8-hydroxyquinoline (HQ) were purchased from Alfa Aesar[†], and sodium dodecylbenzenesulfonate (SDBS) was purchased from Sigma Aldrich[†]. The topcoat was Aerodur®5000 military aircraft topcoat supplied by Akzo Nobel[†].
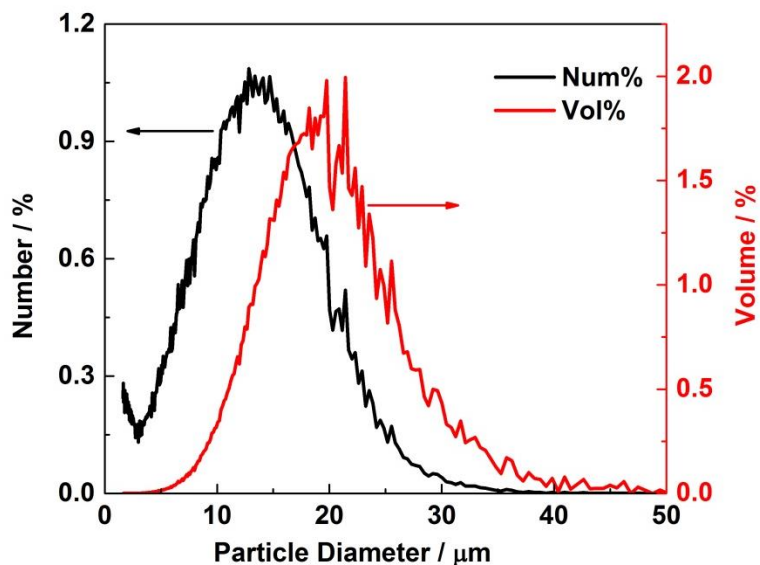

Figure 5.1. Particle size distribution of Mg pigment

5.3.2. Mg pellet electrodes preparation and testing

5.3.2.1. Mg pellet electodes preparation

Mg pellet electrodes were made by compressing Mg powder at 4000 psi using a compressor supplied by International Crystal Laboratories[†]. The pellet was then connected to an Al wire and glued onto a glass substrate as electrode. The edges of the pellet as well as the contact area between the pellet and Al wire were sealed with epoxy. The exposed pellet area for PDS measurement was $1cm^2$. Three inhibitor-added Mg pellet electrodes: Mg+HQ pellet electrode (Mg-HQ), Mg+SB pellet electrode (Mg-SB), and Mg+SDBS pellet electrode (Mg-SDBS) were prepared in the same way using Mg + 5wt.% inhibitor powder mixture. A schematic diagram of making an inhibitor-added Mg pellet electrode is shown in Figure 5.2.
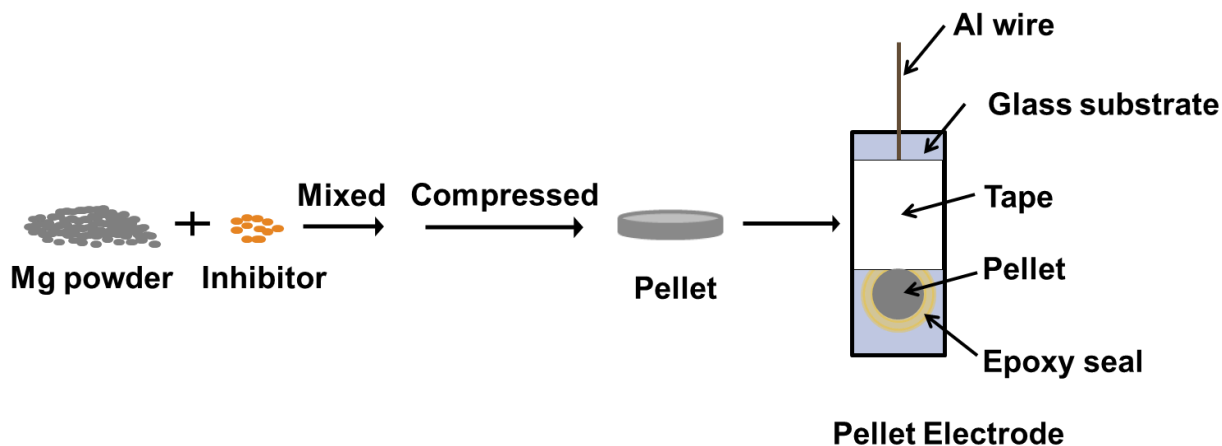
Figure 5.2. Schematic diagram of making an inhibitor-added Mg pellet electrode

5.3.2.1. Potentiodynamic scan (PDS) on Mg pellet electrodes

PDS measurement was conducted through a three-electrode setup. A Mg pellet electrode was used as the working electrode. A saturated calomel electrode (SCE) was used as the reference electrode, and a Pt mesh was used as the counter electrode. The PDS measurement started after 30 mins of immersion. The scan was set at 0.3mV/s and ranged from -1.25 V vs SCE to -0.5V vs SCE, corresponding to the mix potential range of MgRP on AA2024-T3. The same test was conducted on Mg-inhibitor electrodes for comparison.

5.3.3. Coating preparation and testings

5.3.3.1. Coatings preparation

The AA2024-T3 panels were blasted with 80μm Al2O3 grit using Econoline Mini Bench[†] to remove the oxide layer, grease, and oils. The panels were then rinsed with hexane until no residues were observed. Mg-rich primer (MgRP) was prepared by dispersing Mg pigment into the epoxy phase. The pigment volume concentration (PVC) was 40%. Three inhibitor-added primer systems were prepared: MgRP with HQ (MgRP+HQ), MgRP with SB (MgRP+SB), and MgRP with SDBS (MgRP+SDBS). Inhibitors were first mixed separately with Mg pigment, and

then dispersed uniformly into the epoxy phase. The inhibitor concentration in each inhibitor-added primer was 5wt.% based on the weight of Mg pigment. All primers were applied to AA2024-T3 panels by air spray. Primer coated panels were cured at room temperature for 7 days before being tested or topcoated. The topcoated systems are denoted as MgRP-TC, MgRP+HQ-TC, MgRP+SB-TC, and MgRP+SDBS-TC. The thickness of the dry primer was 55 ± 10 μm and the thickness of the topcoat was 50 ± 10 μm, as measured with a digital thickness gauge (Elcometer 345[†]).

5.3.3.2. Adhesion test

In order to ensure that the addition of inhibitors does not compromise the adhesion strength of the primer, pull-off adhesion testing was conducted on MgRP coated samples and compared to the samples with inhibitors. Tests were performed according to the ASTM standard D4541-09. Three sets of measurements were made. The dolly used for the test has a diameter of 14 mm and the pull-off rate was 0.7 MPa/s.

5.3.3.3. Hydrogen volume measurement

A full immersion hydrogen testing assembly was used to measure the volume of H_2 gas generated from MgRP coated aluminum panel[22-24]. The experimental setup (Figure 5. 3) consisted of a glass funnel placed inside a beaker. An inverted volumetric burette was attached to the end of glass funnel to collect H_2 bubbles. A primer coated Al panel was placed at the botton of the beaker, inside the glass funnel. The exposed area of the coating was 9cm^2. The edges and the back of the sample were sealed with epoxy and taped to prevent the penetration of electrolyte. The electrolyte was saturated with H_2 gas prior to exposing the sample by purging the electrolyte with high purity H_2 gas. The test electrolyte was Dilute Harrison's Solution (DHS), which consists of 0.05wt.% NaCl and 0.35wt.% $(NH_4)_2SO_4$. The pH of the DHS was 5.9.
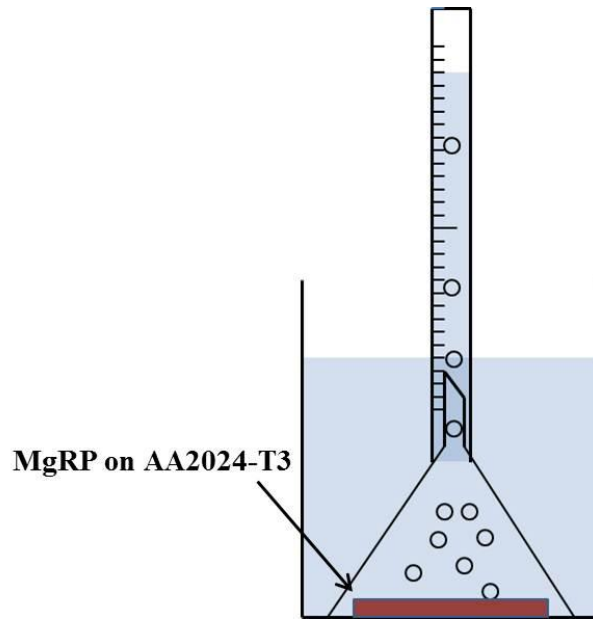
Figure 5.3. Hydrogen collection setup

5.3.3.4. Accelerated weathering test

To compare the performance of MgRP and the inhibitor-added MgRPs under aggressive environment, both primer coated AA2024-T3 samples and primer+topcoated samples were exposed to Prohesion® (ASTM G85-11) weathering. The Prohesion® exposure is cyclic, alternating between one hour of salt fog (DHS) at 25°C and one hour of bake-off at 35°C. The back and the edges of the panels were covered with tape. An X shape scribe was made on topcoated samples until the AA2024-T3 substrate was reached. The primer coated samples were removed from the tester periodically for visual analysis and EIS test. The topcoated samples were removed from the tester periodically for visual inspection. All panels were removed at the end of fog cycle. At least 3 panels were tested for each sample.

5.3.3.5. Electrochemical impedance spectroscopy (EIS)

EIS tests were conducted on primer coated samples before and during Prohesion® exposure. Tests were carried out through a three-electrode setup. A primer coated sample was clamped to a glass cell with a 7.06 cm^2 exposure area and used as the working electrode. A saturated calomel electrode (SCE) was used as the reference electrode, and a Pt mesh was used as the counter electrode. EIS data collection started after 30 mins adding the electrolyte (DHS) to the glass cell. OCP was measured prior to EIS tests. The frequency range of EIS tests is from 10^5 Hz to 0.01Hz with an acquisition rate of 10 points per decade. The amplitude of alternating current (AC) voltage perturbation was ±10 mV with respect to the OCP. All the electrochemical tests were conducted using a Gamry potentiostat[†].

5.4. Results and discussion

5.4.1. Potentiodynamic scans on Mg pellect electrodes

To examine the inhibition effect of sodium benzoate (SB), sodium dodecyl-benzenesulfonate (SDBS), and 8-hydroxyquinoline (HQ) on Mg, potentiodynamic scans (PDS) were conducted on pellet electrodes in DHS (Figure 5.4). The currents obtained from inhibitor-added Mg pellet electrodes were lower than that from Mg pellet electrode, indicating decreased Mg corrosion rate with the presence of inhibitors. In addition, current oscillations are observed from Mg-inhibitor pellet electrodes, which may be due to metastable pitting on Mg surface.

Moreover, among the three inhibitors, HQ shows highest inhibition efficiency. For Mg-SB and Mg-SDBS pellet electrodes, initially, the currents were only slightly lower than that from Mg pellet electrode. With increased polarization potential, a dramatically decrease of current was observed from both Mg-SB and Mg-SDBS electrodes. This might be due to increased absorption efficiency of inhibitive anions on Mg surface with potential[25].
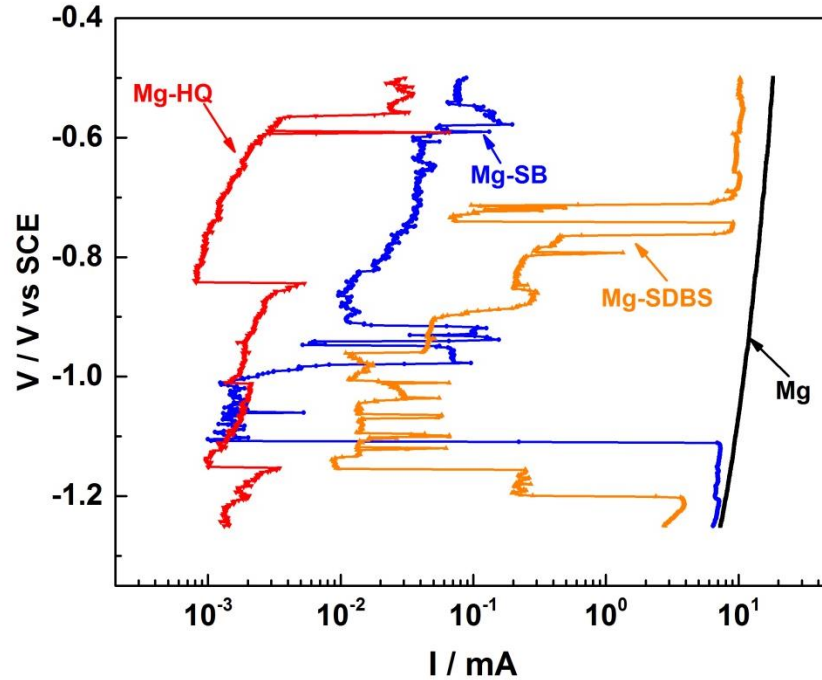
73

Figure 5.4. Polarization behavior of Mg pellet electrodes with and without inhibitors exposed in DHS

5.4.2. Adhesion test

One of the most important properties in corrosion protective coatings is the coating adhesion to the substrate. Thus, pull-off adhesion test was conducted in this research to evaluate if adding inhibitor affected the adhesion strength between MgRP and AA2024-T3 substrate (Figure 5.5). The results show no significant difference in the adhesion strength between MgRPs with and without inhibitors, which suggest the inhibitors do not compromise the adhesion strength of MgRPs.
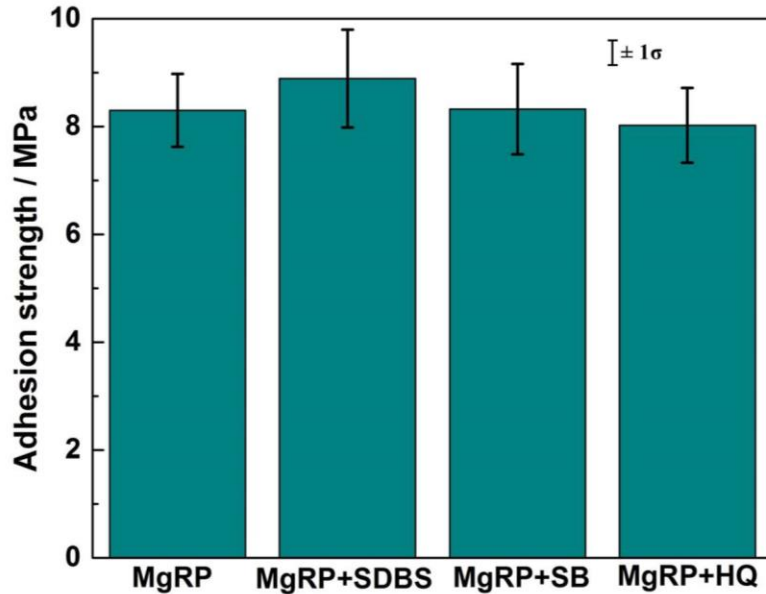
Figure 5.5. Adhesion strength of MgRP with and without inhibitors

5.4.3. Open circuit potential (OCP)

OCP of MgRPs with and without inhibitors were collected after exposure to DHS for 30 mins (Table 5.1). The results show that adding HQ into MgRPs slightly increased the OCP of MgRPs, while adding SB and SDBS into MgRPs decreased the OCP of MgRPs. The change of OCP can be explained by considering the ionic conductivity and inhibition efficiency of the inhibitors. It's reported that HQ is a mixed-type inhibitor and can instantaneously form stable complexes with Mg[18,26]. The complexes layer increased the resistivity between Mg pigment and Al alloy substrate, and therefore increased the OCP as the galvanic couple potential is affected by the resistivity of the system. In contrast, adding SB and SDBS into primers decreased the resistivity through the primers as the two inhibitors are ionic compounds. Even though SB and SDBS are reported as anodic and mixed-type inhibitors for Mg alloy respectively[20], according to PDS results, the inhibition efficiency of SB and SDBS on Mg is low around OCP. Therefore, the

increase of OCP due to absorption is not enough to offset the decreased resistivity through the primers, so the OCP of MgRP+SB and MgRP+SDBS decreased.

Table 5.1. OCP of MgRPs with and without inhibitors after 30 mins immersion in DHS

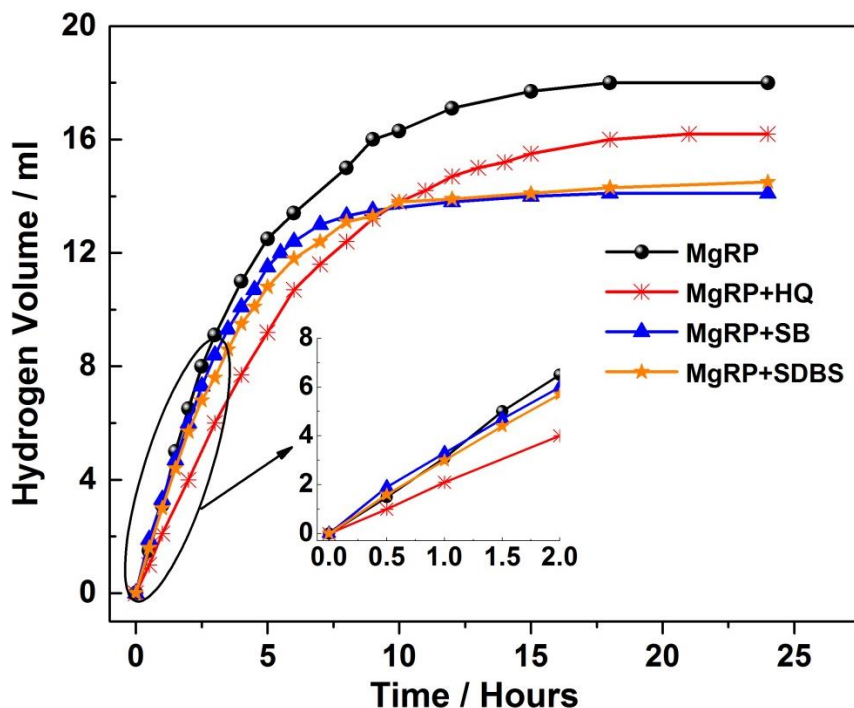|	MgRP	MgRP+HQ	MgRP+SB	MgRP+SDBS
OCP (V vs. SCE)	-1.065±0.029	-1.035±0.031	-1.253±0.012	-1.226±0.015

5.4.4. Hydrogen volume measurement

Figure 5.6. H_2 volume vs. time from MgRPs with and without inhibitors after immersed in DHS

H_2 generated from MgRP with and without inhibitors was collected for 24 hours while immersing in DHS (Figure 5.6). Since the moles of H_2 generated from MgRP is equal to the moles of Mg consumed, H_2 volume measures the amount of Mg pigment consumed in primer. The total moles of Mg pigment in the primer and the amount of Mg reacted in MgRPs with and without inhibitors are estimated and listed in Table 5.2. The results show that the addition of inhibitors into MgRPs reduced the consumption of Mg pigment. That is, more Mg pigment was

76

preserved in inhibitor-added MgRPs, extending the corrosion protection of Al substrate beyond

MgRP without inhibitors.

Table 5.2. Total moles of Mg pigment in the primer and the moles of Mg pigment consumed in MgRPs with and without inhibitors

Total moles of Mg in MgRPs (10^{-3} mole)	Moles of Mg consumed (10^{-3} mole)			
	MgRP	MgRP+HQ	MgRP+SB	MgRP+SDBS
1.433	0.731	0.658	0.573	0.589

In addition, it is observed that, initially, more H_2 was generated from MgRP+SB and

MgRP+SDBS than from MgRP. After 1 hour of immersion, the amount of H_2 generated from

MgRP+SDBS and MgRP+SB became less than that from MgRP. For MgRP+HQ, the amount of

H_2 generated was less than that from MgRP during the immersion. This difference in the H_2

generation behaviors can also be explained by considering the ionic conductivity and inhibition

efficiency of the inhibitors.

For MgRP+HQ, due to the high corrosion inhibition efficiency and the low ionic

conductivity of HQ, the decreased Mg corrosion rate outweighed the effect of increased ionic

conductivity. Therefore, the amount of H_2 generated from MgRP+HQ was less than that from

MgRP during the immersion.

For MgRP+SB and MgRP+SDBS, initially, around the OCP of the primers, the inhibition

efficiency of SB and SDBS is low. Thus, the decreased Mg corrosion rate is not enough to offset

the effect of increased ionic conductivity. Consequently, more hydrogen was generated from

MgRP+SB and MgRP+SDBS. After 1 hour of immersion, due to the consumption of Mg

pigment, potential of the primers increased, which resulted in the increased inhibition efficiency

of SB and SDBS. Therefore, the Mg corrosion rate in MgRP+SB and MgRP+SDBS dramatically decreased, resulting in less H_2 generated from MgRP+SB and MgRP+SDBS than from MgRP.

5.4.5. Visual Inspection (primer only)

H_2 volume collection was conducted for a short period of time, so it only evaluated the consumption behavior of readily exposed Mg pigment. To compare the long term performance of MgRP with and without inhibitors, primer coated samples were exposed to Prohesion® chamber for visual and EIS measurements.

The images of primer coated samples before and after accelerated weathering test are shown in Figure 5.7. After 2000 hours of exposure, white corrosion products were observed on all exposed samples, but with different extend. MgRP coated sample has completely deteriorated. MgRP had peeled off from the Al substrate, and severe corrosion of Al was observed. For inhibitor-added MgRPs, primers still adhered well to Al substrate. However, white corrosion products were observed on a large area of MgRP+HQ surface. For MgRP+SB and MgRP+SDBS coated samples, only scattered corrosion products were observed on the primer surface. It is hard to tell from the visual inspection that the corrosion products are due to the corrosion of Mg pigment, Al alloy substrate or both. Further research will be conducted to identify the corrosion products. The circular areas observed on exposed samples might be due to intermediate EIS measurements.
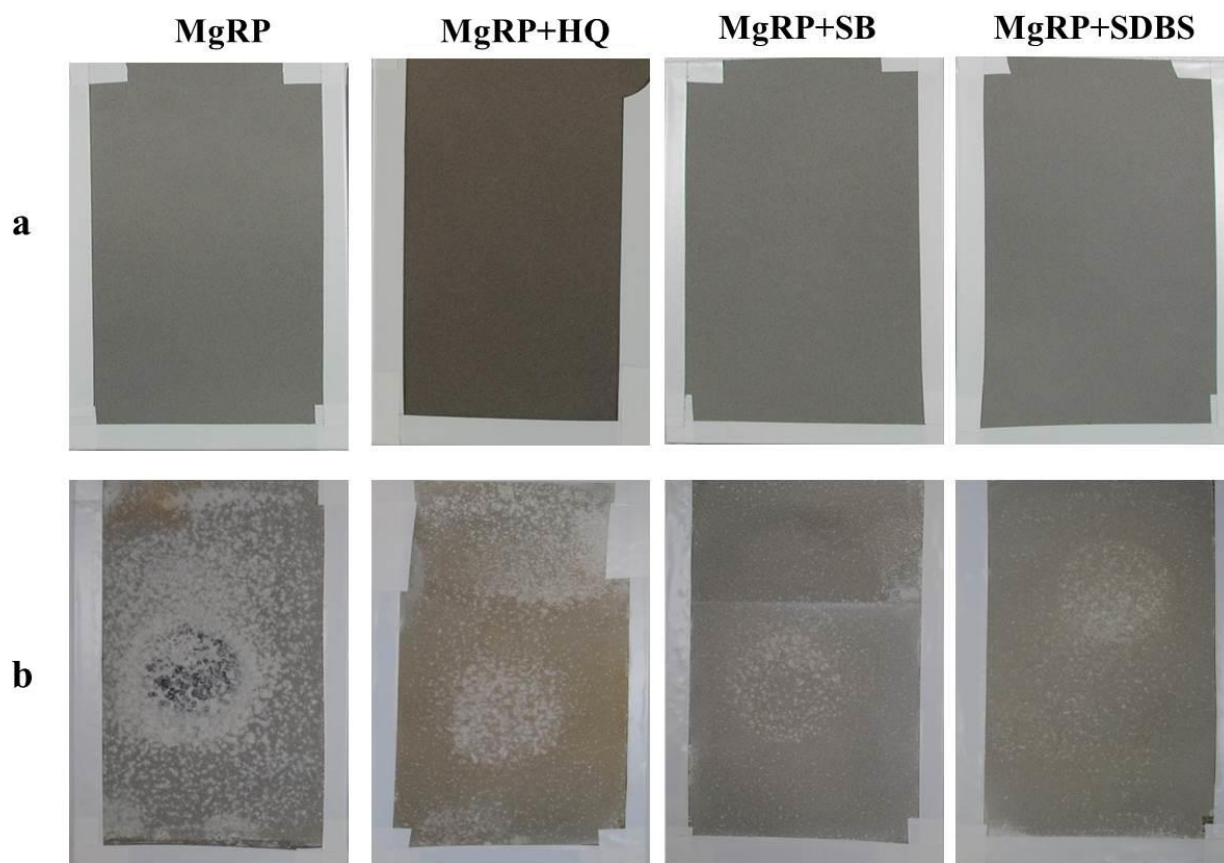
Figure 5.7. Images of MgRPs with and without inhibitors (a) before exposure, (b) after 2000hrs of exposure in Prohesion® chamber

5.4.6. Electrochemical impedance spectroscopy (EIS)

Low frequency (0.01Hz) EIS data were collected on primer coated samples before and during the Prohesion® test to evaluate primer barrier properties [13,27–29](Figure 5.8). Before exposure, the impedance of MgRP+SB and MgRP+SDBS is lower than that of MgRP. This result is expected since SB and SDBS are ionic compounds, which increase the conductivity of the primer. During exposure, the changes of the impedance are characterized by three distinct periods. First, the primers experienced an increase in impedance during the first 240 hours of exposure. This increased impedance can be attributed to the formation of oxide layers on Mg or

Al alloy surface as well as the deposition of Mg corrosion products within primer pores. During this period, the impedance of inhibitor-added MgRPs became greater than that of MgRP, which seems to indicate that the inhibitors helped to form denser oxide layers and corrosion products. During the second period, the impedance values slightly decreased for all samples. This decreased impedance may be due to the dissolution of Mg corrosion products and / or depletion of Mg pigment, which created voids in primers. This period lasted longer for inhibitor-added MgRPs (240-1000hours) than for MgRP (240-750 hours). The third period is characterized by sharp decrease of the impedance, which indicates severe degradation of the primers and the onset of Al corrosion.

In addition, it is observed that during exposure, the impedance of MgRP+HQ was lower than that of MgRP+SB and MgRP+SDBS, which suggests that HQ is not as effective as SB and SDBS in the aspect of improving primer barrier properties. This might explain why MgRP+HQ didn't perform as well as MgRP+SB and MgRP+SDBS during Prohesion® exposure, even though HQ showed best corrosion inhibition efficiency during PDS test.
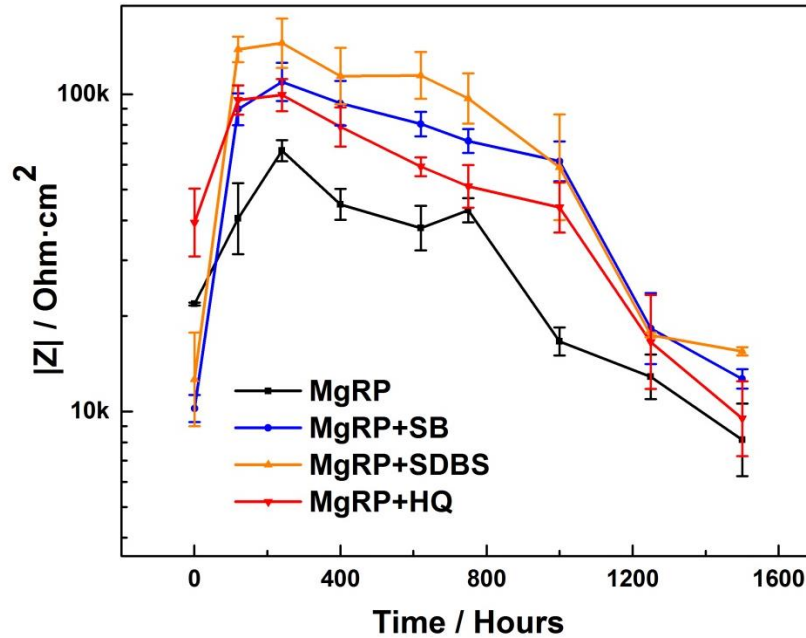
Figure 5.8. Impedance value at 0.01Hz vs. exposure time from MgRPs with and without inhibitors

5.4.7. Visual Inspection (with topcoat)

Coating systems that use MgRP usually include a topcoat for camouflage and barrier effect. Therefore, topcoated samples were scribed and exposed to Prohesion® test to evaluate the response of the coating systems to a defect (Figure 5.9). For MgRP-TC coating systems, severe deterioration of coatings was observed after 3000 hours of exposure. The image of AA2024-T3 substrate after removal of the coatings shows that a large area of the surface was corroded. In contrast, for MgRP+SB-TC coating system, the coating was intact after 3000 hours of exposure. After removal of the coatings, corrosion product was observed only inside the scribe. For MgRP+SDBS-TC and MgRP+HQ-TC coating systems, besides the scribe area, slight corrosion was also observed on the edge of the panel. Visual inspection of both primer coated samples and topcoated samples demonstrates that adding inhibitor improved the corrosion protection

81

performance of MgRP. Among inhibitor-added MgRPs, the MgRP+SB coating system performed best, followed by MgRP+SDBS, and then MgRP+HQ coating system.
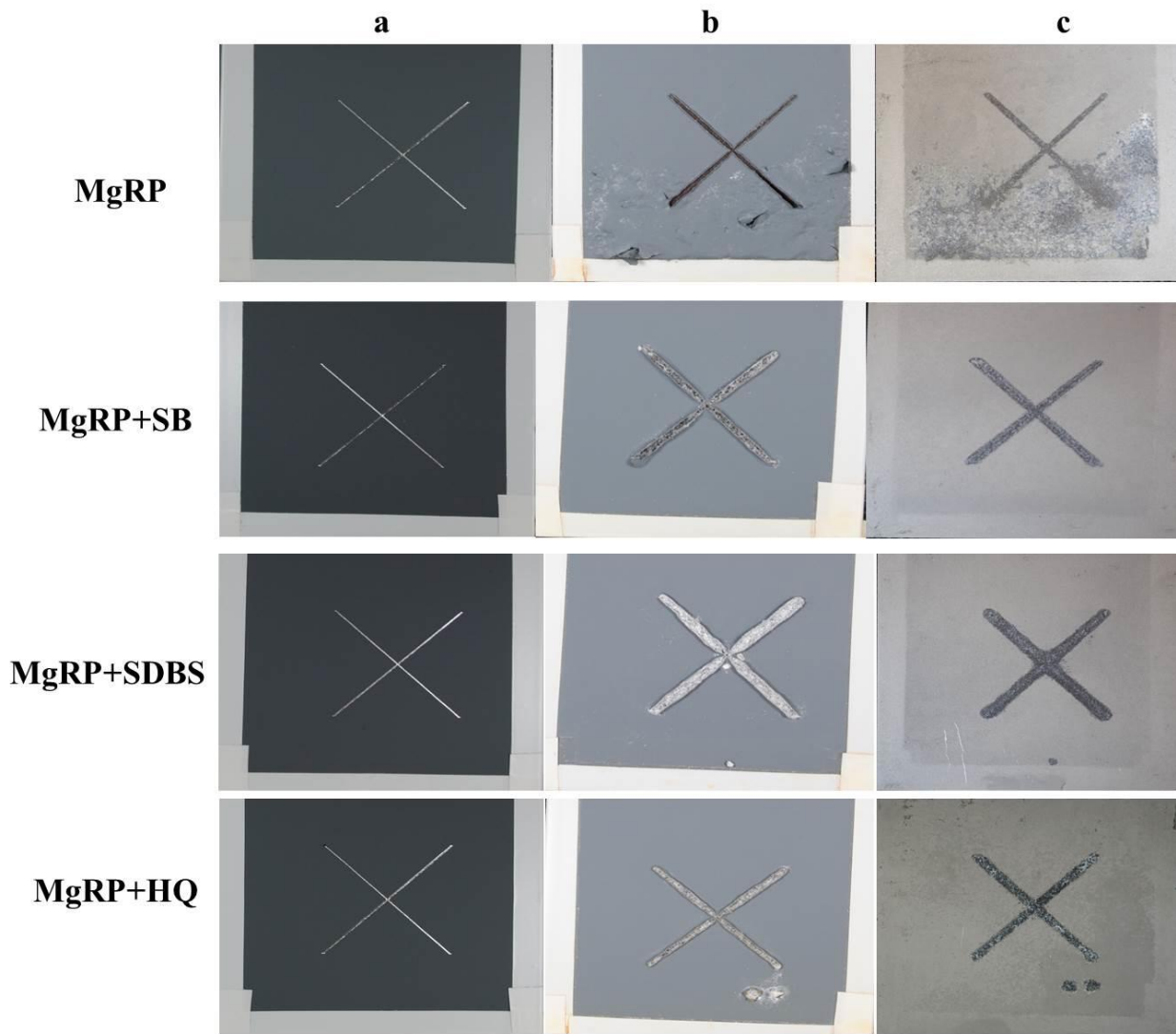

Figure 5.9. Images of topcoated MgRPs with and without inhibitor (a) before exposure, (b) after exposure for 3000hrs, (c) after exposure for 3000hrs, coating removed

5.5. Conclusions

Inhibition effect of three inhibitors: SB, SDBS, and HQ on Mg were verified through PDS. These inhibitors were then added into MgRPs separately for the purpose of prolonging the corrosion protection time of MgRPs. The coating systems with and without inhibitors were compared through hydrogen volume measurement, accelerated weathering tests, electrochemical tests, and adhesion tests. H2 volume measurement shows that adding SB, SDBS and HQ into MgRPs reduced the consumption of Mg pigments. Accelerated weathering tests, EIS tests, and adhesion tests show that the addition of SB, SDBS and HQ into MgRPs could prolong cathodic protection time and improved barrier properties of MgRP, without compromising adhesion strength. However, the presented results do not prove that the inhibitors solely work on Mg pigment. They might as well have inhibition effects on the Al substrate. Future work will consider methods such as SEM, EDX, spectroscopy analysis and EIS modeling to identify corrosion products and investigate inhibition mechanism.

5.6. Acknowledgments

5.7. References

1.   G. Bierwagen, R. Brown, D. Battocchi, and S. Hayes, Prog. Org. Coatings 67 (2010): pp. 48–61.

2.   M.E. Nanna, and G.P. Bierwagen, J. Coatings Technol. Res. 1 (2004): pp. 69–80.

3.   G. Bierwagen, D. Battocchi, A. Simões, A. Stamness, and D. Tallman, Prog. Org. Coatings 59 (2007): pp. 172–178.

4.   G. Bierwagen, R. Brown, D. Battocchi, and S. Hayes, "Observations on the Testing of Mg-Rich Primers for the Totally Chromate-Free Corrosion Protection of Aerospace Alloys," in Dep. Def. Corros. Conf. (Washington DC, 2009).

5.   A.D. King, B. Kannan, and J.R. Scully, 9312 (2014): pp. 536–557.

6.   P. Visser, R. Waddell, and R. Walker, "Reflections," AkzoNobel Aerospace Coatings (2012).

7.   K. Pianoforte, "Aerospace Coatings Market," Coatings World (2015).

8.   W.H. Abbott, The Long Term Degradation of Paint Systems: Effects of Environmental Severity and Acceleration Factors. A Summary of 7 Year Results (Columbus, OH: In Press, n.d.).

9.   D. Battocchi, A.M. Simões, D.E. Tallman, and G.P. Bierwagen, Corros. Sci. 48 (2006): pp. 1292–1306.

10.   A.M. Simões, D. Battocchi, D.E. Tallman, and G.P. Bierwagen, Corros. Sci. 49 (2007): pp. 3838–3849.

11.   B. Maier, and G.S. Frankel, Corrosion 67 (2011): pp. 055001–1–055001–15.

12.   A. Simões, D. Battocchi, D. Tallman, and G. Bierwagen, Prog. Org. Coatings 63 (2008): pp. 260–266.

13.   A.D. King, B. Kannan, and J.R. Scully, Corrosion 70 (2014): pp. 512–535.

14.   X. Lu, Y. Zuo, X. Zhao, and Y. Tang, Electrochim. Acta 93 (2013): pp. 53–64.

15.   S. Shen, Y. Zuo, and X. Zhao, Corros. Sci. 76 (2013): pp. 275–283.

16.   S. Shen, and Y. Zuo, Corros. Sci. 87 (2014): pp. 167–178.

17.   Y. Wang, X. Zhao, and X. Lu, 28 (2012): pp. 407–413.

18.   H. Gao, Q. Li, Y. Dai, F. Luo, and H.X. Zhang, Corros. Sci. 52 (2010): pp. 1603–1609.

19.   L.J. Li, Z.M. Yao, J.L. Lei, H. Xu, S.T. Zhang, and F.S. Pan, Acta Phys. - Chim. Sin. 25 (2009): pp. 1332–1336.

20.   J. Lei, L. Li, and F. Pan, Magnes. Alloy. - Corros. Surf. Treat. (2010): pp. 47–64.

21.   R. Rosliza, W.B. Wan Nik, and H.B. Senin, Mater. Chem. Phys. 107 (2008): pp. 281–288.

22.   J. Lin, V. Upadhyay, X. Qi, D. Battocchi, and G.P. Bierwagen, Corrosion 72 (2016): pp. 377–383.

23. G.S. Frankel, A. Samaniego, and N. Birbilis, Corros. Sci. 70 (2013): pp. 104–111.

24. A.D. King, N. Birbilis, and J.R. Scully, Electrochim. Acta 121 (2014): pp. 394–406.

25. I.A. Raspini, Corrosion 49 (1993): pp. 821–828.

26. A.F. Galio, S. V. Lamaka, M.L. Zheludkevich, L.F.P. Dick, I.L. Müller, and M.G.S. Ferreira, Surf. Coatings Technol. 204 (2010): pp. 1479–1486.

27. D.T.A. Amirudin, A. Amirudin, and D. Thierry, Prog. Org. Coatings 26 (1995): pp. 1–28.

28. B.J.E. Merten, D. Battocchi, and G.P. Bierwagen, Prog. Org. Coatings 78 (2015): pp. 446–454.

29. G. Bierwagen, D. Tallman, J. Li, L. He, and C. Jeffcoate, Prog. Org. Coatings 46 (2003): pp. 148–157.

CHAPTER 6. (MAGNESIUM RICH PRIMER-POWDER TOPCOAT) COATING SYSTEM FOR THE CORROSION PROTECTION OF AL ALLOYS[(1)]

6.1. Abstract

(Mg rich primer-powder topcoat) coating system was first developed and characterized in this research for the corrosion protection of Al alloys. Feasibility of using Mg rich primer (MgRP) as an under layer for powder topcoat was proved through evaluating thermal stability of MgRP, adhesion strength of the (MgRP-powder topcoat) coating system, and cross-section images of the coating system. In addition, corrosion protection effects of (MgRP-powder topcoat) coating system were evaluated by exposing samples to accelerated weathering test. Electrochemical impedance spectroscopy (EIS) and visual inspection were conducted during exposure. The results show that (MgRP-powder topcoat) coating system provided much longer corrosion protection time to Al substrate than the powder coat by itself. Moreover, gloss measurements indicated that for the coating systems tested in this research, using MgRP as under layer does not affect the final coating appearance.

6.2. Introduction

Aluminum alloys are widely used in engineering structures and components due to their light weight and excellent mechanical properties[1, 2]. However, the alloying elements which contribute to the good mechanical properties also make the alloy prone to localized corrosion[3, 4]. One of the most common and economic approaches to protect Al alloys from corrosion is to

---

apply coatings as protective layers. For example, powder coatings and magnesium-rich primers (MgRP) are both widely used for the corrosion protection of Al alloys[5-8]. These two coating systems both have advantages and limitations: powder coatings designed for corrosion protection usually provide very good barrier properties and long lifetime[9]. However, powder coatings by themselves lack corrosion inhibition effect and do not perform well once a defect has developed in the coatings[10, 11]. MgRPs can provide effective cathodic protection to Al alloys[12, 13]. However, since MgRPs are formulated at high pigment volume concentration (PVC) to ensure cathodic protection, they show poor barrier properties and require a topcoat to realize good performance[14,15].

Therefore, this research proposed a (MgRP-powder topcoat) coating system on the premise that the combination of the cathodic protection effect from MgRP and the barrier protection from powder topcoat will achieve superior corrosion protection effect. Furthermore, MgRP is formulated at high PVC, so it might provide desired conductivity for electrostatic spray application, which is the most common application method for powder coating.

To evaluate the corrosion protection effect of (MgRP-powder topcoat) coating system, samples were exposed to accelerated weathering test, and characterized by electrochemical impedance spectroscopy (EIS) and visual inspection. Thermal stability of MgRP, adhesion strength of the (MgRP-powder topcoat) coating system, and gloss change of powder topcoat were also studied in this research.

6.3. Experimental procedures

6.3.1. Samples preparation

The AA2024-T3 panels used in this study were purchased from Q-Lab[†]. The glass panels were purchased from VWR International[†]. The epoxy resin system used was a two component system (Epon 828 and Epikure 3164) purchased from Hexion Inc[†]. BYK 346, from BYK-chemi[†], was used as dispersant, tert-butyl acetate (from TCI American[†]) and p-xylene (from Sunnyside Corporation[†]) were the solvents used. The Mg pigment was supplied by READE Advanced Materials[†]. The powder coat was a polyester based powder coating with b-hydroxyalkylamide (b-HA) as the crosslinker provided by Valspar Corporation[†].

The AA2024-T3 panels were sand blasted with Al_2O_3 grit to remove the oxide layer, grease and oils. The panels were then cleaned with Prekote[†], washed with DI water and dried with paper towel. Mg rich primer was air sprayed onto AA2024-T3 panels and cured at room temperature for seven days before applying powder topcoat. The thickness of MgRP was 40±10μm as measured by a digital thickness gauge elcometer 345[†]. Powder coat was applied on top of MgRP by electrostatic spray and dip methods. For both application methods, the MgRP coated panels were first preheated at 350°F for 20 mins, and then removed from the oven for application. For electrostatic method, a Nordson Versa-Spray II electrostatic spray system was used. Panels were sprayed while suspended by metal hangers in a steel faraday cage grounded to the electrostatic spray unit. Air pressures and electrical settings for the spray unit were 12 psi for the fluidizing air, 15 psi for the powder supply air, 10 psi for the atomization air, and an 80 kV applied voltage potential. After electrostatic spray, the panels were cured at 350°F for 10mins. For dip method, powder topcoats were applied by fully immersing the preheated panels into the

---

[†] Trade name

fluidized powder for approximately two seconds to build proper film thickness. The coated

panels were then removed from the fluidized bed hopper and cured in the oven at 350°F for

10minutes. After curing, panels were removed from the oven and immediately quenched in a

water bath. The coating systems tested in this research and their corresponding thickness are

summarized in Table1. Free films were prepared by air spraying MgRP on Al panels covered

with Mylar®, which has very low surface tension, easing peeling off of the primer.

Table 6.1. Coating systems tested in this research and their thickness

Abbreviation	Coating systems	Thickness (μm)
Al-E	Powder coat on bare Al substrate by electrostatic spray	110±10
Al-D	Powder coat on bare Al substrate by fluidized bed	170±10
MgRP-E	Powder coat on MgRP coated Al substrate by electrostatic spray	160±10 (total)
MgRP-D	Powder coat on MgRP coated Al substrate by fluidized bed	170±10 (total)

6.3.2. Scanning electron microscope

For scanning electron microscope (SEM) investigations, sample cross sections were

mounted in MetLab[†] Jet-Set two part epoxy. After curing, each sample was polished using 800,

1000, and 1200 grit sandpaper. Fine polishing was carried out using 3 μm, and 1 μm diamond

paste followed by 0.05 μm Al_2O_3 on text-met 2500 pads until a mirror finish was achieved. Then

samples were coated with gold using a Hummer II sputter coater[†]. Images of the cross-section

were taken using a JEOL JSM-6490LV scanning electron microscope (from JEOL Ltd[†]) in back

scattering mode with 15KeV acceleration voltage.

6.3.3. Thermal and adhesion measurements

Thermogravimetric analysis (TGA) was conducted using a TA Instruments[†] Q500

Thermogravimetric Analyzer on three samples: 40% Mg rich primer, the same epoxy primer

without Mg pigment, and Mg pigment. All samples were heated in air from 25°C to 300°C at a rate of 10°C/min. Differential scanning calorimetry (DSC) analysis was conducted using a TA Instruments Q1000 series DSC. The testing method used was a heat-cool-heat cycle. The samples were first equilibrated at -75°C and then subjected to a heat cycle at the rate of 10°C/min to 200°C, followed by cooling to -75°C and held isothermally for 5 minutes, and a final heating cycle at a rate of 10°C/min to 250°C. Pull-off adhesion test was conducted on (MgRP-powder topcoat) coating system using Positest® pull-off adhesion tester[†] according to ASTM D4541-09. Loctite 907 Hysol was used for mounting dollies. Five sets of measurements were made on each sample. The dolly used for the test has a diameter of 20 mm and the pull off rate is 1.00 MPa/s.

6.3.4. Accelerated weathering test

Following ASTM standard G85-11 (Prohesion® test), powder coated panels (both scribed and unscribed) were placed into a Q-fog cyclic corrosion tester[†]. The back and the edges of panels were covered with tape. The solution for Prohesion® procedure is Dilute Harrison's Solution (DHS), which consists of 0.05% NaCl and 0.35% $(NH_4)_2SO_4$. Each cycle includes one hour salt fog cycle at 25°C and one hour dry air purge cycle at 35°C. The panels were removed from the tester periodically for visual analysis, gloss measurement and electrochemical impedance spectroscopy test. All panels were removed at the end of fog cycle. At least 3 panels were tested for each sample.

6.3.5. Visual inspection and gloss measurement

The images of the panels were taken by Nikon D3000 digital camera. The light source was above the unexposed panels and to the side of the exposed panels. The position of the light source was changed for exposed panels because the side position of the light cast more visible

90

shadows that make the coating delamination easier to see. Gloss (60°) was measured using Rhopoint IQ Glossmeter & Goniophotometer[†]. Nine sets of measurements were made on each sample

6.3.6. EIS measurement

EIS measurements were performed using a Gamry Reference 600 potentiostat[†] (open lead impedance exceed 10 TΩ at 0.01Hz) with three-electrode setup: a test panel was used as working electrode, a saturated calomel electrode (SCE) was used as reference electrode, and a Pt mesh was used as counter electrode. The exposed area of the working electrode was 7.06 cm^2. The testing electrolyte was DHS. Impedance spectra were collected at the open circuit potential, through a frequency range from 100 kHz to 0.01 Hz with 10mV alternating current (AC) voltage applied.

6.4. Results and discussion

6.4.1. Thermal stability of MgRPs

Since powder topcoat application includes preheat and curing samples at 350ºF (177ºC), thermogravimetric analysis (TGA) was conducted to observe if MgRP can endure the high temperature. The results (Figure 6.1) show that MgRP lost only about 1% weight at 350ºF. To determine the cause of the weight loss from MgRP, TGA was conducted on Mg pigment and epoxy primer without Mg pigment. The results show that Mg pigment didn't undergo any weight loss at 350ºF, but epoxy primer lost about 4% weight at the temperature. It is known that when a coating is cured below glass transition temperature (T_g), residual solvent remains in the coating for years after the coating has formed[16]. T_g of the MgRP was 36.24ºC as measured by DSC (Figure 6.2), which is higher than the curing temperature of MgRP (room temperature). Therefore, it is very likely that the weight loss is from unevaporated solvents. Generally, 10% of

weight loss is considered as the threshold of thermal degradation[17]. Therefore, MgRPs can be

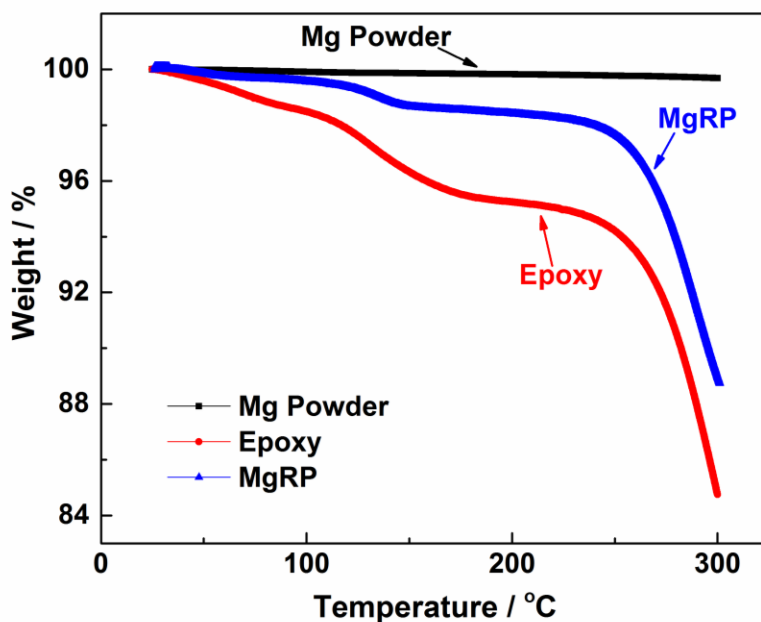considered thermal stable during the application of powder topcoat.

Figure 6.1. Thermogravimetric analysis of MgRP, Mg pigment and epoxy primer
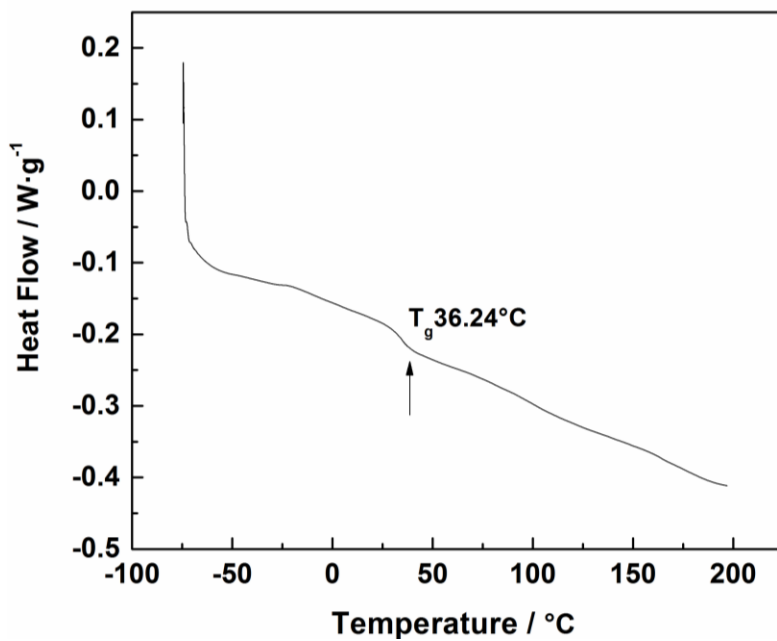

Figure 6.2. DSC analysis of MgRP

6.4.2. Coating application

The application quality of a powder coat will be affected by surface conditions of the substrate. Therefore, SEM Images of coating cross-sections were taken to assess the application quality of powder topcoat on top of MgRP. As shown in Figure 6.3, powder topcoats on MgRP cover the surface of MgRP very well. No difference was observed on powder topcoats between coating systems with and without MgRP, which suggests that the application quality of powder topcoat on MgRP is as good as powder topcoat on Al alloy.
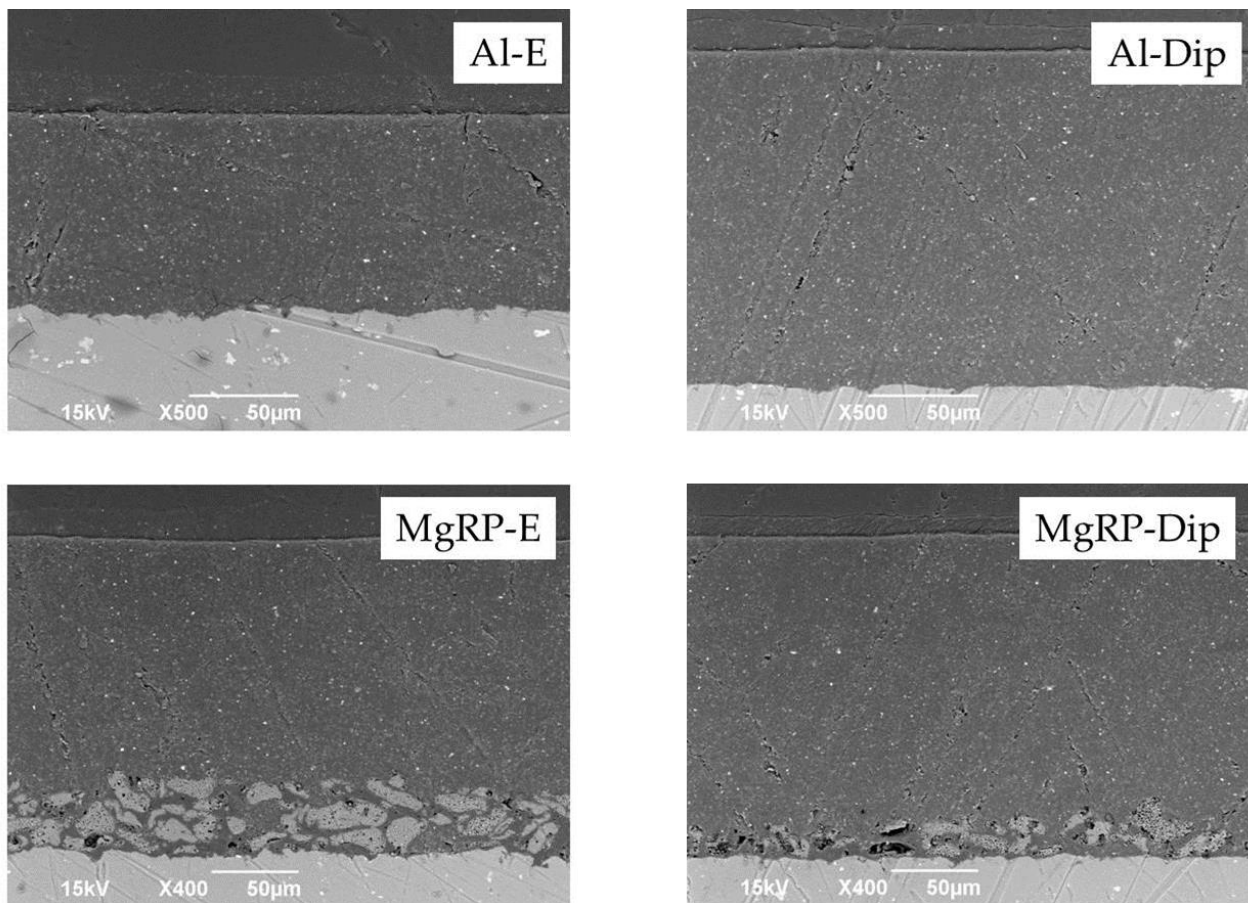

Figure 6.3. SEM images of four samples: Al-E, Al-D, MgRP-E and MgRP-D

6.4.3. Adhesion tests

One of the most important properties in corrosion protective coatings is the coating adhesion to the substrate. Thus, pull-off adhesion test was conducted in this research to evaluate the adhesion strength of the (MgRP-powder topcoat) coating (Figure 6.4). The results show that the adhesion strength is similar between coating systems with and without MgRP. However, when conducting the adhesion tests, coating detached between MgRP/Al interface for the coating systems with MgRP, which suggests that the adhesion strength between MgRP and powder topcoat is greater than the measurement results. This indicates that powder topcoat adheres stronger to MgRP than to Al substrate.
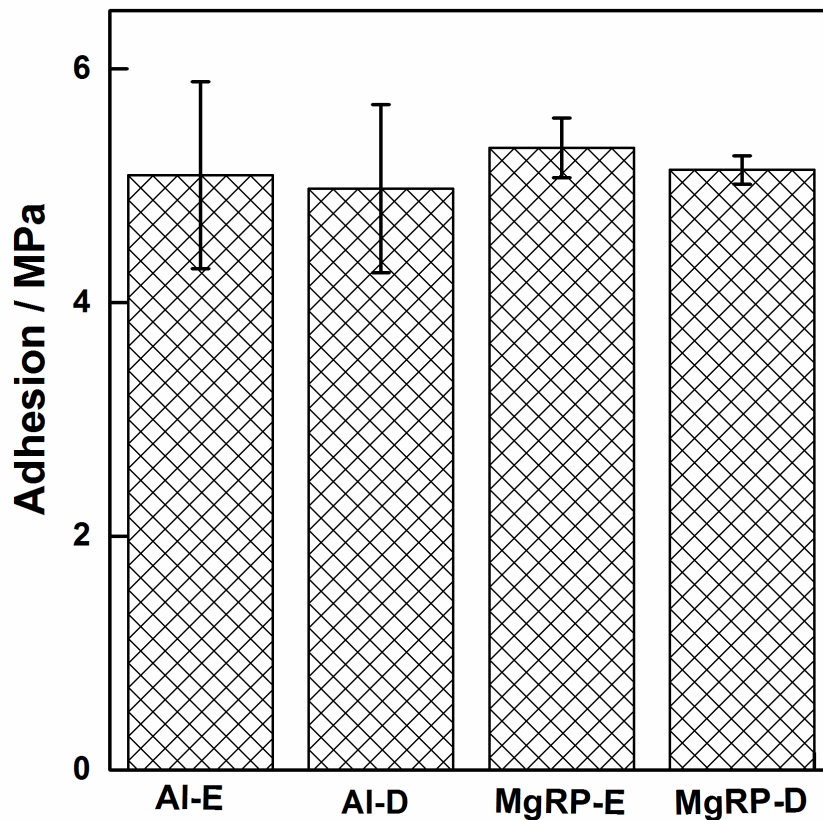
Figure 6.4. Adhesion strength of four samples: Al-E, Al-D, MgRP-E and MgRP-D

6.4.4. EIS measurement

EIS has been used widely in studies of corrosion prevention by organic coatings. The coating barrier properties can be determined by the change of the coating resistance. Generally, for organic coating systems, the low frequency impedance is an indication of coating barrier properties. EIS results on unscribed samples (Figure 6.5) show that, before exposure, all the samples have very high impedance at 0.01Hz, exceeding 10^{10} Ohm. The 0.01Hz impedance remains the same even after 3000 hours of exposure. This indicates that all four coating systems provide excellent barrier protection to the substrate under prohesion test. In addition, the phase angle shifts for all four coating systems are constant around -90 degree over entire exposure (not shown). This suggests purely capacitive behavior of the coating systems, which again indicates that all the coating systems provide very effective barrier protection even after 3000 hours of exposure.
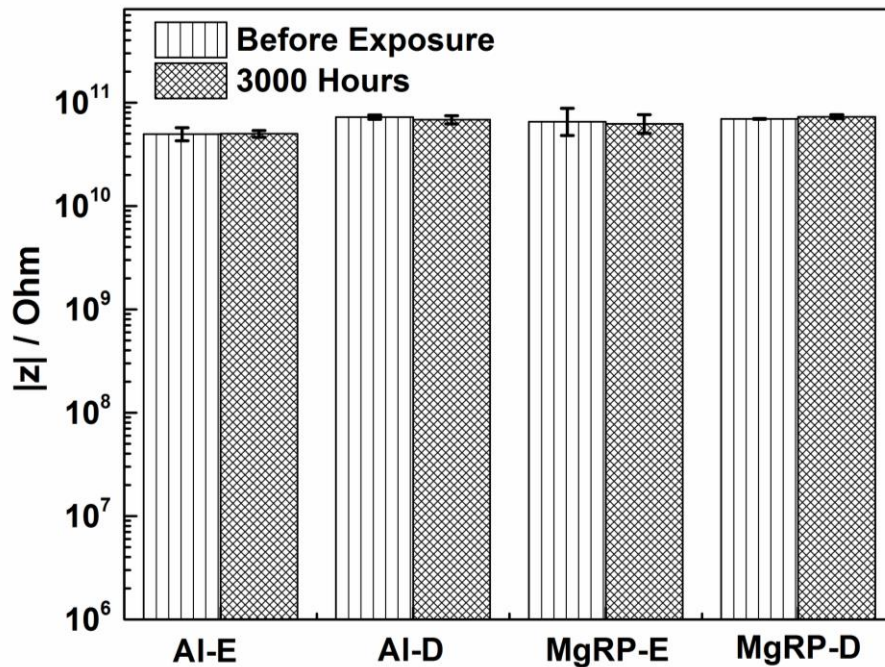

Figure 6.5. $Z_{0.01Hz}$ of four samples: Al-E, Al-D, MgRP-E and MgRP-D

6.4.5. Visual analysis

Visual inspection of the scribed samples after Prohesion® exposure was conducted to evaluate the response of the four coating systems to a defect (Figure. 6.6-6.9). For Al-E coating system (Figure 6.6), delamination of the powder topcoat was observed around the scribe area after 600 hours of exposure. After 1500 hours of exposure, the delamination area has spread to most of the surface. The image of Al alloy substrate after removal of the powder topcoat shows that most of the Al alloy surface was corroded. For Al-Dip system (Figure 6.7), delamination of the powder topcoat was observed after 1100 hours of exposure, and the delamination area spread to most of the surface after 2000 hours of exposure. The image of Al alloy substrate after removal of the powder topcoat also shows that most of the Al alloy surface was corroded. In contrast, for coating systems with MgRP (Figure 6.8&6.9), slight delamination of powder topcoat was observed around the scribed area after 2000 hours of exposure. Even after 3500 hours of exposure, the delamination area was still restricted to the scribed area. The images of Al alloy substrate after removal of the powder topcoat show that corrosion of Al alloy only occurred around the scribed area for both MgRP-E and MgRP-Dip coating systems. The difference between samples with and without MgRP along with the EIS measurements on unscribed samples confirms that powder coat by itself provides corrosion protection through its effective barrier property. However, once a defect developed in the coating, undercoat corrosion started and spread rapidly, because powder coat does not provide any corrosion inhibition effect. By adding MgRP as under layer, when a defect occured, undercoat corrosion can be prevented by MgRP through cathodic protection. Consequently, (MgRP-powder topcoat) coating system provided not only excellent barrier properties but also superior cathodic protection effect. The

corrosion protection time of the (MgRP-powder topcoat) coating system was much longer than
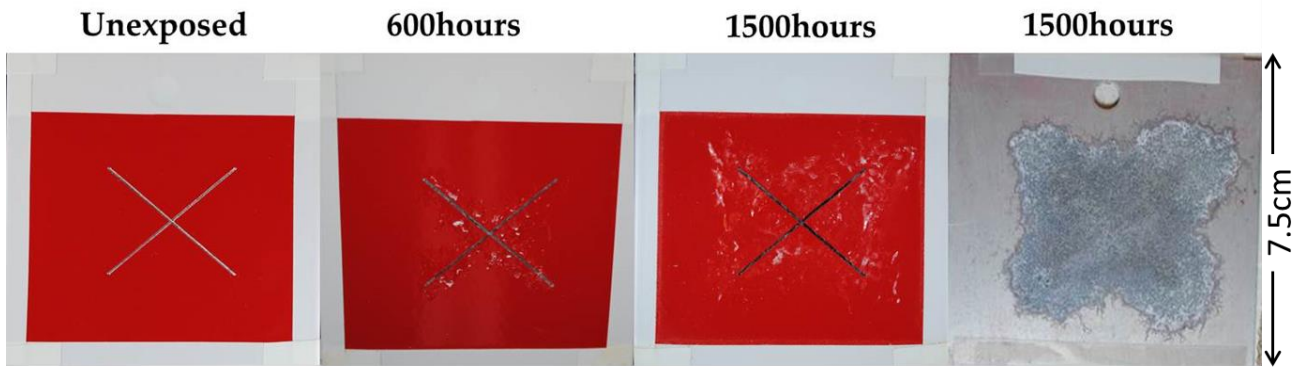
the powder coat by itself.

Figure 6.6. Images of Al-E coating system before and after prohesion exposure
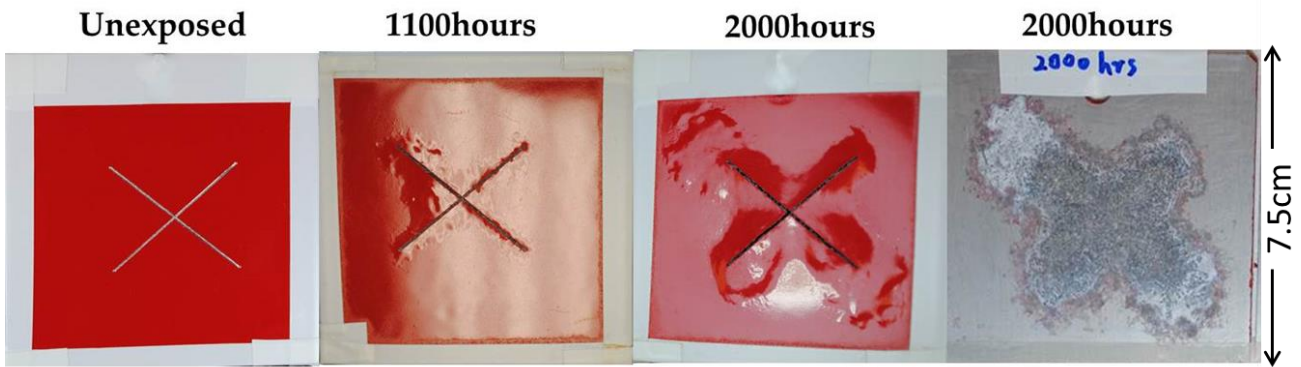

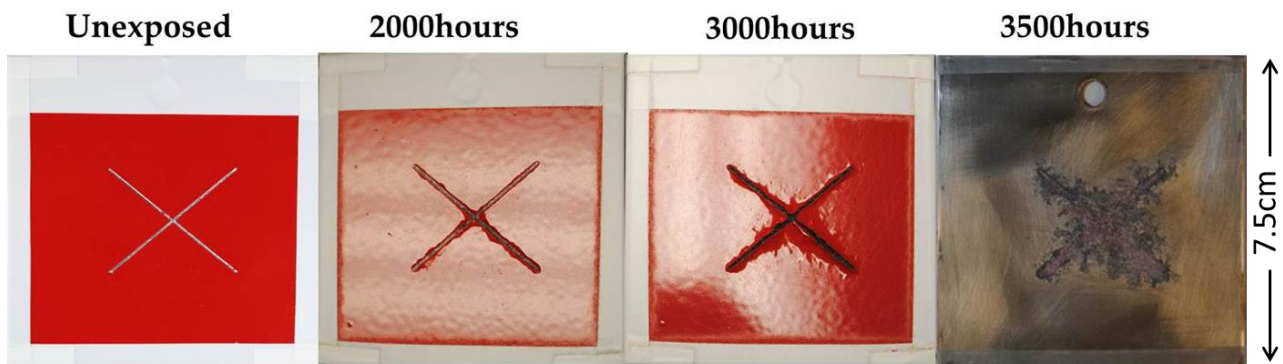Figure 6.7. Images of Al-D coating system before and after prohesion exposure

Figure 6.8. Images of MgRP-E coating system before and after prohesion exposure
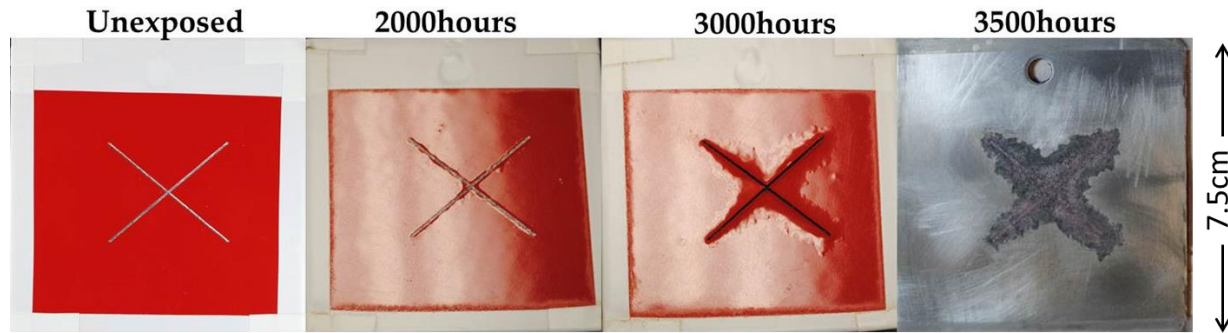
Figure 6.9. Images of MgRP-D coating system before and after prohesion exposure

6.4.6. Gloss measurement

The appearance of a painted surface has always been an important factor, because it is often the first impression of a product seen by the end-user, especially in the automotive and consumer appliances industries[18]. For a multilayer coating system, surface properties of the under layers might influence the appearance of the final paint appearance[19]. Therefore, gloss changes of the powder topcoat were measured to evaluate the influence of MgRP on the final paint appearance. As shown in Figure 6.10, the coating systems with and without MgRPs show similar gloss values before exposure. After 750 hours of exposure, a slight increase of the gloss values was observed for all four coating systems. The increase of gloss value might due to the swelling of the coatings during exposure, which reduces the roughness of the coatings caused by shrinkage during curing[20]. After 3000 hours of exposure, the gloss values started decreasing for all four coating systems due to surface erosion by weathering. The similar gloss values and the same trend of gloss changes for all four coating systems suggest that at least for the coating systems tested in this research, using MgRPs as an under layer does not affect the final coating appearance.
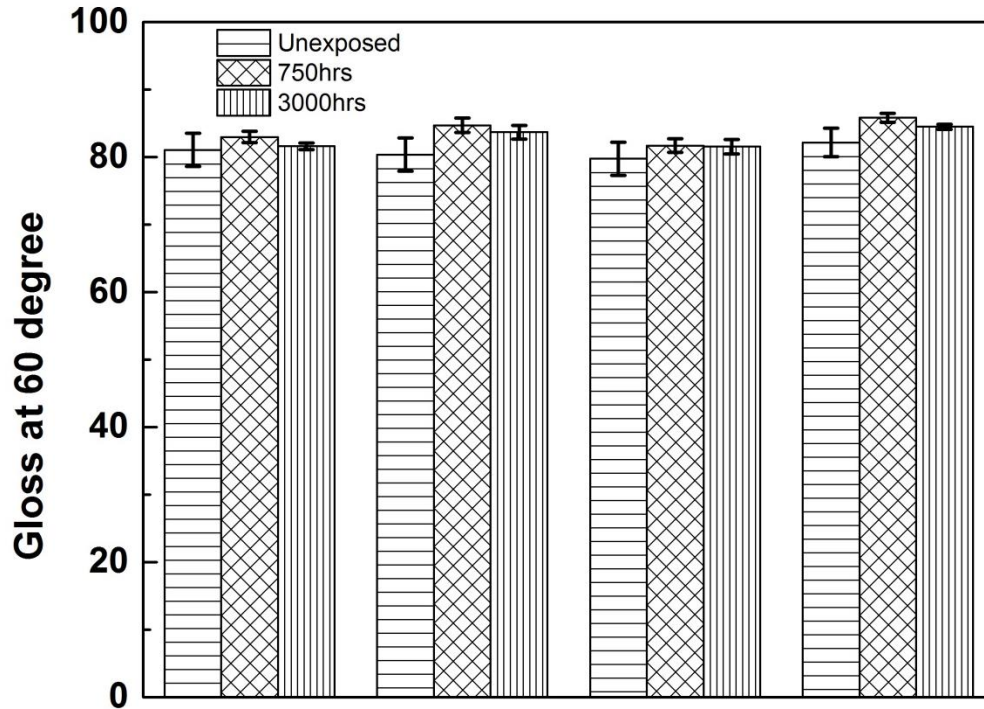
98

Figure 6.10. Gloss measurements of four coating systems before and after prohesion exposure

6.5. Conclusions

1. Powder topcoat can be applied on top of MgRP through both fluidized bed and electrostatic spray methods. SEM images of cross-section of coating systems suggests that using MgRP as an under layer for powder topcoat doesn't undermine the application quality of powder topcoat.

2. TGA results shows that MgRP is thermally stable during the application of powder topcoat; and adhesion tests indicate that powder topcoat adheres stronger to MgRP than to Al substrate.

3. Accelerating weathering test shows that (MgRP-powder topcoat) coating system provides much longer corrosion protection time to Al substrate than the powder coat by itself,

since (MgRP-powder topcoat) coating system provided both excellent barrier properties through powder topcoat, and superior cathodic protection through MgRP.

4. Gloss measurements indicates that for the coating systems tested in this research, using MgRP as under layer does not affect the final coating appearance.

6.6. Acknowledgements

6.7. References

1. B.J.E. Merten, D. Battocchi, and G.P. Bierwagen, Prog. Org. Coatings 78 (2015): pp. 446–454.

2. D. Zhu, and W. J. van Ooij, Corros. Sci. 45 (2003): pp. 2163–2175.

3. Z. Szklarska-Smialowska, Corros. Sci. 41 (1999): pp. 1743–1767.

4. D.E. Beving, A.M.P. McDonnell, W. Yang, and Y. Yan, J. Electrochem. Soc. 153 (2006): p. B325.

5. J.B. Bajat, J.P. Popić, and V.B. Mišković-Stanković, Prog. Org. Coatings 69 (2010): pp. 316–321.

6. R.G. Haverkamp, D.C.W. Siew, and T.F. Barton, Surf. Interface Anal. 33 (2002): pp. 330–334.

7. M.E. Nanna, and G.P. Bierwagen, J. Coatings Technol. Res. 1 (2004): pp. 69–80.

8. S.S. Pathak, S.K. Mendon, M.D. Blanton, and J.W. Rawlins, Metals (Basel). 2 (2012): pp. 353–376.

9. Y. Takeshita, T. Kamisho, S. Sakata, T. Sawada, Y. Watanuki, R. Nishio, and T. Ueda, J. Appl. Polym. Sci. 128 (2013): pp. 1732–1739.

10. M. Bjordal, S.B. Axelsen, and O.O. Knudsen, Prog. Org. Coatings 56 (2006): pp. 68–75.

11. S. Radhakrishnan, N. Sonawane, and C.R. Siju, Prog. Org. Coatings 64 (2009): pp. 383–386.

12. A. Simões, D. Battocchi, D. Tallman, and G. Bierwagen, Prog. Org. Coatings 63 (2008): pp. 260–266.

13. A.M. Simões, D. Battocchi, D.E. Tallman, and G.P. Bierwagen, Corros. Sci. 49 (2007): pp. 3838–3849.

14. A.D. King, B. Kannan, and J.R. Scully, c (2014): pp. 512–535.

15. J. Li, J. He, B.J. Chisholm, M. Stafslien, D. Battocchi, and G.P. Bierwagen, J. Coatings Technol. Res. 7 (2010): pp. 757–764.

16. Z.W. Wicks, F.N. Jones, S.P. Pappas, and D.A. Wicks, "Evaporation of Solvents from Coating Films," in Org. Coatings Sci. Technol., 3rd ed. (New Jersey: John Wiley & Sons, Inc., 2007), pp. 363–365.

17. D. Ajloo, A. Sharifian, and H. Behniafar, Bull. Korean Chem. Soc. 29 (2008): pp. 2009–2016.

18. S. Mezghani, H. Zahouani, and J.J. Piezanowski, J. Mater. Process. Technol. 211 (2011): pp. 205–211.

19. G. Kigle-boeckler, "Surface Smoothness and Its Influence on Paint Appearance . How to Measure and Control It ?," in Color. Technol. Plast. (William Andrew, 1999), pp. 103–111.

20. H.J. Braun, and D.P. Cobranchi., J. Coatings Technol. 67 (1995): pp. 55–62.

CHAPTER 7. CONCLUSIONS AND FUTURE WORK

7.1. Conclusions

With the research goals to develop deeper understanding of the corrosion protection mechanism of Mg-rich primer (MgRPs), improve corrosion protection performance of MgRPs, and extend the application of MgRPs, research of this thesis made significant developments in the following four areas.

7.1.1. Early blistering problems

Early blistering was observed on top-coated MgRPs over Al substrates under constant immersion or constant salt spray tests. This problem has hindered the acceptance of MgRP. Hydrogen entrapment by topcoats was definitively identified as the cause of early blistering in this research. This understanding of the cause of early blistering will allow coating manufacturers to make improvements to the coating formulation and to produce a more realistic accelerated weathering test for the qualification of the metal rich coating systems. Meanwhile, hydrogen volume collection method was applied to MgRP for the first time, and a simultaneous real-time open circuit potential and hydrogen volume collection method was demonstrated as a new approach for studying the corrosion protection mechanism of MgRPs. Moreover, the gas generated from MgRPs was unequivocally identified as hydrogen by cyclic voltammetry.

7.1.2. Corrosion protection mechanisms of MgRP in different solutions

This research compared degradation behaviors of MgRP during constant immersion in DHS and 1% NaCl solution through hydrogen volume collection, electrochemical measurements and scanning electron microscopy analysis. The different behaviors observed during electrochemical measurements and hydrogen volume collection can be explained by the microstructural porosity difference after immersion in DHS and 1% NaCl solution. The effects of

connection modes between Mg pigment and Al substrate, different ions on the formation and stability of Mg oxidation products, and cathodic reaction sites on the microstructure of MgRP were discussed. In addition, an in situ method for the estimation of remaining Mg pigment in MgRP was developed based on H_2 volume collection. The estimation data and the SEM analysis of MgRP confirmed that there was still Mg pigment preserved in MgRP for future protection of Al even though the OCP of MgRP had risen above the OCP of bare AA2024-T3 substrate.

7.1.3. Inhibitor included MgRPs for prolonged corrosion protection time on AA2024-T3

Three inhibitors, sodium benzoate (SB), sodium dodecylbenzenesulfonate (SDBS), and 8-hydroxyquinoline (HQ), were added to MgRP individually. The effects of each inhibitor were investigated through potentiodynamic scans, accelerated weathering tests, electrochemical impedance spectroscopy, visual inspection, adhesion tests, and hydrogen volume measurement. The results show that addition of SB, SDBS and HQ into an MgRP prolonged the corrosion protection time of MgRP by decelerating the oxidation rate of Mg pigment, improving coating barrier properties and inhibiting the corrosion of AA2024-T3. Among the inhibitor-added MgRPs, MgRP+SB coating system performed best, followed by MgRP+SDBS, and then MgRP+HQ coating system.

7.1.4. (MgRP-Powder topcoat) coating system

The (MgRP-powder topcoat) coating system was developed and characterized in this research. Powder topcoats were successfully applied on top of MgRP through both fluidized bed and electrostatic spray. Feasibility of using Mg rich primer (MgRP) as an under layer for powder topcoat was proved through verifying the thermal stability of MgRP during powder coat application, adhesion strength of the (MgRP-powder topcoat) coating system, and cross-section images of the coating system. Accelerated weathering tests show that (MgRP-powder topcoat)

coating system provided much longer corrosion protection time to Al substrate than the powder

coat by itself through the combination of the cathodic protection from MgRP and the barrier

protection from powder topcoat. Moreover, gloss measurements indicated that for the coating

systems tested in this research, using MgRP as under layer does not reduce topcoat gloss.

7.2. Future work

Simultaneous open circuit potential and hydrogen volume collection method was shown

to be an effective approach for studying the protection mechanism of MgRPs. In the future,

combination of hydrogen volume collection method with other electrochemical techniques, such

as electrochemical impedance spectroscopy, could be developed. Through this approach,

information about consumption of Mg, coating barrier properties and the cathodic protection

effect could be obtained simultaneously.

Initial studies of inhibitors added MgRPs shown that SB, SDBS and HQ can prolong

corrosion protection time of MgRPs on AA2024-T3. The concentration of each inhibitor could

be adjusted to optimize the primer formulations. Also, more than one inhibitor could be added

into an MgRP, the synergistic effect between different inhibitors could be studied. In addition,

more characterization techniques, such as SEM, SVET, SECM, and XPS, could be used to study

the working mechanism and structure-properties relationship of each inhibitor. Deeper

understanding of the inhibitor-added MgRP will provide guidelines to select other effective

inhibitors and formulate MgRPs with improved properties.

The effect of powder coat curing temperature on Al alloys should be examined due to the

temperature sensitivity of their mechanical properties[1-4]. The application of (MgRP-powder

topcoat) system then could be extended to other Al alloys. Also, successful development of this

(MgRP-powder topcoat) system gives us guideline to develop other metal rich powder topcoat

systems, such as zinc rich primer/powder topcoat system for the corrosion protection of steel. In addition, developing Mg rich powder primer and (Mg rich powder primer-powder topcoat) system may be highly beneficial from environmental perspective. Continued progress in the field will yield MgRPs that possess better performance and wider applications.

7.3. References

1.   J.C. Malas, S. Venugopal, and T. Seshacharyulu, Mater. Sci. Eng. A 368 (2004): pp. 41–47.

2.   D. Li, and A. Ghosh, Mater. Sci. Eng. A 352 (2003): pp. 279–286.

3.   G.R. Ebrahimi, A. Zarei-Hanzaki, M. Haghshenas, and H. Arabshahi, J. Mater. Process. Technol. 206 (2008): pp. 25–29.

4.   W.S. Lee, W.C. Sue, C.F. Lin, and C.J. Wu, J. Mater. Process. Technol. 100 (2000): pp. 116–122.

APPENDIX. ESTIMATION OF THE TOTAL AREA AND VOLUME OF BLISTERS

(CHAPTER 3)

The total area and volume of the blisters were estimated by assuming the blisters are hemispherical. Figure 3.6(a) was magnified to a 6 in × 6 in (15.24 cm × 15.24 cm) image to clearly show the blisters. Each blister was marked by a circle just large enough to surround the blister (Figure A.1). The radius of each circle was measured as C_i, so the radius of each corresponding blister is $r_i = C_i \frac{3}{6} = \frac{C_i}{2}$ cm. Therefore, the total area and the volume of the blisters can be estimated through the following equations:

$$\text{Total area: } A = \sum_1^n \pi r_i^2 \tag{A.1}$$
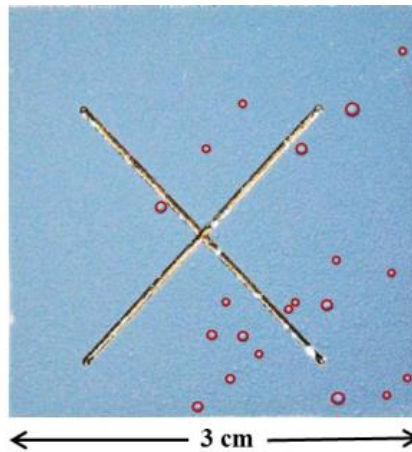
$$\text{Total volume: } V = \sum_1^n \frac{4}{3}\pi r_i^3 \tag{A.2}$$

Figure A.1. Image of blisters marked by circles